"Variational Transition State Theory with Multidimensional Tunneling," A. Fernandez-Ramos, B. A. Ellingson, B. C. Garrett, and D. G. Truhlar, in *Reviews in Computational Chemistry*, Vol. 23, edited by K. B. Lipkowitz and T. R. Cundari (Wiley-VCH, Hoboken, NJ 2007), pp. 125-232.

CHAPTER 3

Variational Transition State Theory with Multidimensional Tunneling

Antonio Fernandez-Ramos,[a] Benjamin A. Ellingson,[b] Bruce C. Garrett,[c] and Donald G. Truhlar[b]

[a]*Departamento de Quimica Fisica, Universidade de Santiago de Compostela, Facultade de Quimica, Santiago de Compostela, Spain*
[b]*Department of Chemistry and Supercomputing Institute, University of Minnesota Minneapolis, MN*
[c]*Chemical and Materials Sciences Division, Pacific Northwest National Laboratory, Richland, WA*

INTRODUCTION

"The rate of chemical reactions is a very complicated subject"

Harold S. Johnston, 1966

"The overall picture is that the validity of the transition state theory has not yet been really proved and its success seems to be mysterious."

Raymond Daudel, Georges Leroy, Daniel Peeters, and Michael Sana, 1983

This review describes the application of variational transition state theory (VTST) to the calculation of chemical reaction rates. In 1985, two of us, together with Alan D. Isaacson, wrote a book chapter on this subject entitled "Generalized Transition State Theory" for the multi-volume series entitled *Theory of Chemical Reaction Dynamics*.[1] Since that time, VTST has undergone

Reviews in Computational Chemistry, Volume 23
edited by Kenny B. Lipkowitz and Thomas R. Cundari

important improvements due mainly to the ability of this theory to adapt to more challenging problems. For instance, the 1985 chapter mainly describes the application of VTST to bimolecular reactions involving 3–6 atoms, which were the state-of-the-art at that moment. The study of those reactions by VTST dynamics depended on the construction of an analytical potential energy surface (PES). Nowadays, thanks to the development of more efficient algorithms and more powerful computers, the situation is completely different, and most rate calculations are based on "on the fly" electronic structure calculations, which together with hybrid approaches, like combined quantum mechanical molecular mechanical methods (QM/MM), allow researchers to apply VTST to systems with hundreds or even tens of thousands of atoms. Three other major advances since 1985 are that transition state dividing surfaces can now be defined much more realistically, more accurate methods have been developed to include multidimensional quantum mechanical tunneling into VTST, and the theory has also been extended to reactions in condensed phases.

This review progresses from the simplest VTST treatments applicable to simple systems to more advanced ones applicable to complex systems. The next four sections describe the use of VTST for gas-phase unimolecular or bimolecular reactions for which we can afford to build a global analytical PES or to use a high-level electronic structure method to run the dynamics without invoking special methods or algorithms to reduce the computational cost. In the second part (the subsequent three sections on pages 190–212), we deal with VTST in complex systems; this often involves the use of interpolative or dual-level methods, implicit solvation models, or potentials of mean force to obtain the potential energy surface. Two sections also discuss the treatment of condensed-phase reactions by VTST.

A fundamental theoretical construct underlying this whole chapter is the Born–Oppenheimer approximation. According to this approximation, which is very accurate for most chemical reactions (the major exceptions being electron transfer and photochemistry), the Born–Oppenheimer energy, which is the energy of the electrons plus nuclear repulsion, provides a potential energy surface V for nuclear motion. At first we assume that this potential energy surface is known and is available as a potential energy function. Later we provide more details on interfacing electronic structure theory with nuclear dynamics to calculate V by electronic structure calculations "on the fly," which is called direct dynamics. The geometries where ∇V is zero play a special role; these geometries are called stationary points, and they include the equilibrium geometries of the reactants, products, and saddle points, and geometries of precursor and successor complexes that are local minima (often due to van der Waals forces) between reactants and the saddle point and between products and the saddle point. In general V is required at a wide range of geometries, both stationary and nonstationary.

A word on nomenclature is in order here. When we say transition state theory, we refer to the various versions of the theory, with or without including tunneling. When we want to be more specific, we may say conventional

transition state theory, variational transition state theory, canonical variational transition state theory (also called canonical variational theory or CVT), and so forth. For each of the versions of VTST, we can further differentiate, for example, CVT without tunneling, CVT with one-dimensional tunneling, or CVT with multidimensional tunneling; and we can further specify the specific approximation used for tunneling. Sometimes we use the term generalized transition state theory, which refers to any version of transition state theory in which the transition state is not restricted to the saddle point with the reaction coordinate along the imaginary frequency normal mode.

In this chapter we explain the algorithms used to implement VTST, especially CVT, and multidimensional tunneling approximations in the POLYRATE[2–6] computer program. We also include some discussion of the fundamental theory underlying VTST and these algorithms. Readers who want a more complete treatment of theoretical aspects are referred to another review.

The beginning of the next section includes the basic equations of VTST, paying special attention to canonical variational transition state theory (CVT), although other theories are discussed briefly in the third subsection. The reason for centering attention mainly on CVT is that it is very accurate but requires only a limited knowledge of the PES. The basic algorithms needed to run the dynamics calculations are then discussed in detail, including harmonic and anharmonic calculations of partition functions. Multidimensional tunneling corrections to VTST are discussed in the fourth section. Approaches to build the PES information needed in the VTST calculations are then discussed, including direct-dynamics methods with specific reaction parameters, interpolated VTST, and dual-level dynamics. The sixth section is dedicated to reactions in condensed media, including liquid solutions and solids. Then ensemble-averaged VTST is highlighted. The eighth and ninth sections describe some practical examples that show in some detail how VTST works, including a brief discussion of kinetic isotope effects. The last section provides a summary of the review.

VARIATIONAL TRANSITION STATE THEORY FOR GAS-PHASE REACTIONS

Conventional Transition State Theory

Transition state theory (TST), also known as conventional TST, goes back to the papers of Eyring[8] and Evans and Polanyi[9] in 1935. For a general gas-phase reaction of the type

$$A + B \rightarrow \text{Products} \qquad [1]$$

where *A* and *B* may be either atoms or molecules, the theory assumes that there is an activated complex called the transition state that represents the bottleneck in the reaction process. The fundamental assumption of TST (also

called the no-recrossing assumption) is only expressible in classical mechanics. It states that

(1) this transition state is identified with a dividing hypersurface (or surface, for brevity) that separates the reactant region from the product region in phase space, and
(2) all the trajectories that cross this dividing surface in the direction from reactants to products originated as reactants and never return to reactants;

that is, they cross the dividing surface only once. For this reason, the TST dividing surface is sometimes called the dynamical bottleneck. Rigorously, we can say that TST makes only four assumptions:

(1) that the Born–Oppenheimer approximation is valid, and so the reaction is electronically adiabatic;
(2) that the reactants are equilibrated in a fixed-temperature (canonical) ensemble or fixed-total-energy (microcanonical) ensemble;
(3) that there is no recrossing; and
(4) that quantum effects can be included by quantizing vibrations and by a multiplicative transmission coefficient to account for tunneling (nonclassical transmission) and nonclassical reflection.

In a world where nuclear motion is strictly classical, we need not consider (4), and the TST classical rate constant, $k_C^\ddagger$, for Eq. [1] is given by

$$k_C^\ddagger = \frac{1}{\beta h}\frac{Q_C^\ddagger(T)}{\Phi_C^R(T)}\exp[-\beta V^\ddagger] \qquad [2]$$

where $\beta = (k_B T)^{-1}$ (k_B is the Boltzmann constant, and T is the temperature), h is the Planck constant, $V^\ddagger$ is the potential energy difference between reactants and the transition state (the barrier height, also called classical barrier height), $Q_C^\ddagger$ is the classical (C) partition function of the transition state, and Φ_C^R is the classical partition function of reactants per unit volume. (For a unimolecular reaction, we would replace Φ_C^R by the unitless classical reactant partition function Q_C^R.)

Note that the transition state has one less degree of freedom than does the full system; that particular degree of freedom is called the reaction coordinate, and it is missing in $Q_C^\ddagger$. Throughout this chapter, the symbol ‡ is used to denote the conventional transition state, which is a system confined to the vicinity of the saddle point by constraining the coordinate corresponding to the saddle point's imaginary-frequency normal mode to have zero extension. This coordinate is the reaction coordinate in conventional transition state theory. The zero of energy for the potential is taken as the energy of the minimum energy configuration in the reactant region. The partition functions are proportional to configurational integrals of Boltzmann factors of the potential. For the reactant partition function, the zero of energy is the same as that for the potential, whereas for the partition function of the transition state, the zero

of energy is taken as the local minimum in the bound vibrational modes at the saddle point, which is $V^{\ddagger}$.

We can establish a connection between Eq. [2] and thermodynamics by starting with the relation between the free energy of reaction, ΔG_T^0 at temperature T, and the equilibrium constant K, which is given by

$$K = K^0 \exp\left[-\Delta G_T^0/RT\right] \qquad [3]$$

where K^0 is the value of the reaction quotient at the standard state. (For a reaction where the number of moles decreases by one, this is the reciprocal of the standard-state concentration.) Then we rewrite Eq. [2] in quasithermodynamic terms[8,10,11] as

$$k_C^{\ddagger} = \frac{1}{\beta h} K_C^{\ddagger}(T) \qquad [4]$$

where $K_C^{\ddagger}$ is the quasiequilibrium constant for forming the transition state.. (The transition state is not a true thermodynamic species because it has one degree of freedom missing, and therefore we add the prefix "quasi".) The thermodynamic analog of Eq. [1] is now given by

$$k_C^{\ddagger} = \frac{1}{\beta h} K^{\ddagger,o} \exp\left[-\Delta G_{C,T}^{\ddagger,o}/RT\right] \qquad [5]$$

where $\Delta G_{C,T}^{\ddagger,o}$ represents the classical free energy of activation for the reaction under consideration.

The siren song of TST when it was first proposed was that "all the quantities may be calculated from the appropriate potential surface,"[8] and in fact from very restricted regions of that surface. Specifically, one "only" needs to obtain the properties (energies, geometries, moments of inertia, vibrational frequencies, etc.) of the reactants and the transition state from the PES and to be sure that the transition state is unequivocally joined to reactants by a reaction path. One approach to ensuring this is to define the reaction path as the minimum energy path, which can be computed by steepest descent algorithms. (These techniques will be discussed in detail in the subsection entitled "The Reaction Path".) The fact that conventional transition state theory needs the potential energy surface only in small regions around the reactant minimum and saddle point is indeed enticing. We will see that when one adds variational effects, one needs a more extensive region of the potential energy surface that is, nonetheless, still localized in the valley connecting reactants to products. Then, when one adds tunneling, a longer section of the valley is needed, and sometimes the potential for geometries outside the valley, in the so-called tunneling swath, is required. Nevertheless, the method often requires only a manageably small portion of the potential energy surface, and the calculations can be quite efficient.

It is possible to improve the results of Eq. [2] by incorporating a factor γ_C, called the transmission coefficient, that accounts for some of the above approximations. The "exact" classical thermal rate constant will be given as

$$k_C = \gamma_C(T)k_C^{\ddagger}(T) \qquad [6]$$

We can factor the transmission coefficient into two approximately independent parts,

$$\gamma_C(T) = \Gamma_C(T)g(T) \qquad [7]$$

that account, respectively, for corrections to the fundamental assumption being made and to approximation (2) described earlier. When conventional TST is compared with classical trajectory calculations, one is testing the no-recrossing assumption; i.e., we are assessing how far Γ_C is from unity, with TST being an upper bound to the classical rate constant ($\Gamma_C \leq 1$). Both classical trajectory simulations (also called molecular dynamics simulations) and TST invoke the local-equilibrium approximation[12] where the microstates of reactants are in local equilibrium with each other, but it has been shown that for gas-phase bimolecular reactions, the deviation of g from unity is usually very small.[13–18] In the case of gas-phase unimolecular reactions, the reacting molecules need to be activated, and so there is a competition between energy transfer and reaction. At low pressures, the rate constant is pressure dependent ("falloff region") and controlled by the activation and deactivation of the activated species. Only when the pressure is sufficiently high is energy redistribution much faster than the product-forming step such that TST can be applied. In this context, we can consider TST as the high-pressure limit rate constant of a unimolecular rate constant.

The justification of variational transition state theory is rigorous only in a classical mechanical world because, when the local equilibrium assumption is valid, VTST provides an upper bound on the classical mechanical rate constant. One optimizes the definition of the transition state to minimize recrossing, and the calculated rate constant converges to the exact rate constant from above.

The derivation of TST involves calculating the flux, i.e., counting the species that pass through the dividing surface located at the transition state. This only can be stated with certainty in the realm of classical mechanics. In other words, to formulate classical TST requires that, at a given moment, we know exactly the location in coordinate space of our reactive system, which is passing through the dividing surface, and we know the sign of the momentum, which has to be positive, because the molecule is heading toward products. This violates the uncertainty principle. Nevertheless, the classical framework provides a starting point for real systems, which have quantum effects that are incorporated in two ways. First, quantum effects on motion in all degrees of freedom except the reaction coordinate near the dynamical bottleneck are included by replacing classical vibrational partition functions by quantum

mechanical ones. Second, tunneling and nonclassical reflection are included through another temperature-dependent transmission coefficient, κ.

In this review we consider reactions for which auxiliary assumption (1), the Born–Oppenheimer approximation, is met or is assumed to be met. Furthermore, we assume that energy transfer processes are occurring fast enough to replenish the populations of depleted reactant states, so $g \cong 1$ for all gas-phase reactions considered here. Therefore, the true quantum mechanical rate constant is given by

$$k = \gamma(T)k^{\ddagger}(T) = \Gamma(T)\kappa(T)k^{\ddagger}(T) \qquad [8]$$

where κ takes into account nonclassical effects on the reaction coordinate, and $k^{\ddagger}$ is a quantized version of $k_C^{\ddagger}$. Then we have to find a methodology to evaluate $\Gamma(T)$ and $\kappa(T)$, which are discussed in the following sections. In particular, VTST may be considered a way to calculate Γ by finding a better transition state that has less recrossing, and semiclassical tunneling calculations may be used to estimate κ. In practical calculations on real systems, even when we optimize the transition state by VTST, we do not find a transition state that eliminates all recrossing. Thus there is still a non-unit value of $\Gamma(T)$. As we carry out better optimizations of the transition state, the exact Γ should converge to unity. The essence of transition state theory is that one finally approximates Γ as unity for one's final choice of transition state.

Canonical Variational Transition State Theory

Conventional TST provides only an approximation to the "true" rate constants, in part because we are calculating the one-way flux through the dividing surface that is appropriate only for small, classical vibrations around the saddle point.[19] We should be considering the net flux in a way that accounts for global dynamics, quantization of modes transverse to the reaction coordinate, and tunneling. It is important to note that "transverse" modes consist of all modes except the reaction coordinate. The first way in which the calculated rate constants can be improved is to change the location of the dividing surface, which in conventional TST[8] is located at the saddle point. More generally we should also consider other dividing surfaces. The conventional transition state dividing surface is a hyperplane perpendicular to the imaginary-frequency normal mode (the reactive normal mode) of the saddle point; it is the hyperplane with displacement along the reaction normal mode set equal to zero (see Figure 1). Any other dividing surface is by definition a "generalized transition state."[20] We search for generalized transition state dividing surfaces (even if they are not saddle points) that are located where the forward flux is a minimum.[20–27] The practical problem involves locating this particular dividing surface S, which in principle is a function of

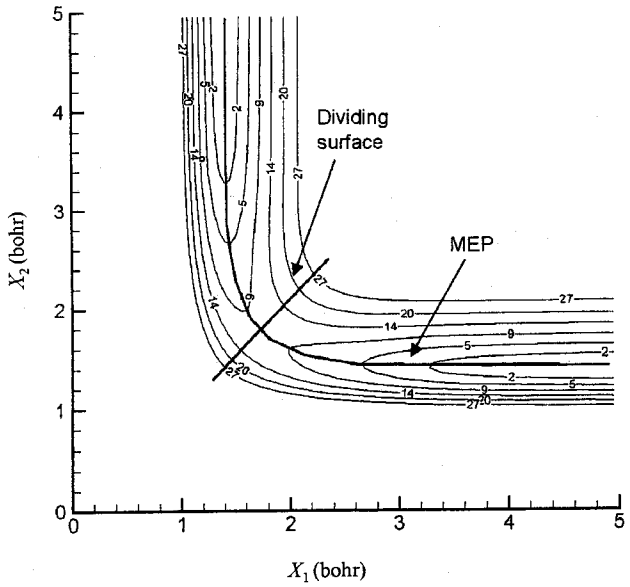

Figure 1 Contour plot of the $H_a + H_b - H_c \rightarrow H_a - H_b + H_c$ collinear reaction showing the dividing surface at the transition state and minimum energy path (MEP). X_1 and X_2 indicate the $H_a \ldots H_b$ and $H_b \ldots H_c$ distances, respectively. The contour labels are in kcal/mol.

all the coordinates $\mathbf{q}$ and momenta $\mathbf{p}$ of the system; that is, $S = S(\mathbf{p},\mathbf{q})$. One way of doing this is to consider the surface as being a function of coordinates only and then simplify further this dependency by considering a few-parameter set of dividing surfaces of restricted shape and orientation (together specified by $\boldsymbol{\Omega}$) at a distance s along a given reaction path (instead of allowing arbitrary definitions) such that $S(\mathbf{p},\mathbf{q})$ is reduced to $S(s,\Omega)$. We can go further and fix the shape of the dividing surface and use the unit vector $\hat{\mathbf{n}}$ perpendicular to the surface, instead of $\boldsymbol{\Omega}$, to define the dividing surface $S(s,\hat{\mathbf{n}})$. These two parameters (one scalar and one vector) are optimized variationally until the forward flux through the dividing surface is minimized.

In POLYRATE, the default for the reaction path is the minimum energy path (MEP) in isoinertial coordinates. The minimum-energy path is the union of the paths of steepest descent on the potential energy surface down from the saddle point toward reactants and products. The path of steepest descent depends on the coordinate system, and when we refer to the MEP, we always mean the one computed by steepest descents in isointertial coordinates. Isoinertial coordinates are rectilinear coordinates in which the kinetic energy consists of diagonal square terms (that is, there are no cross terms between different components of momenta), and every coordinate has the same reduced mass. (Rectilinear coordinates are linear functions of Cartesian coordinates.) Some examples of isoinertial coordinates that one encounters are mass-weighted

Cartesians, mass-weighted Cartesian displacements, mass-scaled Cartesians, and mass-scaled Jacobis. In mass-weighted coordinates,[28] mass is unity and unitless, and the "coordinates" have units of length times square root of mass; in mass-scaled coordinates, the reduced mass for all coordinates is a constant μ (with units of mass), and the coordinates have units of length. We almost always use mass-scaled coordinates; the main exception is in the subsection on curvilinear internal coordinates, where much of the analysis involving internal coordinates is done in terms of unscaled coordinates.

The original choice[27] of dividing surface for polyatomic VTST was a hyperplane in rectilinear coordinates orthogonal to the MEP. With this choice of dividing surface, the direction of the gradient along the MEP coincides with the direction along $\hat{\mathbf{n}}$. Therefore, in this case, the dividing surface depends only on s, and the minimum rate is obtained by variationally optimizing the location of the surface along the MEP. The coordinate perpendicular to the dividing surface is the reaction coordinate, and the assumption that systems do not recross the dividing surface may be satisfied if this coordinate is separable from the other $3N - 1$ degrees of freedom, where N is the number of atoms. The set of coordinates $\{u_1(s), \ldots u_{3N-1}(s), s\}$ or $(\mathbf{u},s)$ are called natural collision coordinates.[29]

It can be shown[30] that all isoinertial coordinates can be obtained from one another by uniform scaling and an orthogonal transformation. Therefore, the MEP is the same in all such coordinate systems. This MEP is sometimes called the intrinsic reaction coordinate or IRC.[31]

It is not necessary to use the MEP as the reaction path; one could alternatively use a path generated by an arbitrarily complicated reaction coordinate,[32] and for reactions in the condensed phase, some workers have allowed a collective bath coordinate[33] to participate in the definition of the reaction path. The transition state dividing surface is defined by the MEP only on the reaction path itself. In the variational reaction path algorithm,[34] the dividing surface is not necessarily perpendicular to the gradient along the MEP. Instead, it is the dividing surface that maximizes the free energy of activation,[20] and so, in this case, we also optimize $\hat{\mathbf{n}}$ (discussed above and in the subsection entitled "The Reaction Path"), which allows us to make a better estimate of the net flux through the dividing surface.

It is possible to write an expression for the rate constant similar to Eq. [2] by using generalized transition state dividing surfaces. We start by describing the formulation of VTST for the original choice of dividing surface—a hyperplane in rectilinear coordinates orthogonal to the MEP—and intersecting it at s. In this case, the generalized transition state rate constant is given by

$$k_C^{GT} = \frac{1}{\beta h} \frac{Q_C^{GT}(T,s)}{\Phi_C^R(T)} \exp[-\beta V_{MEP}(s)] \qquad [9]$$

where by convention $s = 0$ indicates the location of the saddle point and $s < 0$ and $s > 0$ indicate the reactant and product side of the reaction path, respectively, $V_{MEP}(s)$ is the potential evaluated on the MEP at s, and Q_C^{GT} is the classical generalized transition state partition function. The zero of energy for the generalized transition state partition function is taken as the minimum of the local vibrational modes orthogonal to the reaction path at s, which is equal to $V_{MEP}(s)$. The value of the rate constant in Eq. [9], when minimized with respect to s, corresponds to canonical variational transition state theory, also simply called canonical variational theory (CVT)[20,27,30,35,36]

$$k_C^{CVT} = \min_s k_C^{GT}(T,s) = k_C^{GT}\left[T, s_{C,*}^{CVT}(T)\right] \qquad [10]$$

where $s_{C,*}^{CVT}$ indicates the optimum classical position of the dividing surface. (In general, an asterisk subscript on s denotes the value of s at a variational transition state.) The expression for the classical CVT rate constant is then

$$k_C^{CVT} = \frac{1}{\beta h}\frac{Q_C^{GT}\left(\left[T, s_{C,*}^{CVT}(T)\right]\right)}{\Phi_C^R(T)}\exp\left\{-\beta V_{MEP}\left(s_{C,*}(T)\right)\right\} \qquad [11]$$

The CVT rate constant can account for most of the recrossing (depending on the reaction) that takes place at the conventional transition state. It should be noted that to minimize the recrossing does not generally mean to eliminate it, and for a particular reaction, we may find that even the "best" dividing surface obtained by CVT yields a rate constant larger than the exact classical rate constant, although it can be shown that in a classical world, we can always eliminate all recrossing by optimizing the dividing surface in phase space with respect to all coordinates and momenta.[37] On the other hand, assuming local equilibrium of reactant states, the CVT rate constant always improves the result obtained by conventional TST, and therefore, the following inequality holds:

$$k_C^{CVT} \leq k_C^{\ddagger}(T) \qquad [12]$$

Thus, CVT takes into account the effect of the factor $\Gamma_C^{\ddagger}(T)$ on the thermal rate constant, where the superscript ‡ means recrossing of the conventional transition state, and the subscript C reminds us that we are still discussing the classical mechanical rate constant. CVT is considered to be an approximation to the exact classical rate constant

$$k_C \cong k_C^{CVT}(T) = \Gamma_C^{CVT}(T)k_C^{\ddagger}(T) \qquad [13]$$

where

$$\Gamma_C^{CVT} = \frac{k_C^{CVT}(T)}{k_C^{\ddagger}(T)} \qquad [14]$$

Now we consider how to incorporate quantum effects into the thermal rate constant. For the modes perpendicular to the reaction coordinate, this is done in what is often considered to be an ad hoc way by quantizing the partition functions.[8] Actually, this is not totally ad hoc; it was derived, at least to order h^2 in Planck's constant, by Wigner[38] in 1932. Because the reaction coordinate is missing in the transition state partition functions of Eqs. [2] and [9], the rate constant is still not fully quantized at the transition state. At this point, to denote that we have incorporated quantum effects in all degrees of freedom of reactants and all but one degrees of freedom of the transition state by using quantum mechanical partition functions instead of classical mechanical partition functions, we drop the subscript (C) from all remaining expressions. The CVT rate constant is then given by

$$k^{CVT} = \frac{1}{\beta h}\frac{Q^{GT}\left(T, s_*^{CVT}(T)\right)}{\Phi^R(T)} \exp\left\{-\beta V_{MEP}\left(s_*^{CVT}(T)\right)\right\} \qquad [15]$$

where Φ^R is the quantized reactant partition function per unit volume and $Q^{GT}(T,s)$ is the quantized generalized transition state partition function at s. Note that the value s_*^{CVT} that minimizes the quantized generalized transition state rate constant at temperature T is not necessarily equal to the value $s_{C,*}^{CVT}(T)$ that minimizes the classical expression.

Another way to write Eq. [9] is to relate it to the free energy of activation profile $G_T^{GT,o}$ by analogy to Eq. [5]:

$$\begin{aligned} k^{GT} &= \frac{1}{\beta h} K^{\ddagger,o} \exp\left\{-\left[G^{GT,o}(T,s) - G_T^{R,o}\right]\Big/RT\right\} \\ &= \frac{1}{\beta h} K^{\ddagger,o} \exp\left[-\Delta G_T^{GT,o}(T,s)\Big/RT\right] \end{aligned} \qquad [16]$$

where $K^{\ddagger,o}$ is the reciprocal of concentration in the standard state for bimolecular reactions or unity for unimolecular reactions, $G_T^{GT,o}$ is the standard-state free energy of the system at the dividing surface perpendicular to the MEP, and $G_T^{R,o}$ is the classical standard-state free energy of reactants at temperature T. The free energy of activation profile is given as

$$\Delta G^{GT,o} = V_{MEP}(s) - RT \ln\left[\frac{Q^{GT}(T,s)}{K^{\ddagger,o}\Phi^R(T)}\right] \qquad [17]$$

Therefore, the CVT rate constant can be rewritten as

$$k^{\mathrm{CVT}} = \frac{1}{\beta h} K^{\ddagger,o} \exp\left\{-\Delta G_T^{\mathrm{CVT},0}\left(s_*^{\mathrm{CVT}}(T)\right)\Big/RT\right\} \qquad [18]$$

When comparing Eqs. [16] and [18], it can be seen that the minimum value of k^{GT} as a function of s is reached when the free energy of activation is maximum.[20,27,39,40] This can be restated in terms of first and second derivatives; that is,

$$\frac{\partial}{\partial s} k^{\mathrm{GT}}(T,s)\Big|_{s=s_*^{\mathrm{CVT}}(T)} = \frac{\partial}{\partial s} \Delta G_T^{\mathrm{GT},o}(s)\Big|_{s=s_*^{\mathrm{CVT}}(T)} = 0 \qquad [19a]$$

with

$$\frac{\partial^2}{\partial s^2} k^{\mathrm{GT}}(T,s)\Big|_{s=s_*^{\mathrm{CVT}}(T)} > 0 \qquad [19b]$$

and

$$\frac{\partial^2}{\partial s^2} \Delta G_T^{\mathrm{GT}}(s)\Big|_{s=s_*^{\mathrm{CVT}}(T)} < 0 \qquad [19c]$$

Initially we have taken the dividing surface to be perpendicular to the MEP. In the reorientation of the dividing surface (RODS) algorithm, the dividing surface is oriented to yield the most physical free energy of activation, which is the dividing surface that maximizes $\Delta G_T^{\mathrm{GT},o}(S(s_i,\hat{\mathbf{n}}))$ at a given T and s_i. In this case, the dividing surface is defined by the location s_i where it intersects the MEP and a unit vector $\hat{\mathbf{n}}$ that is orthogonal to the dividing surface at the MEP. The value of the free energy with the optimum orientation at point s_i is given by

$$\Delta G_T^{\mathrm{OGT},o} = \max_{\hat{\mathbf{n}}} \Delta G_T^{\mathrm{GT},o}(S(s_i,\hat{\mathbf{n}})) \qquad [20]$$

and the CVT free energy is the maximum of the orientation optimized free energies:

$$\Delta G_T^{\mathrm{CVT},o} = \max_s \Delta G_T^{\mathrm{OGT},o}(s) \qquad [21]$$

The algorithm used to evaluate $\Delta G_T^{\mathrm{OGT},o}$ will be discussed below.

Other Variational Transition State Theories

Canonical variational theory finds the best dividing surface for a canonical ensemble, characterized by temperature T, to minimize the calculated canonical rate constant. Alternative variational transition state theories can also be

defined. This is done for other ensembles by finding the dividing surfaces that minimize the rate constants for those ensembles. For example, a microcanonical ensemble is characterized by a total energy E, and the generalized transition state theory rate constant for this ensemble is proportional to $N_{vr}^{GT}(E,s)$, which is the number of vibrational–rotational states with energy smaller than E at a generalized transition state at s. Microcanonical variational transition state[1] theory (μVT) is obtained by finding the dividing surface that minimizes N_{vr}^{GT}; i.e.,

$$N^{\mu VT} = \min_s N_{vr}^{GT}(E,s) \qquad [22]$$

The location of the dividing surface that minimizes Eq. [22] is defined as $s_*^{\mu VT}$, which specifies the microcanonical variational transition state; thus,

$$\left.\frac{\partial N_{vr}^{GT}(E,s)}{\partial s}\right|_{s=s_*^{\mu VT}(E)} = 0 \qquad [23]$$

Notice that the minimum-number-of-states criterion corresponds correctly to variational transition state theory, whereas an earlier minimum-density-of-states criterion does not.[27] The microcanonical rate constant can be written as

$$k^{\mu VT} = \frac{Q_{el}(T)\int_0^\infty N_{vr}^{\mu VT}(E)\exp(-\beta E)dE}{h\Phi_R(T)} \qquad [24]$$

Where the electronic partition function is defined below. Evaluating the microcanonical number of states can be very time consuming at high energies for big molecules. To avoid this problem, one can instead optimize the generalized transition states up to the microcanonical variational threshold energy and then use canonical theory for higher energy contributions. This approach is called improved canonical variational theory (ICVT).[1,41] ICVT has the same energy threshold as μVT, but its calculation is much less time consuming. A microcanonical criterion is more flexible than is a canonical one, and therefore,

$$k^{\ddagger}(T) \geq k^{CVT}(T) \geq k^{ICVT}(T) \geq k^{\mu VT}(T) \qquad [25]$$

As we go to the right in the above sequence, the methods account more accurately for recrossing effects.

Sometimes it is found that even the best dividing surface gives too high rate constants because another reaction bottleneck exists. Those cases can be handled, at least approximately, by the unified statistical (US) model.[42,43] In this method, the thermal rate constant can be written as

$$k^{US} = \frac{Q_{el}(T)\int_0^\infty N_{vr}^{US}(E)\exp(-\beta E)dE}{h\Phi_R(T)} \qquad [26]$$

where

$$N_{vr}^{US} = N_{vr}^{\mu VT}(E)\Gamma^{US}(E) \quad [27]$$

The Γ^{US} recrossing factor due to the second bottleneck is defined as

$$\Gamma^{US} = \left\{1 + \frac{N_{vr}^{\mu VT}(E)}{N_{vr}^{min}(E)} - \frac{N_{vr}^{\mu VT}(E)}{N_{vr}^{max}(E)}\right\}^{-1} \quad [28]$$

where $N_{vr}^{min}(E)$ is the second lowest minimum of the accessible number $N_{vr}^{GT}(E,s)$ of vibrational–rotational states, and $N_{vr}^{max}(E)$ is the maximum of $N_{vr}^{GT}(E,s)$ located between the two minima in the number of vibrational–rotational states. This approach is nonvariational but always satisfies the relation

$$k^{\mu VT} \geq k^{US} \quad [29]$$

In the case that the same physical approximations are applied to fluxes in a canonical ensemble, we call this canonical unified statistical theory (CUS)[44] and the recrossing factor Γ^{CUS} is given by

$$\Gamma^{CUS} = \left\{1 + \frac{q_{vr}^{CVT}(T)}{q_{vr}^{max}(T)} - \frac{q_{vr}^{CVT}(T)}{q_{vr}^{min}(T)}\right\}^{-1} \quad [30]$$

where

$$q_{vr}^{CVT} = Q_{vr}^{GT}(T, s_*^{CVT}) \exp[-\beta V_{MEP}(s)] \quad [31]$$

is the partition function evaluated at the maximum of the free energy of activation profile, q_{vr}^{max} is evaluated at the second highest maximum, and $q_{vr}^{min}(T)$ is evaluated at the lowest minimum between the two maxima. The CUS rate constant is given by

$$k^{CUS} = \Gamma^{CUS}(T)k^{CVT}(T) \quad [32]$$

In the limit that there are two equivalent maxima in the free energy of activation profile with a deep minimum between them, the statistical result is obtained; i.e., $\Gamma^{CUS} = 0.5$. Note that signs appear different in Eqs. [28] and [30] because in the former, "max" and "min" are associated with local maxima and minima, respectively, of the flux, whereas in the latter, they are associated with maxima and minima, respectively, of the free energy of activation profile—not of the flux.

Quantum Effects on the Reaction Coordinate

Up to this point we have incorporated quantum mechanics in the $F-1$ bound degrees of freedom (where F is the total number of bound and unbound

vibrations and equals $3N - 6$, where N is the number of atoms except that it is $3N - 5$ for linear species) through the partition functions, and therefore, both the TST and the CVT rate constants are quantized. The difference between both theories is still given by the factor

$$\Gamma^{\mathrm{CVT}}(T) = k^{\mathrm{CVT}}(T)/k^{\ddagger}(T) \qquad [33]$$

which takes into account the recrossing. To quantize all degrees of freedom requires incorporation of quantum effects into the reaction coordinate, through a multiplicative transmission coefficient $\kappa(T)$. For example, for CVT, we write

$$k^{\mathrm{CVT/Y}}(T) = \kappa^{\mathrm{CVT/Y}}(T)k^{\mathrm{CVT}}(T) \qquad [34]$$

where Y indicates the method to evaluate the quantum effects. The main quantum effect to account for is tunneling through the reaction barrier. We can classify tunneling calculations into three levels depending on level of approximation:[45]

(1) one-dimensional approximations,
(2) multidimensional zero-curvature approximations, and
(3) multidimensional corner-cutting approximations.

Early models that were developed correspond to the first level of approximation and are based on the probability of penetration of a mass point through a one-dimensional barrier,[46,47] whose shape was usually given by an analytical function, for example, a parabola[48–50] or an Eckart barrier,[51] that is fitted to the shape of the potential along the reaction path. The method of Wigner[38] actually corresponds to the leading term in an expansion in $\hbar$; as it depends only on the quadratic force constant along the reaction path at the saddle point, it may be considered an approximation to the one-dimensional parabolic result. These one-dimensional models, although historically important, are not very accurate because they do not take into account the full dimensionality of the system under study. Detailed discussion of multidimensional tunneling methods is provided below.

PRACTICAL METHODS FOR QUANTIZED VTST CALCULATIONS

In this section, we provide details of methods used in computations of quantities needed in quantized VTST rate constant calculations. We start by discussing methods used to define dividing surfaces. As the reaction path plays an important role in parameterizing dividing surfaces, we first describe methods for its evaluation. We then discuss calculations of partition functions and numbers of states needed in the rate constant calculations.

The Reaction Path

This section describes some algorithms used to calculate the reaction path efficiently. The evaluation of the CVT rate constants requires the knowledge of at least part of a reaction path, which can be calculated by some of the steepest-descent methods briefly described in the first Subsection. The second Subsection explains a reaction-path algorithm that, at a given value of the reaction coordinate, finds the orientation of the hyperplanar dividing surface that maximizes the free energy. Later on, more general shapes for the dividing surface are discussed.

The Minimum Energy Path

The minimum energy path is the path of steepest descents in isoinertial coordinates from the saddle point into the reactant and product regions. For the general reaction of Eq. [1] in which the reactive system is composed of N atoms ($N = N_A + N_B$) and $i = 1, 2, \ldots, N$ labels the atoms, we define the $3N$ Cartesian coordinates as $\mathbf{R}$. The origin of the coordinate system is arbitrary, although it is often convenient to define it as the center of the mass of the system. The saddle point geometry in Cartesian coordinates, denoted $\mathbf{R}^{\ddagger}$, is a stationary point and first derivatives of the potential energy, V, with respect to the coordinates at $\mathbf{R}^{\ddagger}$, is zero:

$$\nabla V = \frac{\partial V}{\partial \mathbf{R}}\bigg|_{\mathbf{R}=\mathbf{R}^{\ddagger}} = 0 \qquad [35]$$

It is useful to change from Cartesian coordinates to a mass-scaled coordinate system defined by

$$x_{i\alpha} = \left(\frac{m_i}{\mu}\right)^{1/2} R_{i\alpha} \qquad [36]$$

where m_i is the mass of nucleus i, μ is an arbitrary mass, and α denotes the Cartesian component (x, y, or z). For bimolecular reactions like Eq. [1], it is common either to use the reduced mass of reactants

$$\mu_{\text{rel}} = \frac{m_A m_B}{m_A + m_B} \qquad [37]$$

or to use a value of 1 amu for μ. For these isoinertial coordinates, the kinetic energy of the nuclear motion simplifies from

$$T = \frac{1}{2}\sum_{i=1}^{N} m_i \sum_{\alpha=x,y,z} \dot{R}_{i\alpha}^2 \qquad [38]$$

to a diagonal form

$$T = \frac{1}{2}\mu \sum_{i=1}^{N} \sum_{\alpha=x,y,z} \dot{x}_{i\alpha}^2 \qquad [39]$$

where $\dot{x}_{i\alpha}$ represents the derivative of $x_{i\alpha}$ with respect to time. With the latter choice, the numerical value of coordinates expressed in Å is identical to the numerical value of a mass-weighted[28] Cartesian coordinate in amu$^{1/2}$ Å. The motion of the polyatomic system is reduced to the motion of a point mass μ on a potential surface V with the classical equations of motion given by

$$\mu \frac{d}{dt}\dot{x}_{i\alpha} = -\frac{\partial V}{\partial x_{i\alpha}} \qquad [40]$$

A generalized transition state is a tentative dynamical bottleneck, and a tentative reaction coordinate is a nearly separable coordinate in a direction from reactants to products. Thermal rate constants are dominated by near-threshold events, and near the reaction threshold, a nearly separable coordinate in a direction from reactants to products is given by following the equations of motion but damping out the velocity along the trajectory. With this damping, the equations of motion can be rewritten for an infinitesimal time interval t as

$$\mu \dot{x}_{i\alpha} = -\frac{\partial V}{\partial x_{i\alpha}} t \qquad [41]$$

The integration constant is zero because of the assumption of infinitesimal velocity ($\dot{\mathbf{x}} = 0$ at $t = 0$). We can rewrite Eq. [41] in vector form as

$$\mu d\mathbf{x} = -\nabla V(\mathbf{x}) d\tau = -\mathbf{G}(\mathbf{x}) d\tau \qquad [42]$$

where $d\tau = t\, dt$. If we define a infinitesimal mass-scaled distance along the path as ds, then

$$ds = \left[\sum_{i=1}^{N} \sum_{\alpha=x,y,z} dx_{i\alpha}^2\right]^{1/2} = \frac{|G(x)|}{\mu} d\tau \qquad [43]$$

with $|\mathbf{G}|$ being the modulus of the gradient. Substituting Eq. [43] in Eq. [42], we obtain

$$\frac{d\mathbf{x}}{ds} = -\hat{\mathbf{G}}(\mathbf{x}) = \mathbf{v}(\mathbf{x}) \qquad [44]$$

where $\hat{\mathbf{G}} = \mathbf{G}/|\mathbf{G}|$ is the normalized gradient, and $\mathbf{v}$ is a vector with opposite direction to the gradient. The MEP can be followed by solving the above differential equation. The displacement on the MEP is given by the steepest descent direction along $\mathbf{v}$, where s indicates the progression along the path[52–55] and $\mathbf{x}(s)$ the geometry.

For a practical evaluation of the MEP, the first stage involves the knowledge of the transition state (or first-order saddle point) geometry. By convention we locate the transition state at $s = 0$, and we denote its scaled-mass Cartesian-coordinates geometry by $\mathbf{x}^{\ddagger}$. Reactants and products sides are given by values of $s < 0$ and $s > 0$, respectively. There are very efficient algorithms to evaluate transition state geometries,[56–58] which are available in many popular electronic structure packages. We cannot use Eq. [44] to take a step from the saddle point along the reaction path because the gradient is zero. At the saddle point, the direction of the MEP is given by the unbound vibrational mode, which requires evaluation of the normal mode frequencies and eigenvectors at the saddle point. At stationary points, the vibrational frequencies are calculated by diagonalization of the $3N \times 3N$ matrix of force constants F, which are the second derivatives of the potential with respect to isoinertial Cartesian coordinates scaled to a mass μ. F is also called the Hessian. For instance, for the conventional transition state geometry $\mathbf{x}^{\ddagger}$, this matrix can be diagonalized by performing the unitary transformation:

$$\mathbf{L}(\mathbf{x}^{\ddagger})^{\dagger}\mathbf{F}(\mathbf{x}^{\ddagger})\mathbf{L}(x^{\ddagger}) = \Lambda(\mathbf{x}^{\ddagger}) \qquad [45]$$

where $\dagger$ denotes transpose, Λ is the $3N \times 3N$ diagonal matrix with eigenvalues λ_m on the diagonals (with $m = 1, 2, \ldots, 3N$) and with eigenvectors arranged as a matrix L whose columns $\mathbf{L}_m$ correspond to the $3N$ normal-mode directions. The normal-mode frequencies at the saddle point can be obtained from the eigenvalues by the relation:

$$\omega_m(s = 0) = \left[\lambda_m(\mathbf{x}^{\ddagger})/\mu\right]^{1/2} \qquad [46]$$

The saddle point has 6 zero eigenvalues (5 if it is linear), which correspond to the overall rotation and translation of the molecule. We define F as the number of vibrational modes ($F = 3N - 6$ for a nonlinear molecule or $3N - 5$ for a linear molecule), where for a saddle point, the first $F - 1$ modes are bound with positive eigenvalues and real frequencies. Mode F is unbound with an imaginary frequency ($\omega^{\ddagger}$) corresponding to motion parallel to the MEP at the saddle point. The eigenvector associated with this frequency is denoted by $\mathbf{L}_F(\mathbf{x}^{\ddagger})$. The first geometry along the MEP toward reactants (− sign) and toward products (+ sign) is given by

$$\mathbf{x}(s_1 = \pm\delta s) = \mathbf{x}^{\ddagger} \pm \delta s \mathbf{L}_F(\mathbf{x}^{\ddagger}) \qquad [47]$$

where δs is the step length. The sign of $\mathbf{L}_F(\mathbf{x}^{\ddagger})$ is chosen so that the vector points from reactants towards products.

For the geometry $\mathbf{x}(s)$ ($\mathbf{x}$ hereafter), the gradient is different than zero, and so for the next $\mathbf{x}_2$ geometry, or in general for a geometry $\mathbf{x}_n$, with $n > 1$, we can apply Eq. [44] and follow the opposite direction of the normalized gradient:

$$\mathbf{x}_n = \mathbf{x}_{n-1} - \delta s \hat{\mathbf{G}}_{n-1} = \mathbf{x}_{n-1} + \delta s \mathbf{v}_{n-1} \qquad [48]$$

where we use the shorthand notation $\hat{\mathbf{G}}_n = \hat{\mathbf{G}}(\mathbf{x}_n)$ and $\mathbf{v}_n = \mathbf{v}(\mathbf{x}_n)$. The above first-order equation gives the MEP geometries by the so-called Euler steepest-descent (ESD) method.[59] For an accurate evaluation of the MEP, the step size has to be small because the error is proportional to $(\delta s)^2$. Some other Euler-type methods try to minimize the error, like the predictor-corrector algorithm,[60,61] the optimized Euler stabilization method,[59] and the backward Euler method.[62] Of all of the Euler-based steepest descent methods, the optimized Euler stabilization method, version 1 (ES1*), is the one that produces the best-converged paths.[59] The ESD method provides an initial geometry

$$\mathbf{x}_n^{(0)} = \mathbf{x}_{n-1} + \delta s \mathbf{v}_{n-1} \qquad [49]$$

Then a corrector step is specified as a point at a minimum of a parabolic fit along a line that goes through $\mathbf{x}_n^{(0)}$ and parallel to a "bisector" vector $\mathbf{d}_n$, which is given by[60]

$$\mathbf{d}_n = \frac{\mathbf{v}(x_{n-1}) - \mathbf{v}(x_n^{(0)})}{\left|\mathbf{v}(x_{n-1}) - \mathbf{v}(x_n^{(0)})\right|} \qquad [50]$$

The new geometry is given by

$$\mathbf{x}_n = \mathbf{x}_n^{(0)} + \zeta \mathbf{d}_n \qquad [51]$$

where ζ is a step along $\mathbf{d}_n$, with a step size proportional to a user provided parameter δ_2. The correction is not carried out if $|\mathbf{v}(\mathbf{x}_{n-1}) - \mathbf{v}(\mathbf{x}_n^{(0)})| < \omega$, with ω being a small value characteristic of some small angle between gradients. The algorithm is sensitive to the values of δ_2 and ω, and in the ES1* method, it is recommended that both values are set according to recommendations[59] that were based on systematic studies of convergence, those values being $\delta_2 = \delta s$ and $\omega = 0.01$.

The above methods are based on a local linear approximation to the energy, with quadratic information being used only at the saddle point. Another possibility is to use algorithms, which in general are more accurate, that exploit higher order information about the potential energy. Page and McIver[63] have presented a successful method that does this. First, a cubic expansion of the potential energy surface around the saddle point was proposed to take the initial step along the MEP. In this case, the first point along the reaction path is given by

$$\mathbf{x}(s_1 = \pm\delta s) = \mathbf{x}^{\ddagger} \pm \delta s \mathbf{L}_F(\mathbf{x}^{\ddagger}) \pm \frac{1}{2}(\delta s)^2 \mathbf{c}(\mathbf{x}^{\ddagger}) \qquad [52]$$

where the vector $\mathbf{c}(\mathbf{x}^\ddagger)$ is defined by

$$\mathbf{A}\mathbf{c}(\mathbf{x}^\ddagger) = \mathbf{C}(\mathbf{x}^\ddagger)\mathbf{L}_F(\mathbf{x}^\ddagger) - \mathbf{L}_F^\dagger(\mathbf{x}^\ddagger)\mathbf{C}(\mathbf{x}^\ddagger)\mathbf{L}_F(\mathbf{x}^\ddagger)\mathbf{L}_F(\mathbf{x}^\ddagger) \quad [53a]$$

where

$$\mathbf{A} = 2\mathbf{L}_F^\dagger(\mathbf{x}^\ddagger)\mathbf{F}(\mathbf{x}^\ddagger)\mathbf{L}_F(\mathbf{x}^\ddagger)\mathbf{I} + \left[2\mathbf{L}_F(\mathbf{x}^\ddagger)\mathbf{L}_F^\dagger(\mathbf{x}^\ddagger) - \mathbf{I}\right]\mathbf{F}(\mathbf{x}^\ddagger) \quad [53b]$$

with $\mathbf{I}$ being the identity matrix, and $\mathbf{C}(\mathbf{x}^\ddagger)$ is given by a finite difference expansion of the force constants matrix around the saddle point with a preselected step δ_3:

$$\mathbf{C}(\mathbf{x}^\ddagger) = \frac{\mathbf{F}(\mathbf{x}^\ddagger + \delta_3\mathbf{L}_F(\mathbf{x}^\ddagger)) - \mathbf{F}(\mathbf{x}^\ddagger - \delta_3\mathbf{L}_F(\mathbf{x}^\ddagger))}{2\delta_3} \quad [54]$$

Although the algorithm is cubic, it requires calculations of Hessian matrices only near the saddle point.

One of the most popular second-order methods for following the steepest descent path is the local quadratic approximation of Page and McIver,[63] which we call the Page–McIver (PM) algorithm and we describe next. At a given geometry $\mathbf{x}_n$ along the path, we evaluate the Hessian matrix $\mathbf{F}_n$ and diagonalize it using

$$\boldsymbol{\alpha}_n = \mathbf{U}_n^\dagger\mathbf{F}_n\mathbf{U}_n \quad [55]$$

where $\mathbf{U}_n$ is an orthogonal matrix of column eigenvectors and $\boldsymbol{\alpha}_n$ is a diagonal matrix of eigenvalues. The geometry at the next step along the MEP is given by

$$\mathbf{x}_{n+1} = \mathbf{x}_n + \mathbf{D}_n(\zeta)\mathbf{v}_n \quad [56]$$

where

$$\mathbf{D}_n(\zeta) = \mathbf{U}_n\mathbf{M}_n(\zeta)\mathbf{U}_n^\dagger \quad [57]$$

and $\mathbf{M}_n$ is a diagonal matrix with diagonal elements given by

$$M_{ii}(\zeta) = [\exp(-\alpha_{n,ii}\zeta) - 1)]/\alpha_{n,ii} \quad [58]$$

The variable ζ is a progress variable that is zero at $\mathbf{x}_n$ and is related to the reaction coordinate s by

$$\frac{ds}{d\zeta} = \left[\frac{d\mathbf{x}^\dagger}{d\zeta}\frac{d\mathbf{x}}{d\zeta}\right]^{1/2} \quad [59]$$

which can be rewritten

$$\frac{d\zeta}{ds} = \sum_{i=1}^{3N} h_i^2 \exp(-2\alpha_{n,ii}\zeta) \qquad [60]$$

where

$$\mathbf{h}_n = \mathbf{U}_n^{\dagger}\mathbf{G}_n \qquad [61]$$

The next value of the reaction path coordinate $s_{n+1} = s_n + \delta s$ is given by choosing the value of ζ to satisfy the following integral equation:

$$\delta s = \int_0^{\zeta} d\zeta' \left(\sum_{i=1}^{3N} h_i^2 \exp(-2\alpha_{n,ii}\zeta') \right)^{-1} \qquad [62]$$

which is numerically integrated by the trapezoidal rule. An option is to evaluate a new Hessian after a given number of steps along the reaction path rather than after each step; in which case, we call it the modified Page–McIver algorithm.[59]

Variational Reaction Path Algorithm

The original approach for defining variational dividing surfaces, once the MEP is determined, is to choose them to be hyperplanes in rectilinear coordinates, which are constrained to be orthogonal to the MEP. In this case the dividing surfaces are characterized by a single parameter, the location s along the MEP. In the reorientation of the dividing surface (RODS) method, the dividing surface is not constrained to be orthogonal to the MEP and its orientation is optimized to maximize the free energy for points along the MEP. The previously described algorithms allow calculation of a well-converged MEP by the steepest-descent path from the saddle point to reactants or to products. However, to obtain a well-converged path may be computationally very demanding and so some alternative strategies have been suggested[34,64] for defining optimum dividing surfaces even if the MEP is not well converged. One such approach is the variational reaction path algorithm (VRP) that is a combination of the ESD and RODS algorithms. The first geometry along the path can be obtained from Eq. [47] or Eq. [52] as discussed above. The geometries along the path, for instance, a given geometry $\mathbf{x}_n$, are obtained by applying first the ESD method to obtain a zero-order approximation to the geometry on the MEP

$$\mathbf{x}_n^{(0)} = \mathbf{x}_{n-1} - \delta s\, \hat{\mathbf{G}}_{n-1} \qquad [63]$$

We define the dividing surface as a hyperplane in rectilinear coordinates, which is orthogonal to the unit vector $\hat{\mathbf{n}}$ and passes through the geometry

$x_n^{(0)}$. The potential in the hyperplane is approximated through quadratic terms and is most easily expressed in terms of the generalized normal modes for motion in the $(F-1)$-dimensional space of the hyperplane (note that conventional normal modes are defined only at stationary points, so this concept must be generalized to use it at geometries where the gradient of the potential does not vanish):

$$V(\mathbf{x}) = V(\mathbf{x}_n^{(0)}) + \sum_{m=1}^{F-1} \left[G_{n,m}^{\mathrm{E}}(\hat{\mathbf{n}}) Q_m + \frac{1}{2} \lambda_{n,m}^{\mathrm{E}}(\hat{\mathbf{n}}) Q_m^2 \right] \qquad [64]$$

where Q_m is the displacement from $x_n^{(0)}$ in generalized normal mode m and the gradient and force along mode m are defined as follows. The gradient vector and Hessian matrix evaluated at $\mathbf{x}_n^{(0)}$ are denoted $\mathbf{G}_n^{(0)}$ and $\mathbf{F}_n^{(0)}$, respectively. Motion along the vector $\hat{\mathbf{n}}$, as well as rotations and translations, are projected out to give

$$\mathbf{G}_n^{\mathrm{P},(0)}(\hat{\mathbf{n}}) = \left(\mathbf{I} - \hat{\mathbf{n}}\hat{\mathbf{n}}\right)\left(\mathbf{I} - \mathbf{P}^{\mathrm{RT}}\right)\mathbf{G}_n^{(0)} \qquad [65]$$

and a projected Hessian matrix

$$\mathbf{F}_n^{\mathrm{P},(0)}(\hat{\mathbf{n}}) = \left(\mathbf{I} - \hat{\mathbf{n}}\hat{\mathbf{n}}^{\dagger}\right)\left(\mathbf{I} - \mathbf{P}^{\mathrm{RT}}\right)\mathbf{F}_n^{(0)}\left(\mathbf{I} - \mathrm{P}^{\mathrm{RT}}\right)\left(\mathbf{I} - \hat{\mathbf{n}}\hat{\mathbf{n}}^{\dagger}\right) \qquad [66]$$

where $\mathbf{P}^{\mathrm{RT}}$ is the matrix that projects onto the translations and rotations.[65] The gradient vector and force constant matrix in the eigenvalue representation are then given by

$$\mathbf{G}_n^{\mathrm{E}}(\hat{\mathbf{n}}) = \left[\mathbf{L}_n^{\mathrm{P}}(\hat{\mathbf{n}})\right]^{\dagger} \mathbf{G}_n^{\mathrm{P},(0)}(\hat{\mathbf{n}}) \qquad [67]$$

and

$$\mathbf{\Lambda}_n^{\mathrm{E}}(\hat{\mathbf{n}}) = \left[\mathbf{L}_n^{\mathrm{P}}(\hat{\mathbf{n}})\right]^{\dagger} \mathbf{F}_n^{\mathrm{P},(0)}(\hat{\mathbf{n}}) \mathbf{L}_n^{\mathrm{P}}(\hat{\mathbf{n}}) \qquad [68]$$

where $\mathbf{\Lambda}_n^{\mathrm{E}}$ is a diagonal matrix with elements $\lambda_{n,m}^{\mathrm{E}}$ along the diagonal and $\mathbf{L}_n^{\mathrm{P}}$ is the matrix of eigenvectors that diagonalizes the projected Hessian matrix. The eigenvalues and eigenvectors are ordered so that the first $F-1$ correspond to the modes in the hyperplane and modes $F, F+1, \ldots, 3N$ correspond to the modes along $\hat{\mathbf{n}}$ and translations and rotations, which have zero eigenvalues. The normal mode coordinates are defined by

$$\mathbf{Q} = \left[\mathbf{L}_n^{\mathrm{P}}(\hat{\mathbf{n}})\right]^{\dagger} \left(\mathbf{x} - \mathbf{x}_n^{(0)}\right) \qquad [69]$$

and the elements $F, F+1, \ldots, 3N$ will be zero for motion constrained to the hyperplane.

The coordinate along the variational reaction path is then defined as the location of the minimum of the local quadratic potential in the hyperplane as given by Eq. [63], which is given by

$$\mathbf{x}_n = \mathbf{x}_n^{(0)} + \mathbf{L}_n^{\mathrm{P}}(\hat{\mathbf{n}})\mathbf{Q}^{\mathrm{M}}(\hat{\mathbf{n}}) \qquad [70]$$

where the minimum in the normal mode coordinates is given by

$$Q_m^{\mathrm{M}}(\hat{\mathbf{n}}) = \begin{cases} -G_{n,m}^{\mathrm{E}}(\hat{\mathbf{n}})/\lambda_{n,m}^{\mathrm{E}}(\hat{\mathbf{n}}), & m = 1, \ldots, F-1 \\ 0, & m = F, \ldots, 3N \end{cases} \qquad [71]$$

In the ESD algorithm, for which $\mathbf{x}_n = \mathbf{x}_n^{(0)}$, the value of s along the path is simply given by the arc length between adjacent points on the MEP

$$s_n = s_{n-1} \pm \delta s \qquad [72]$$

where the sign is negative on the reactant side and positive on the product side of the saddle point. Although $\mathbf{x}_n$ is not necessarily equal to $\mathbf{x}_n^{(0)}$ for the variational reaction path, it has been found that use of Eq. [72] provides a better estimate of computed rate constants than a method that uses the difference between $\mathbf{x}_n$ and $\mathbf{x}_{n-1}$ in evaluating s.

A complete description of the variational reaction path approach still requires definition of the vector $\hat{\mathbf{n}}$. If $\hat{\mathbf{n}}$ is chosen to be along the gradient vector $\hat{\mathbf{G}}_n^{(0)}$, then $\mathbf{G}_n^{\mathrm{P},(0)}(\hat{\mathbf{n}})$ and $\mathbf{G}_n^{\mathrm{E}}(\hat{\mathbf{n}})$ are zero [i.e., $(1 - \hat{\mathbf{n}}\hat{\mathbf{n}}^{\dagger})\hat{\mathbf{n}} = 0$, $\mathbf{Q}^{\mathrm{M}}(\hat{\mathbf{n}}) = 0$, and $\mathbf{x} = \mathbf{x}_n^{(0)}$]. In the variational reaction path approach, the RODS algorithm is used to determine the direction of $\hat{\mathbf{n}}$. The free energy of activation of Eq. [17] is generalized to

$$\Delta G^{\mathrm{GT,o}}(T, x_n^{(0)}, \hat{\mathbf{n}}) = V_n^{\mathrm{M}}(\hat{\mathbf{n}}) - RT \ln\left[\frac{Q_{\mathrm{C}}^{\mathrm{GT}}(T, x_n^{(0)}, \hat{\mathbf{n}})}{K^{\ddagger,\mathrm{o}}\Phi_{\mathrm{C}}^{\mathrm{R}}(T)}\right] \qquad [73]$$

where $V_n^{\mathrm{M}}(\hat{\mathbf{n}})$ is the minimum value of the local quadratic potential in Eq. [64], which can be expressed

$$V_n^{\mathrm{M}}(\hat{\mathbf{n}}) = V\left(\mathbf{x}_n^{(0)}\right) - \sum_{m=1}^{F-1}\left[G_{n,m}^{\mathrm{E}}(\hat{\mathbf{n}})\right]^2 \Big/ 2\lambda_{n,m}^{\mathrm{E}}(\hat{\mathbf{n}}) \qquad [74]$$

Calculation of the partition function needed in the evaluation of the free energy of activation is described in the next section. Once the partition function is evaluated, the optimum value of $\Delta G^{\mathrm{GT,o}}\left(T, \mathbf{x}_n^{(0)}, \hat{\mathbf{n}}\right)$ with respect to $\hat{\mathbf{n}}$ is obtained by applying the conjugate gradient algorithm for which the vector of derivatives $\partial \Delta G^{\mathrm{GT,o}}(T, \mathbf{x}_n^{(0)}, \hat{\mathbf{n}})/\partial \hat{\mathbf{n}}$ is needed. These derivatives are obtained by finite differences. We denote the optimum value of the unit vector for a point s

along the variational reaction path as $\hat{\mathbf{n}}(s)$. This algorithm eliminates some instabilities of the calculated reaction path and of the generalized normal mode frequencies. At the same time, it allows a larger step size than the normal steepest-descent algorithms.[34,64]

Evaluation of Partition Functions

Calculation of the rate constant involves the ratio of partition functions for the generalized transition state and for reactants. The three degrees of freedom corresponding to translation of the center of mass of the system are the same in the reactants and transition state, and they are therefore removed in both the numerator and the denominator of Eq. [15]. The reactant partition function per unit volume for bimolecular reactions is expressed as the product of partition functions for the two reactant species and their relative translational motion

$$\Phi^{R}(T) = \Phi_{rel}^{A,B}(T)Q^{A}(T)Q^{B}(T) \qquad [75]$$

where

$$\Phi_{rel}^{A,B}(T) = \left(\frac{2\pi\mu_{rel}}{\beta h^2}\right)^{3/2} \qquad [76]$$

and Q^A and Q^B include contributions from internal degrees of freedom (vibrational, rotational, and electronic) for each species. For unimolecular reactions, the reactant partition function involves contributions from just one reactant species. For an atomic reactant, $Q^A(T)$ and $Q^B(T)$ have contributions only from the electronic degrees of freedom, whereas for polyatomic species, they are approximated as shown for reactant A:

$$Q^{A} = Q_{el}^{A}(T)Q_{vib}^{A}(T)Q_{rot}^{A}(T) \qquad [77]$$

In this expression, couplings among the electronic, vibrational, and rotational degrees of freedom are neglected. The calculation of partition functions for bound species is standard in many textbooks and is repeated here for completeness. The electronic partition function is given by

$$Q_{el}^{A} = \sum_{\alpha=1} d_{\alpha}^{A} \exp\left[-\beta E_{el}^{A}(\alpha)\right] \qquad [78]$$

where α is the index over electronic states and d_α^A and $E_{el}^A(\alpha)$ are the degeneracy and energy of electronic state α, respectively. Note that the energy of the ground state (i.e., $\alpha = 1$) is zero. Rotational partition functions approximated

for the rotational motion of a rigid molecule have shown that there is little loss of accuracy (not more than about 1%) if the quantum partition function is replaced by the classical one. For a linear reactant, the classical rigid-rotor partition function is given by

$$Q^{A}_{rot} = \frac{2I^{A}}{\hbar^2 \beta \sigma^{A}_{rot}} \qquad [79]$$

where I^A is the moment of inertia, σ^A_{rot} is the rotational symmetry number, and $\hbar = h/2\pi$. If the reactant is nonlinear, the rotational partition function is approximated by

$$Q^{A}_{rot} = \frac{1}{\sigma^{A}_{rot}} \left[\left(\frac{2}{\hbar^2 \beta} \right)^3 \pi I^{A}_1 I^{A}_2 I^{A}_3 \right]^{1/2} \qquad [80]$$

where I^A_1, I^A_2, and I^A_3 are the principal moments of inertia of reactant A.

The vibrational partition function is treated quantum mechanically, and as a first approximation, it is evaluated within the harmonic approximation as

$$Q^{A}_{vib}(T) = \prod_{m=1}^{F_A} \sum_{n_m} \exp\left[-\beta E^{A}_{vib,m}(n_m) \right] \qquad [81]$$

where $F_A = 3N_A - 5$ (linear) or $F_A = 3N_A - 6$ (nonlinear), N_A is the number of atoms in reactant A, and $E^A_{vib,m}(n_m)$ is the energy of the harmonic vibrational level n in mode m and is given by

$$E^{A}_{vib,m}(n_m) = \left(n_m + \frac{1}{2} \right) \hbar \omega^{A}_m \qquad [82]$$

where ω^A_m is the frequency of normal mode m in reactant A. Anharmonic corrections to the vibrational partition functions are discussed below.

Generalized Transition State Partition Functions in Rectilinear Coordinates

Evaluation of the generalized transition state partition function Q^{GT} involves contributions from the $3N - 4$ internal degrees of freedom in the dividing surface. The three degrees of freedom for overall center-of-mass translation and motion out of the dividing surface are removed. Calculations of generalized transition state partition functions require definition of the dividing surface, which in the most general case described above is specified by a location $\mathbf{x}(s)$ along the reaction coordinate and the orientation of the planar dividing surface given by the unit normal vector $\hat{\mathbf{n}}(s)$. In this section, we describe

calculations for dividing surfaces that are hyperplanes in rectilinear coordinates. Calculations for curvilinear coordinates are described in the next section.

As for reactant partition functions, we assume that the coupling among rotation, vibration, and electronic motion may be neglected, so that the generalized partition function can be written as the product of three partition functions:

$$Q^{GT}(T,s) = Q^{GT}_{rot}(T,s)Q^{GT}_{vib}(T,s)Q^{GT}_{el}(T,s) \qquad [83]$$

The electronic partition function is given by

$$Q^{GT}_{el} = \sum_{\alpha=1} d^{GT}_{\alpha}(s) \exp\left[-\beta E^{GT}_{el}(\alpha,s)\right] \qquad [84]$$

where $\alpha = 1,\ldots$ indicates the electronic state, $\alpha = 1$ denotes the ground electronic state, and $d^{GT}_{\alpha}(s)$ and $E^{GT}_{el}(\alpha,s)$ are the degeneracy and energy of electronic state α. The electronic energies are measured relative to the energy at the local minimum in the dividing surface with the ground state energy $E^{GT}_{el}(\alpha = 1,s) = 0$. For many molecules, it is sufficient to consider only the electronic ground state, because it is the only one that contributes significantly to the sum. Furthermore, it is usually a very good approximation to make the electronic partition function independent of s in the interaction region.

Rotational partition functions are calculated for rigid rotations of the transition state complex and only require knowledge of the geometry $\mathbf{x}(s)$. As noted, classical rotational partition functions accurately approximate the quantum mechanical ones. For a linear transition state complex, the classical rotational partition function is given by

$$Q^{GT}_{rot} = \frac{2I(s)}{\hbar^2 \beta \sigma_{rot}} \qquad [85]$$

where $I(s)$ is the moment of inertia and σ_{rot} is the rotational symmetry number. The rotational partition function for a nonlinear transition state complex is

$$Q^{GT}_{rot}(T,s) = \frac{1}{\sigma_{rot}}\left[\left(\frac{2}{\hbar^2\beta}\right)^3 \pi I_1(s)I_2(s)I_3(s)\right]^{1/2} \qquad [86]$$

where $I_1(s)$, $I_2(s)$, and $I_3(s)$ are the principal moments of inertia.

Vibrational partition functions are evaluated within the harmonic approximation

$$Q^{GT}_{vib} = \prod_{m=1}^{F-1} Q^{GT}_{vib,m}(T,s) \qquad [87]$$

Each of the m vibrational partition functions is given by

$$Q^{GT}_{vib,m} = \sum_{n_m} \exp\left[-\beta E^{GT}_{vib,m}(n_m, s)\right] \quad [88]$$

where $E^{GT}_{vib,m}(n_m, s)$ is the energy of the harmonic vibrational level n_m in mode m, measured relative to $V_{MEP}(s)$, and is given, analogous to Eq. [82], by

$$E^{GT}_{vib,m}(n_m, s) = \left(n_m + \frac{1}{2}\right)\hbar\omega_m(s) \quad [89]$$

where $\omega_m(s)$ is the frequency of normal mode m for the dividing surface defined by $\mathbf{x}(s)$ and $\hat{\mathbf{n}}(s)$. The sum in Eq. [88] should terminate when the lowest dissociation energy of the system is reached,[30] but because, in general, the contribution from high energy levels is negligible, the sum can include all harmonic levels and so we get an analytical expression of the type:

$$Q^{GT}_{vib,m}(T, s) = \frac{\exp\left[-\frac{1}{2}\beta\hbar\omega_m(s)\right]}{\{1 - \exp[-\beta\hbar\omega_m(s)]\}} \quad [90]$$

The harmonic frequencies $\{\omega_1(s), \ldots, \omega_{F-1}(s)\}$ needed for the vibrational partition functions correspond to those obtained by making a quadratic expansion of the potential in the vicinity of the reaction path for motion constrained to stay on the dividing surface. Calculation of harmonic frequencies for planar dividing surfaces in rectilinear coordinates is straightforward and described here. At stationary points, the vibrational frequencies are calculated by diagonalization of the $3N \times 3N$ Hessian matrix, **F**, which are the second derivatives of the potential with respect to isoinertial Cartesian coordinates scaled to a mass μ. For instance, for the transition state geometry, $\mathbf{x}^{\ddagger}$, this matrix is diagonalized as in Eq. [45] to yield the eigenvalues $\lambda_m(\mathbf{x}^{\ddagger})$. The normal-mode frequencies at the saddle point can be obtained from the eigenvalues using Eq. [46].

For a location s along the reaction path that is off the saddle point, we want the set of vibrational frequencies $\{\omega_1(s), \ldots, \omega_{F-1}(s)\}$ for motions that are orthogonal to the dividing surface at s. Diagonalization of $\mathbf{F}[\mathbf{x}(s)]$ for locations where the gradient is not zero will yield normal modes that mix motion in the dividing surface with those orthogonal to it. In this case, motion parallel to $\hat{\mathbf{n}}(s)$ and the six degrees of freedom corresponding to translations and rotation of the molecule can be projected out of the Hessian. In the case where the dividing surface is a hyperplane and $\hat{\mathbf{n}}(s)$ is parallel to the gradient vector, the expression for the projection matrix, **P**, can be found in the article of Miller,

Handy and Adams.[65] The generalization to cases where $\hat{\mathbf{n}}(s)$ is not parallel to the gradient vector is given by an expression similar to Eq. [66]

$$\mathbf{F}^{\mathrm{P}} = (\mathbf{I} - \hat{\mathbf{n}}(s)\hat{\mathbf{n}}(s)^{\dagger})(\mathbf{I} - \mathbf{P}^{\mathrm{RT}})\mathbf{F}[\mathbf{x}(s)](\mathbf{I} - \mathbf{P}^{\mathrm{RT}})(\mathbf{I} - \hat{\mathbf{n}}(s)\hat{\mathbf{n}}(s)^{\dagger}) \quad [91]$$

Now $\mathbf{F}^{\mathrm{P}}$ can be diagonalized using the relation:

$$[\mathbf{L}^{\mathrm{GT}}(s)]^{\dagger}\mathbf{F}^{\mathrm{P}}(s)\mathbf{L}^{\mathrm{GT}}(s) = \mathbf{\Lambda}(s) \quad [92]$$

The resulting $m = 1, \ldots, F-1$ eigenvalues are given by

$$\omega_m(s) = [\lambda_m(s)/\mu]^{1/2} \quad [93]$$

with directions given by the corresponding vectors $\mathbf{L}_m^{\mathrm{GT}}(s)$, whose phases ("signs") are discussed below Eq. [167].

Generalized Partition Functions in Curvilinear Internal Coordinates

In the previous subsections, the dividing surfaces were hyperplanes in rectilinear coordinates; they were orthogonal to the reaction path at the point where they intersect it, and they were labeled by the location s at which they intersect the reaction path. In this section, we consider more general dividing surfaces defined in terms of curvilinear coordinates such as stretch, bend, and torsion coordinates (which are called valence coordinates or valence force coordinates and which are curvilinear because they are nonlinear functions of atomic Cartesians). In general, defining the reaction path provides the value of the reaction coordinate only for points on the reaction path. Defining the dividing surface assigns a value to the reaction coordinate even when the geometry is off the reaction path because one defines the generalized transition state dividing surface so that s is constant in the dividing surface; this means that defining the reaction coordinate off the reaction path is equivalent to defining the dividing surface and vice versa. Making the dividing surface curvilinear means that the expression for the flux in phase space through the dividing surface no longer matches the expression for a classical partition function.[32] Therefore one should introduce an additional term C, in addition to the free energy of activation, in the exponent of equations like Eq. [5]. However, as we only calculate the generalized transition state partition function approximately, we do not include this term (which is expected to be small for dividing surfaces defined in terms of stretch, bend, and torsion coordinates[32]). Changing the definition of the dividing surface changes the generalized transition state partition function even if one makes the harmonic approximation for transverse coordinates because generalized normal mode frequencies computed with the constraint that s is constant will also change if the definition of s off the reaction path changes.[66–68]

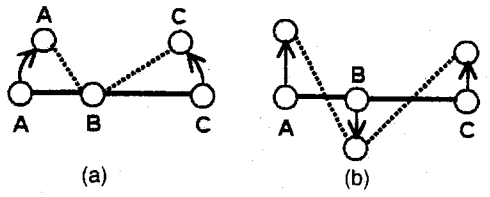

An example showing why curvilinear coordinates are more physical than rectilinear coordinates is provided by an atom–diatom reaction (A + BC → AB + C) with a collinear reaction path where it is clearly more physical to define the reaction coordinate in terms of the AB and BC distances and the ABC bond angle than to define it as a function of the Cartesian coordinates. Displacements from the linear geometry for fixed values of s produce different effects on the geometry when the reaction coordinate is defined in curvilinear coordinates, in which the bond distances stay fixed, as shown in part (a) of Scheme 1, than when it is defined in rectilinear coordinates, in which atoms move along straight-line paths in Cartesian coordinates, as shown in part (b) of Scheme 1. This effect is illustrated in Figure 2. The difference is important because the evaluation of the second derivatives of the potential with different frozen variables produces different harmonic frequencies. The above example indicates that the choice between rectilinear and curvilinear coordinates for the harmonic treatment is equivalent to choosing between two different definitions of the reaction coordinate, s and s', for points that are off the reaction path. These two reaction coordinates are equal for geometries on the

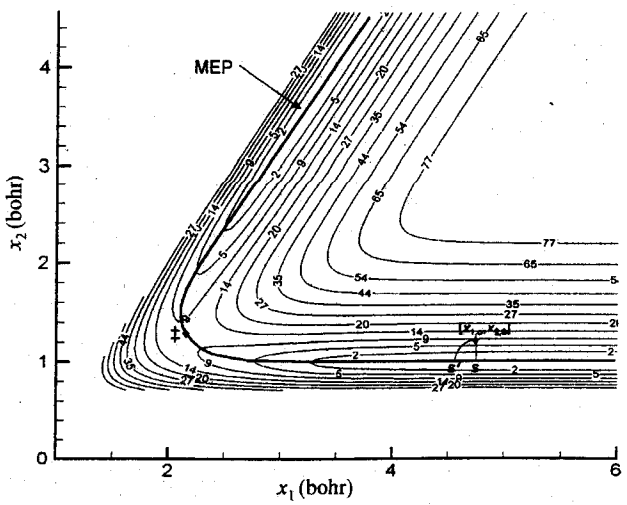

Figure 2 Contour plot that shows the projection over the reaction coordinate of a geometry close to the MEP when curvilinear (s') or rectilinear (s) coordinates are used.

reaction path but differ for general geometries. The relation between them is given by the expression:[67]

$$s' = s + \frac{1}{2}\sum_{i=1}^{F-1}\sum_{j=1}^{F-1} b_{ij} q_i q_j + O(q_i^3) \qquad [94]$$

where q_i represents a curvilinear coordinate that is zero on the reaction path and measures the distortion away from it; b_{ij} involves second-order partial derivatives of s' with respect to q_i with s held fixed. The Hessian elements evaluated with the two definitions are related by[66,67]

$$\left(\frac{\partial^2 V}{\partial q_i \partial q_j}\right)_{s'}\Bigg|_{\mathbf{q}'=(0,\ldots,0,s')} = \left(\frac{\partial^2 V}{\partial q_i \partial q_j}\right)_{s} - b_{ij}\left(\frac{\partial V}{\partial s}\right)_{\mathbf{q}}\Bigg|_{\mathbf{q}=(0,\ldots,0,s)} \qquad [95]$$

where $\mathbf{q}' = \{q_1, q_2, \ldots, q_{F-1}, s'\}$ and $\mathbf{q} = \{q_1, q_2, \ldots, q_{F-1}, s\}$. It is clear from the above relation that the Hessian and (therefore) the harmonic frequencies depend on the definition of the reaction coordinate except at stationary points, where $\partial V/\partial s = 0$. As the calculated vibrational frequencies of the generalized normal modes depend on the coordinate system, it is important to make the most physically appropriate choice. It has been shown that the curvilinear coordinates produce more physical harmonic frequencies than do the rectilinear coordinates.[67,68] This results because the atoms move along straight lines in rectilinear generalized normal modes,[69] whereas motions along paths dictated by valence coordinates[28,68–72] are much less strongly coupled. (Valence coordinates, also called valence force coordinates, are stretches, bends, torsions, and improper torsions.) The frequencies in the more physical curvilinear coordinates can be obtained by following a generalization of the scheme described by Pulay and Fogarasi,[71] as described next.

For the N-atom system, the energy V at a geometry (denoted by $\mathbf{x}$ in Cartesian coordinates and by $\mathbf{q}$ in internal coordinates) close to a reference geometry (denoted by $\mathbf{x}^0$ in Cartesian coordinates and by $\mathbf{q}^0$ in internal coordinates) can be obtained by a second-order Taylor expansion. In unscaled Cartesian and curvilinear coordinates, the expansions are given by

$$V = V_0 + \sum_{i=1}^{3N} G_i^R (R_i - R_i^0) + \frac{1}{2}\sum_{i,j}^{3N} F_{ij}^R (R_i - R_i^0)(R_j - R_j^0) \qquad [96]$$

and

$$V = V_0 + \sum_{i=1}^{F_{\text{curv}}} g_i (q_i - q_i^0) + \frac{1}{2}\sum_{i,j}^{F_{\text{curv}}} f_{ij} (q_i - q_i^0)(q_j - q_j^0) \qquad [97]$$

respectively, where F_{curv} is the number of curvilinear coordinates that are to be used, g_i is a component of the gradient in internal coordinates, and f_{ij} is an

element of the Hessian in curvilinear coordinates. However, three problems are related to the use of curvilinear coordinates:

(1) They are not mutually orthogonal;
(2) for more than four atoms, there are more than $3N-6$ valence coordinates; and
(3) the transformation to Cartesian coordinates is nonlinear.

Specifically, the curvilinear coordinates can be written as a power series of the displacements in Cartesian coordinates:[28]

$$q_i = \sum_{j}^{3N} B_{ij}(R_j - R_j^0) + \frac{1}{2}\sum_{j,k}^{3N} C_{jk}^i (R_j - R_j^0)(R_k - R_k^0) + \ldots \qquad [98]$$

where a superscript zero indicates a reference geometry (a stationary point or a point on the reaction path), B_{ij} is an element of the $F_{\text{curv}} \times 3N$ Wilson B matrix,

$$B_{ij} = \left(\frac{\partial q_i}{\partial R_j}\right)\Bigg|_{\{R_j\}=\{R_j^0\}} ; i = 1, \ldots F_{\text{curv}};\ j = 1, \ldots, 3N \qquad [99]$$

and C_{jk}^i is an element of the $3N \times 3N$ tensor $\mathbf{C}^i$ that represents the quadratic term

$$C_{jk}^i = \left(\frac{\partial^2 q_i}{\partial R_j \partial R_k}\right)\Bigg|_{\{R_k\}=\{R_k^0\}} ; i = 1, \ldots F_{\text{curv}};\ j,k = 1, \ldots, 3N \qquad [100]$$

For reactions involving more than four atoms, it is often not obvious which set of $3N-6$ internal coordinates best describes the whole reaction path, and in those cases, it is very useful to define the reactive system in terms of redundant internal coordinates.[72] Using redundant internal coordinates circumvents

(1) destroying the symmetry of the system for highly symmetric reaction paths by omitting a subset of symmetry related coordinates and
(2) using an incomplete set of $3N-6$ internal coordinates that does not fully span the vibrational space.

Therefore, the recommendation is that, for more than four atoms, one should always use redundant internal coordinates to evaluate the generalized normal mode frequencies.

In practice, the following procedure[68,72] is carried out to calculate the frequencies and generalized normal mode eigenvectors in redundant internal coordinates, where nonredundant internal coordinates are simply a special case and may be used in the same manner.

First, the Wilson B and C matrices[28] must be constructed. When using redundant internal coordinates, the formulas for the Wilson B and C matrices given above are used, except the number of internal coordinates, F_{curv}, is not restricted to be $3N-6$. The formulas given above for these matrices are deceptively simple, and in practice, this is the most difficult step,[68] although once computer code is available (as in POLYRATE), the code is very general, and no new

issues need to be considered for further applications. Once these matrices have been constructed, the Wilson G matrix, called $\mathbf{G}^{\mathrm{W}}$, is constructed as

$$\mathbf{G}^{\mathrm{W}} = \mathbf{BuB}^{\dagger} \tag{101}$$

where $\mathbf{u}$ is a $3N \times 3N$ diagonal matrix with the reciprocals of the atomic masses on the diagonal. Next, the matrix $\mathbf{G}^{\mathrm{W}-}$ is created using

$$\mathbf{G}^{\mathrm{W}-} = (\mathbf{K}\,\mathbf{K}') \begin{pmatrix} \Gamma^{-1} & 0 \\ 0 & 0 \end{pmatrix} \begin{pmatrix} \mathbf{K}^{\dagger} \\ (\mathbf{K}')^{\dagger} \end{pmatrix} \tag{102}$$

where $\mathbf{K}$ is defined to consist of the eigenvectors of $\mathbf{G}^{\mathrm{W}}$ corresponding to nonzero eigenvalues, $\mathbf{K}'$ is defined to consist of the remaining eigenvectors, and Γ is defined to contain the nonzero eigenvalues. The generalized inverse of the Wilson B matrix is[71]

$$\mathbf{A} = \mathbf{uB}^{\dagger}\mathbf{G}^{\mathrm{W}-} \tag{103}$$

Now, the construction of the gradient and force constant matrices in internal coordinates is possible:

$$\mathbf{g} = \mathbf{A}^{\dagger}\mathbf{G}^{R} \tag{104}$$

$$\mathbf{f} = \mathbf{A}^{\dagger}\mathbf{F}^{R}\mathbf{A} - \sum_{i}^{F_{\mathrm{curv}}} g_i \mathbf{A}^{\dagger}\mathbf{C}^{i}\mathbf{A} \tag{105}$$

Then, the gradient and force constant matrices needed to project out the reaction coordinate are created:

$$\mathbf{P} = \mathbf{G}^{\mathrm{W}}\mathbf{G}^{\mathrm{W}-} \tag{106}$$

$$\tilde{\mathbf{f}} = \mathbf{PfP} \tag{107}$$

$$\tilde{\mathbf{g}} = \mathbf{Pg} \tag{108}$$

The projected Hessian $\mathbf{f}^{\mathrm{P}}$ is given by

$$\mathbf{f}^{\mathrm{P}} = \{1 - \mathbf{p}(s)[\mathbf{BuB}^{\dagger}]\}\tilde{\mathbf{f}}(s)\{1 - [\mathbf{BuB}^{\dagger}]\mathbf{p}(s)\} \tag{109}$$

where $\mathbf{p}$, the nonorthogonal coordinate projection operator, is given at s by

$$\mathbf{p} = \frac{\tilde{\mathbf{g}}\tilde{\mathbf{g}}^{\dagger}}{\tilde{\mathbf{g}}^{\dagger}[\mathbf{BuB}^{\dagger}]\tilde{\mathbf{g}}} \tag{110}$$

Now it is possible to evaluate the vibrational frequencies using the Wilson GF matrix method,[28,73–75]

$$\mathbf{G}^{\mathrm{W}}\mathbf{F}^{\mathrm{W}}\mathbf{L}^{\mathrm{W}} = \mathbf{L}^{\mathrm{W}}\Lambda \tag{111}$$

where $\mathbf{G}^{\mathrm{W}}$ is defined above, the projected Hessian $\mathbf{f}^{\mathrm{P}}$ is used for $\mathbf{F}^{\mathrm{W}}$, $\mathbf{L}^{\mathrm{W}}$ is the matrix of generalized normal mode eigenvectors, and Λ is the diagonal

eigenvalue matrix. Vibrational frequencies are given in terms of the eigenvalues by

$$\omega_m = (\Lambda_{mm})^{1/2} \quad [112]$$

Next, the vibrational eigenvectors must be normalized. The normalized eigenvector matrix is given by

$$\hat{\mathbf{L}}^{\mathrm{W}} = \mathbf{L}^{\mathrm{W}}\mathbf{W} \quad [113]$$

where

$$W_{ij} = \sqrt{C_{ij}}\delta_{ij} \quad [114]$$

and

$$\mathbf{C} = (\mathbf{L}^{\mathrm{W}})^{-1}\mathbf{G}^{\mathrm{W}}\left[(\mathbf{L}^{\mathrm{W}})^{-1}\right]^{\dagger} \quad [115]$$

The Cartesian displacement normal-mode eigenvectors are

$$\chi = \mathbf{u}\mathbf{B}^{\dagger}(\mathbf{G}^{\mathrm{W}})^{-1}\hat{\mathbf{L}}^{\mathrm{W}} = \mathbf{A}\hat{\mathbf{L}}^{\mathrm{W}} = \mathbf{A}\mathbf{L}^{\mathrm{W}}\mathbf{W} \quad [116]$$

Finally, the elements of the rectilinear eigenvector matrix, $\mathbf{L}^{\mathrm{GT}}$, which are needed for multidimensional tunneling calculations (see Eqs. [164], [170], and [171]) are given by

$$L_{ij}^{\mathrm{GT}} = \frac{(m_i/\mu)^{1/2}}{\left[\sum_k (m_k/\mu)\chi_{kj}^2\right]^{1/2}} = \frac{m_i^{1/2}\chi_{ij}}{\left[\sum_k m_k\chi_{kj}^2\right]^{1/2}} \quad [117]$$

Loose Transition States

Although the POLYRATE program is very general, the definitions it uses for the generalized transition state dividing surfaces are most appropriate for reactions with non-negligible barriers and tight transition states. For many association–dissociation reactions, the transition state is located at a position where two fragments have nearly free internal rotation; in such cases, one may wish to use even more general definitions of the dividing surfaces;[76,77] these are not covered in the current tutorial. We note though that the methods used above have been used successfully to treat the association of hydrogen atoms with ethylene to form the ethyl radical.[78–80]

In recent years, there has been tremendous progress in the treatment of barrierless association reactions with strictly loose transition states.[76,77,81–89] A strictly loose transition state is defined as one in which the conserved vibrational modes are uncoupled to the transition modes and have the same frequencies in the variational transition state as in the associating reagents.[81,82,84] (Conserved vibrational modes are modes that occur in both

the associating fragments and the association complex, whereas transition modes include overall rotation of the complex and vibrations of the complex that transform into fragment rotations and relative translational upon dissociation of the complex.) Progress has included successively refined treatments of the definition of the dividing surface and of the definition of the reaction coordinate that is missing in the transition state[76,77,81–88] and elegant derivations of rate expression for these successive improvements.[85–88] The recent variational implementation of the multifaceted–dividing-surface variational-reaction-coordinate version of VTST seems to have brought the theory to a flexible enough state that it is suitable for application to a wide variety of practical applications to complex combustion reactions of polyatomic molecules. Although some refinements (e.g., the flexibility of pivot point placement for cylindrical molecules like O_2[88]) would still be useful, the dynamical formalism is now very well developed. However, this formalism is not included in POLYRATE, and so it is not reviewed here.

Harmonic and Anharmonic Vibrational Energy Levels

The partition functions thus far have been assumed to be calculated using the harmonic approximation. However, real vibrations contain higher-order force constants and cross terms between the harmonic normal modes, and they are coupled to rotations. If the cross terms and couplings are neglected, each of the vibrational degrees of freedom is bound by an anharmonic potential given by

$$V_m = \frac{1}{2}k_{mm}(s)Q_m^2 + k_{mmm}(s)Q_m^3 + k_{mmmm}(s)Q_m^4 + \ldots \qquad [118]$$

where k_{mm}, k_{mmm}, and k_{mmmm} are the quadratic, cubic, and quartic normal coordinate force constants and Q is the vector of normal mode coordinates. In rectilinear coordinates, the relationship between normal modes is given by

$$\mathbf{Q} = \left[\mathbf{L}^{GT}(s)\right]^{\dagger}[\mathbf{x} - \mathbf{x}(s)] \qquad [119]$$

where the transformation matrix is defined by the diagonalization in Eq. [92]. In curvilinear coordinates, the normal modes are defined by the Wilson GF matrix method as described above. For the harmonic approximation, the series is truncated after the first term, and the frequency ω is given by

$$\omega_m = \sqrt{k_{mm}/\mu} \qquad [120]$$

The partition function for the harmonic approximation is

$$Q_{vib}^{HO} = e^{-\beta E_0^{HO}}\tilde{Q}_{vib}^{HO} \qquad [121]$$

$$= e^{-\beta E_0^{HO}}\prod_{m=1}^{F}\tilde{Q}_m^{HO} \qquad [122]$$

E_0^{HO} is the harmonic ground-state energy, which is calculated by

$$E_0^{HO} = \frac{\hbar}{2}\sum_{m=1}^{F}\omega_m \qquad [123]$$

where

$$\tilde{Q}_m^{HO} = \frac{1}{1-e^{-\beta\hbar\omega_m/2}} \qquad [124]$$

and ω_m is the harmonic vibrational frequency of mode m, given by Eq. [120]. For generalized transition states, F is replaced by $F-1$ in Eqs. [122] and [123] such that the imaginary frequency is not included.

Hindered Internal Rotations (Torsions)

One type of anharmonic motion is a hindered internal rotation, or torsion, which can differ substantially from a harmonic normal mode motion. Unlike many other anharmonic motions, torsions can be readily accounted for even in large systems. It has been shown[92–95] that a vibrational partition function that includes a torsion can be written as

$$Q_{vib} = e^{-\beta E_0}\tilde{Q}_{tor}\tilde{Q}_{sb} \qquad [125]$$

where $\tilde{Q}_{tor}$ is a torsion partition function and $\tilde{Q}_{sb}$ is the stretch-bend partition function that ignores the torsional twist angle. A simple and effective equation[90] for calculating $\tilde{Q}_{tor}$ is

$$\tilde{Q}_{tor} = \tilde{Q}_m^{HO}\tanh\left(\frac{Q^{FR}}{Q^{I}}\right) \qquad [126]$$

where Q^{FR} is the free rotor partition function given by

$$Q^{FR} = \frac{(2\pi IkT)^{\frac{1}{2}}}{\hbar\sigma} \qquad [127]$$

where I is the effective moment of inertia and σ is the effective symmetry number. Q^I is called the intermediate partition function, which is the high-temperature limit of the harmonic oscillator partition function given by

$$Q^{I} = \frac{kT}{\hbar}\frac{1}{\omega} \qquad [128]$$

where ω is the normal mode frequency relating to the torsion. The method thus far has been defined for a single well or multiple wells that are symmetrically equivalent. For multiple wells that are not symmetrically equivalent, the extended method has been defined by Chuang and Truhlar.[90]

The frequency, the effective moment of inertia, and the barrier height W, are related to one another by the expression[90,91]

$$\omega = \left(\frac{W}{2I}\right)^{\frac{1}{2}} M \qquad [129]$$

where M is the number of wells as the torsion rotates 360 degrees. Therefore, under the assumptions that the effective potential for the torsion is a single cosine term and that the moment of inertia is a constant, only two of the three variables need to be specified to calculate the torsion partition function. The frequency can be determined from normal mode analysis, the barrier height can be determined from electronic structure methods, and the effective moment of inertia is described next.

There are several schemes for calculating the effective moment of inertia for internal rotation: the curvilinear (C) scheme of Pitzer and Gwinn,[92,93] which requires the choice of an axis (typically a bond) about which the tops are rotating; the rectilinear (R) scheme of Truhlar,[94] which only requires that one identify the generalized normal mode that corresponds to the torsion and divide the molecule into parts that rotate against each other; the ωk scheme of Ellingson et al.,[95] which requires that one identify a torsion coordinate as well as the generalized normal mode frequency corresponding to the torsion; and the ωW scheme of Chuang and Truhlar.[90] When the torsion is mixed with stretching, bending, or other torsional motions in the generalized normal modes, the user must pick the generalized normal mode that is most dominated by the torsion under consideration. It is not always clear which scheme is most correct, in part because real torsions are usually coupled strongly to overall rotation and sometimes to other vibrational modes as well. As the tops become significantly asymmetric, the R scheme begins to fail, and one should use one of the other methods.

The method of calculating the moment of inertia in the C scheme is described here. Let M be the mass of the entire molecule and m_i be the mass of atom i, and let the principal moment of inertia be defined as I_j, where $j = 1, 2$, or 3. All atoms in the molecule are divided into two groups rotating with respect to one another; each group is called a top, and the lighter top is taken as the rotating top. Let the coordinate system be defined such that the z axis is the chosen axis of rotation and the x axis is perpendicular to the z axis and passes through the center of mass of the rotating top, and let the y axis be perpendicular to both x and z. At this point, there are three sets of axes: the original Cartesian axes, the principal moment of inertia axes (labeled 1, 2, or 3), and the axes for the rotating top (labeled x, y, and z). It is important that these sets of axis are all either right handed or left handed. The direction of cosines between the axes of the top and the principal moment of inertia axis j are defined as α^{jx}, α^{jy}, and α^{jz}. The vector from the molecule's center of gravity to the origin of coordinates for the rotating top is given by $\mathbf{r}$, with its components r_1, r_2, and r_3 on the principal moment of inertia axes.

The moment of inertia for the rotating top about the z axis is given by

$$A = \sum_i m_i(x_i^2 + y_i^2) \qquad [130]$$

where the sum is over the atoms in the rotating top and x_i, y_i, and z_i (used below) refer to the location of atom i on the newly created x, y, and z axis, respectively. The xz product of inertia is given by

$$B = \sum_i m_i x_i z_i \qquad [131]$$

The yz produce of inertia is given by

$$C = \sum_i m_i y_i z_i \qquad [132]$$

The off-balance factor is given by

$$U = \sum_i m_i x_i \qquad [133]$$

The reduced moment of inertia for internal rotation is given by

$$I = A - \sum_j \left\{ \frac{(\alpha^{jy} U)^2}{M} + \frac{(\beta^j)^2}{I_j} \right\} \qquad [134]$$

where

$$\beta^j = \alpha^{jz} A - \alpha^{jx} B - \alpha^{jy} C + U(\alpha^{j-1,y} r_{j+1} - \alpha^{j+1} r_{j-1}) \qquad [135]$$

and the superscripts refer to cyclic shifts of axes, such that $j - 1 = 3$ if $j = 1$, and $j + 1 = 1$ if $j = 3$. POLYRATE uses the value of I calculated for the lighter of the two tops as the C scheme moment of inertia.

The R scheme does not require that the axis of rotation be chosen a priori, but it relies on the generalized normal mode eigenvector of the mode corresponding to the torsion to determine the axis. The equations for I in this scheme are given elsewhere.[90,91]

The ωk scheme simply takes the moment of inertia as[95]

$$I = \frac{1}{\omega_{\text{torsion}}^2} \frac{\partial^2 V}{\partial \varphi^2} \qquad [136]$$

where ω_{torsion} is the frequency of the normal mode that most corresponds to the torsion, φ is the torsion angle, and the partial derivative in Eq. [136] must be supplied by the user. The partial derivative may be evaluated with other internal coordinates fixed or along a torsion path where other degrees of freedom are optimized for each value of φ. The ωW scheme uses the barrier height rather than the second derivative with respect to the torsion angle.[90]

Morse Approximation I and Other Corrections for Principal Anharmonicity

Many other anharmonic methods can be applied, especially for smaller systems. One way to approximate the accurate anharmonic potential along a stretching vibrational coordinate is to use a Morse function:[96]

$$V_{M,m} = D_e(s)\{\exp[-\beta_{M,m}(s)Q_m(s)] - 1\}^2 \qquad [137]$$

where D_e is the dissociation energy and the range parameter $\beta_{M,m}$ is chosen such that the force constant is correct at the minimum of the Morse potential:

$$\beta_{M,m}(s) = \left[\frac{k_{mm}(s)}{2D_e(s)}\right]^{\frac{1}{2}} \qquad [138]$$

The energy levels for the Morse approximation I are given by

$$E^{GT}_{vib,m} = \hbar\omega_m(s)\left(n+\frac{1}{2}\right)\left[1 - x_{M,m}(s)\left(n+\frac{1}{2}\right)\right] \qquad [139]$$

where n is the level index, ω_m is the harmonic frequency, and $x_{M,m}$ is the Morse anharmonicity constant:

$$x_{M,m} = \frac{\hbar\omega_m(s)}{4D_e(s)} \qquad [140]$$

The choice of D_e as the lowest dissociation energy of the system relative to $V_{MEP}(s)$ is referred to as the Morse approximation I.[20,30,97]

The Morse approximation is not appropriate for modes that have $k_{mmm} = 0$. These types of modes include bending modes of linear systems, out-of-planes bends, and certain stretching motions. Often such modes are better treated by a quadratic-quartic model, given by

$$V_m = \frac{1}{2}k_{mm}(s)[Q_m(s)]^2 + k_{mmmm}(s)[Q_m(s)]^4 \qquad [141]$$

Accurate approximations for this model can be determined using a perturbation–variation method.[98,99]

Spectroscopists call the force constants that have all indices the same the principal force constants, while the anharmonicity associated with the principal force constants is called principal anharmonicity. The Morse and quadratic–quartic approximations treat only principal anharmonicity. However, as mentioned in Eq. [95], neglecting the cross terms between modes is a much more serious approximation in rectilinear coordinates.[70] Explicitly including cross terms in rectilinear coordinates is expensive and cumbersome

because of the large number of quartic cross terms. One practical step that can be taken to minimize the importance of cross terms is to use curvilinear internal coordinates.[68,72,100,101] Not only are the harmonic frequencies more physical in curvilinear coordinates, but anharmonicity is much better approximated by retaining only principal terms in the potential and neglecting couplings.

Calculations of Generalized Transition State Number of States

The generalized transition state number of states needed for microcanonical variational theory calculations counts the number of states N_{vr}^{GT} in the transition state dividing surface at s that are energetically accessible below an energy E. Consistent with approximations used in calculations of the partition functions, we assume that rotations and vibrations are separable to give

$$N_{vr}^{GT} = \sum_{\mathbf{n}} H\left[E - V_{MEP}(s) - E_{vib}^{GT}(\mathbf{n}, s)\right] N_{rot}^{GT}\left[E - V_{MEP}(s) - E_{vib}^{GT}(\mathbf{n}, s), s\right] \quad [142]$$

where $H(x)$ is the Heaviside step function [$H(x) = 0$ for $x < 0$ and $H(x) = 1$ for $x > 0$] and the rotational number of states are calculated classically.

QUANTUM EFFECTS ON REACTION COORDINATE MOTION

In the previous sections, we quantized the $F - 1$ degrees of freedom in the dividing surface, but we still treated the reaction coordinate classically. As discussed, such quantum effects, which are usually dominated by tunneling but also include nonclassical reflection, are incorporated by a multiplicative transmission coefficient $\kappa(T)$. In this section, we provide details about methods used to incorporate quantum mechanical effects on reaction coordinate motion through this multiplicative factor.

In practice, we have developed two very useful approaches to the multidimensional tunneling problem. In both of these methods, we estimate the rate constant semiclassically, in which case it involves averaging the tunneling probabilities calculated for a set of tunneling energies and tunneling paths. In a complete semiclassical theory, one would optimize the tunneling paths;[102] the optimum tunneling paths minimize semiclassical imaginary action integrals, which in turn maximizes the tunneling probabilities. We have found[103] that sufficiently accurate results can be obtained by a simpler criterion[91] in which, for each energy, we choose the maximum tunneling probability from two approximate results, one, called small-curvature tunneling[3,104] (SCT), calculated by assuming that the curvature of the reaction path is small, and the other, called

large-curvature tunneling (LCT),[1,3,7,91,105–110] calculated by assuming that it is large. The result is called microcanonically optimized multidimensional tunneling (μOMT) or, for short, optimized multidimensional tunneling (OMT). The resulting VTST/OMT rate constants have been carefully tested against accurate quantum dynamics,[103,111,112] and the accuracy has been found to be very good.

The SCT, LCT, and OMT tunneling calculations differ from one-dimensional models of tunneling in two key respects:

(1) These approximations include the quantized energy requirements of all vibrational modes along the tunneling path. As the vibrational frequencies are functions of the reaction coordinate, this changes the shape of the effective potential for tunneling.
(2) These approximations include corner-cutting tunneling. Corner cutting means that the tunneling path is shorter than the minimum energy path.

The wave function decays most slowly if the system tunnels where the effective barrier is lowest; however, the distance over which the decay is operative depends on the tunneling path. Therefore, the optimum tunneling paths involve a compromise between path length and effective potential along the path. As a consequence, the optimum tunneling paths occur on the concave side of the minimum energy path; i.e., they "cut the corner."[7,52,102,107,113–119] For the purpose of analyzing the results, it is sometimes of interest to also compute an intermediate result, called zero-curvature tunneling (ZCT), that includes effect (1) but not (2).

The rest of this section will provide the details of the ZCT, SCT, LCT, and OMT tunneling approximations.

Multidimensional Tunneling Corrections Based on the Adiabatic Approximation

The adiabatic separation between the reaction coordinate and all other $F-1$ vibrational degrees of freedom means that quantum states in those modes are conserved through the reaction path. With this approximation, we can label the levels of the generalized transition states in terms of the "one-dimensional" vibrationally and rotationally adiabatic potentials

$$V_a = V_{MEP}(s) + E_{int}^{GT}(\boldsymbol{\alpha}, s) \qquad [143]$$

where $\boldsymbol{\alpha}$ is the collection of vibrational and rotational quantum numbers and $E_{int}^{GT}(\boldsymbol{\alpha}, s)$ is the vibrational–rotational energy level for quantum state $\boldsymbol{\alpha}$ and generalized, transition state at s. Making the rigid-rotor–harmonic-oscillator approximation, $E_{int}^{GT}(\boldsymbol{\alpha}, s)$ for the ground rotational state reduces to the energy level for vibrational state $\mathbf{n} = \{n_1, \ldots n_{F-1}\}$ and is given by

$$E_{vib}^{GT}(\mathbf{n}, s) = \sum_m \hbar\omega_m(s)\left(n_m + \frac{1}{2}\right) \qquad [144]$$

The ground-state adiabatic potential is defined with $\alpha = 0$, and only the vibrations contribute to the internal energy through zero-point energies in each mode to give

$$V_a^G = V_{MEP}(s) + \sum_m \frac{\hbar\omega_m(s)}{2} \qquad [145]$$

The transmission coefficient is written in terms of the classical and quantum probabilities, P_C^A and P_Q^A, respectively, for transmission through or above the adiabatic potential: $V_A(\alpha, s)$:[54]

$$\kappa^A = \frac{\int_0^\infty dE\ \exp(-\beta E) \sum_\alpha P_Q^A(\alpha, E)}{\int_0^\infty dE\ \exp(-\beta E) \sum_\alpha P_C^A(\alpha, E)} \qquad [146]$$

The probabilities for classical motion along the reaction coordinate within the adiabatic approximation are simply zero when the energy E is below the maximum V_a^A of the vibrationally adiabatic potential for state α, and one for energies above the barrier; i.e.,

$$P_C^A(\alpha, E) = H\left[E - V_a^A(\alpha)\right] \qquad [147]$$

where H is the Heaviside unit-step function defined below Eq. [142]. Evaluation of the quantum probabilities P_Q^A is more difficult, and two approximations are made to facilitate evaluation of the numerator of the transmission coefficient.

The first approximation is that excited-state probabilities are approximated by the probabilities for the ground state P_Q^{AG}, but for a shifted energy,

$$P_Q^A = P_Q^{AG}[E - V_a^A(\alpha) + V_a^{AG}] \qquad [148]$$

where V_a^{AG} is the barrier height of the ground-state vibrationally adiabatic potential,

$$V_a^{AG} = V_a^A(\alpha = 0) \qquad [149]$$

This approximation assumes that the vibrationally adiabatic potentials of all excited states have the same shape as the ground-state vibrationally adiabatic potential. Although this approximation is not strictly valid, it is adequate for two reasons. First, when tunneling is important, the temperature is usually low enough that the transmission coefficient is dominated by the ground state or excited states close to the ground state. Second, contributions of tunneling to the rate constant become unimportant (i.e., $\kappa \to 1$) as T becomes high enough that excited states with significantly different vibrationally adiabatic potential curves contribute more to the rate constant.

The second approximation consists in the replacement of quantum probabilities P_Q^{AG} by semiclassical ones

$$P^{SAG} = \{1 + \exp[2\theta(E)]\}^{-1} \qquad [150]$$

where θ is the imaginary action integral:

$$\theta(E) = \hbar^{-1} \int_{s_<(E)}^{s_>(E)} ds \left\{2\mu_{eff}(s)\left[V_a^G(s) - E\right]\right\}^{\frac{1}{2}} \qquad [151]$$

where V_a^G is the ground-state adiabatic potential defined in Eq. [145], and $s_<$ and $s_>$ are the classical turning points, i.e., locations where V_a^G equals E. The effective mass $\mu_{eff}(s)$ for motion along the reaction coordinate is discussed in the next section. After these approximations, the semiclassical adiabatic ground-state transmission coefficient takes the simplified form

$$\kappa^{SAG} = \frac{\beta \int_0^\infty dE\ \exp(-\beta E) P^{SAG}(E)}{\exp(-\beta V_a^{AG})} \qquad [152]$$

which requires evaluation of semiclassical reaction probabilities for the ground state only.

The integrals in Eq. [146] extend to infinity, but Eqs. [150] and [151] are only valid for energies below the top of the barrier (i.e., for $E \leq V_a^{AG}$), which is the tunneling region. For energies above V_a^{AG}, the quantum effects (nonclassical reflection) are incorporated by assuming that close to the top of the barrier the shape of the potential is parabolic, and in that case,[47]

$$P^{SAG}(V_a^{AG} + \Delta E) \cong 1 - P^{SAG}(V_a^{AG} - \Delta E) \qquad [153]$$

where $\Delta E = E - V_a^{AG}$. This equation provides a natural extension to Eq. [150], and therefore, the semiclassical probability in the whole range of energies is given by

$$P^{SAG} = \begin{cases} 0, & E < E_0 \\ \{1 + \exp[2\theta(E)]\}^{-1}, & E_0 \leq E \leq V_a^{AG} \\ 1 - P^{SAG}(2V_a^{AG} - E), & V_a^{AG} \leq E \leq 2V_a^{AG} - E_0 \\ 1, & 2V_a^{AG} - E_0 < E \end{cases} \qquad [154]$$

where E_0 is the lowest energy at which it is possible to have tunneling (also called the quantum threshold energy). For instance, for a bimolecular reaction $A + B \rightarrow C + D$

$$E_0 = \max\left[V_a^G(s = -\infty), V_a^G(s = \infty)\right] \qquad [155]$$

and for a unimolecular reaction A → B

$$E_0 = \max\left[V_a^G(s = s_R) + \frac{1}{2}\hbar\omega_F^R, V_a^G(s = s_P) + \frac{1}{2}\hbar\omega_F^P\right] \qquad [156]$$

where s_R and s_P indicate the value of s at the reactant and the product minima, respectively.

Accurate Incorporation of Classical Threshold Energies

The transmission coefficient described above is appropriate[41] for correcting the adiabatic theory or equivalently[20,30] the microcanonical variation theory,
which can be written

$$k^{\mu VT} = \frac{1}{h\Phi^R(T)}\int_0^\infty dE\ \exp(-\beta E)\sum_\alpha P_C^A(\alpha, E)$$
$$= \frac{k_B T}{h\Phi^R(T)}\sum_\alpha \exp\left[-\beta V_a^A(\alpha)\right] \qquad [157]$$

Reaction coordinate motion is treated classically in this expression and the lowest energy for reaction [i.e., at which $P_C^A(E, \alpha)$ is not zero], or the classical threshold energy, is the barrier maximum for the ground-state adiabatic potential V_a^{AG}. CVT has a different classical threshold energy, which can be seen by writing the CVT rate constant as

$$k^{CVT} = \frac{1}{\beta h\Phi^R(T)}\sum_\alpha \exp\left\{-\beta V_a\left[\alpha, s_*^{CVT}(T)\right]\right\} \qquad [158]$$

where $s_*^{CVT}(T)$ is the value of s that minimizes the quantized generalized transition state rate constant at temperature T as defined after Eq. [15] above. The classical threshold energy inherent in this expression is $V_a^G[s_*^{CVT}(T)]$ instead of V_a^{AG}. Using the transmission coefficient κ^{SAG} to correct CVT instead of μVT (or the adiabatic theory) requires correction for the different classical threshold. The CVT rate constant including multidimensional tunneling (MT) in the reaction coordinate is given by

$$k^{CVT/MT} = \kappa^{CVT/MT}(T)\, k^{CVT}(T) \qquad [159]$$

where

$$\kappa^{CVT/MT} = \frac{\beta\int_0^\infty dE\ \exp(-\beta E)P^{SAG}(E)}{\exp\{-\beta V_a^G[s_*^{CVT}(T)]\}} \qquad [160]$$

Similarly, corrections are needed for other theories that have inherent classical thresholds different from V_a^{AG}, such as conventional TST, in which V_a^{AG} in Eq. [152] is replaced by

$$V_a^{\ddagger G} = V_a^G(s = 0) \qquad [161]$$

Some of the variables explained here are shown in Figure 3 for more clarity.

POLYRATE actually calculates the transmission coefficent as

$$\kappa^{MT} = \frac{\beta \int_0^\infty dE \, \exp(-\beta E) P^{SAG}(E)}{\exp(-\beta V_a^{AG})} \qquad [162]$$

where V_a^{AG} is $V_a^G(s = s^{AG})$. Then, instead of using Eq. [159], one uses Eq. [162] but first multiplies the CVT rate by

$$\kappa^{CVT/CAG}(T) = \exp\left\{\beta\left[V_a^G(s_*^{CVT}(T)) - V_a^{AG}\right]\right\} \qquad [163]$$

In early papers we were careful to distinguish $\kappa^{CVT/MT}$ from κ^{MT}, but in recent papers, we often call both of these quantities κ^{MT} and let the reader figure out which one is involved from the context.

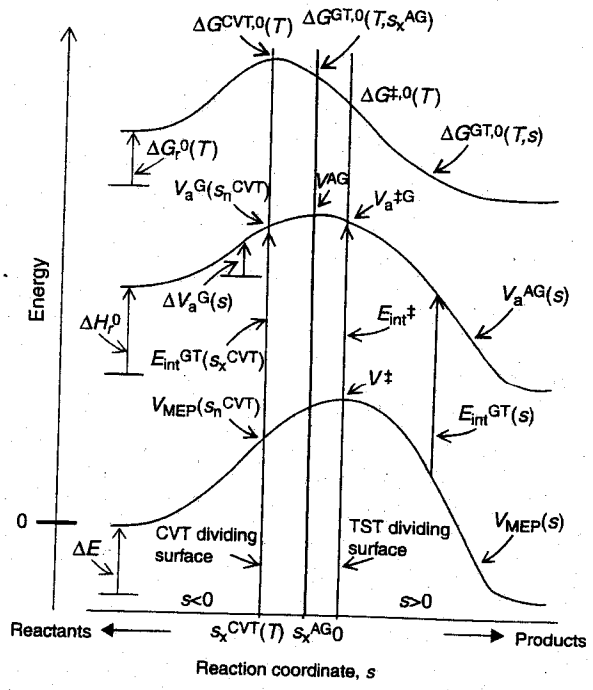

Figure 3 Graphic illustration of some important quantities that often appear in variational transition state theory. The transition state is indicated by the ‡ symbol.

Zero-Curvature and Small-Curvature Multidimensional Tunneling

From the relation between Eq. [150] and Eq. [151], at equal barrier heights, tunneling effects are more important if the particle has a small mass or if the barrier is narrower. This is the reason why tunneling is important when a light particle (for instance, a proton) is being transferred between donor and acceptor. The width at the top of the barrier in V_{MEP} is determined by the magnitude of the imaginary frequency at the transition state, and it is sometimes assumed that a large imaginary frequency indicates a narrower barrier and, as a consequence, more tunneling. However, $V_{MEP}(s)$ is not the effective barrier for tunneling, but as described above, the adiabatic barrier should be used. Complete description of the adiabatic tunneling probabilities requires definition of the effective mass in Eq. [151], which we discuss next.

The adiabatic prescription presented above may appear to be a one-dimensional approach, because the adiabatic potential is a function of the reaction coordinate s only. However, the reaction path is a curvilinear coordinate and the curvature of the path couples motion along the reaction coordinate to local vibrational modes that are perpendicular to it. The coupling enters into the Hamiltonian for the system through the kinetic energy term and leads to a negative internal centrifugal effect that moves the tunneling path to the concave side of the reaction path. In other words, as also concluded above from a different perspective, the coupling causes the system to "cut the corner" and tunnel through a shorter path than the reaction coordinate.[7,52,102,107,113–119] The effect of the coupling is to shorten the tunneling path (relative to the reaction path), decreasing the tunneling integral in Eq. [151] and thereby increasing the tunneling probabilities. Neglecting the coupling in evaluating the tunneling is known as the zero-curvature tunneling (ZCT) approximation. In this case, the tunneling path is the reaction path and the effective mass simplifies to $\mu_{eff}(s) = \mu$. The ZCT method has the drawback that tunneling is usually seriously underestimated.[54]

Marcus and Coltrin[115] showed that the effect of the reaction path curvature was to give an optimum tunneling path for the collinear $H + H_2$ reaction that is the path of concave-side turning points for the stretch vibration orthogonal to the reaction coordinate. If we define $d\xi$ as the arc length along this new tunneling path, then the effective mass in Eq. [151] is given in terms of the s-dependent Jacobian factor $d\xi/ds$ by $\mu_{eff} = \mu\,(d\xi/ds)^2$. The small-curvature tunneling (SCT) method was developed to extend this approach to three-dimensional polyatomic reactions and to eliminate problems with the Jacobian becoming unphysical.[1,116] In this approach, an approximate expression for $d\xi/ds$ is written in terms of the curvature components coupling the reaction path to the vibrational modes and the vibrational turning points.[3,116]

The coupling between the reaction coordinate and a mode m perpendicular to it is given by a curvature component defined by[65]

$$B_{mF} = -[\text{sign}(s)] \sum_{i=1}^{3N} \frac{d\hat{n}_i(s)}{ds} L_{i,m}^{GT}(s) \qquad [164]$$

where $\hat{n}_i$ is component i of the unit vector perpendicular to the generalized transition-state dividing surface at s and $L_{i,m}^{GT}$ is component i of the eigenvector for vibrational mode m perpendicular to $\hat{\mathbf{n}}$ at s. If the reaction path is the MEP, then

$$\hat{\mathbf{n}} = \mathbf{v}(s) \qquad [165]$$

where $\mathbf{v}(s)$ is the unit vector tangent to the MEP at s as defined in Eq. [44]. If the reaction path is the VRP, then $\hat{\mathbf{n}}(s)$ is defined by the procedure in the subsection "Variational Reaction Path Algorithm". Note that in either case, the sign of the unit vector is chosen to be opposite or approximately opposite the gradient vector. The modulus of these $F-1$ couplings corresponds to the curvature along the reaction path:

$$\kappa = \left\{ \sum_{m=1}^{F-1} [B_{mF}(s)]^2 \right\}^{1/2} \qquad [166]$$

To evaluate the turning points we make the independent normal mode approximation, where the potential $V_m(s, Q_m)$ in mode m at s along the reaction coordinate is given by Eq. [118]. The turning point for vibrational state n_m in this mode is obtained by solving the equation:

$$V_m[s, Q_m = t_m(n_m, s)] = E_{\text{vib},m}^{GT}(n_m, s) \qquad [167]$$

The sign of B_{mF} depend on the phase assigned to the vector $\mathbf{L}_m^{GT}$. This is not an issue for harmonic calculations because in such calculations it always enters quadratically. However, for calculations of anharmonic turning points, as in Eq. [167], we must make the physical choice. With the sign of $\hat{\mathbf{n}}$ chosen as stated after eq. [165], we choose the turning point so that $B_{mF}Q_m < 0$, which insures that the turning point is on the concave side.

In the harmonic approximation, the vibrational turning point of mode m is given by the expression

$$t_m(n_m, s) = \left[\frac{(2n_m + 1)\hbar}{\mu\omega_m(s)} \right]^{1/2} \qquad [168]$$

The latest version of the SCT method is limited to treatment of tunneling for the ground vibrational state with harmonic treatment of vibrations. In this case, we use the shorthand notation $t_m(n_m = 0, s) = t_m(s)$ for the ground-state turning points.

In the original SCT method, we assumed that all modes were extended to their turning points along the tunneling path, and this led to unphysically large

tunneling correction factors for reactions with many vibrational modes coupled to the reaction coordinate motion. The final version of SCT, called the centrifugal-dominant small-curvature approximation in the original publication,[3] assumes that the corner cutting occurs in the direction along the vector of coupling components $B_F(s)$ in the space of the local vibrational coordinates Q. We make a local rotation of the vibrational axes so that $B_F(s)$ lies along one of the axes, u_1, and by construction, the curvature coupling in all other vibrational coordinates, u_i, $i = 2$ to $F-1$, are zero in this coordinate system. The effective harmonic potential for the u_1 vibrational mode is written as

$$V = V_{MEP}(s) + \frac{1}{2}\mu[\bar{\omega}(s)]^2 u_1^2 \qquad [169]$$

where the harmonic frequency for this motion is given by

$$\bar{\omega} = \left(\sum_{m=1}^{F-1} \left[\frac{B_{m,F}(s)}{\kappa(s)} \omega_m(s) \right]^2 \right)^{\frac{1}{2}} \qquad [170]$$

The turning point $\bar{t}$ for zero-point motion in this harmonic potential takes the form

$$\bar{t} = \left[\frac{\hbar}{\mu\bar{\omega}(s)} \right]^{\frac{1}{2}} = \left(\sum_{m=1}^{F-1} \left[\frac{B_{m,F}(s)}{\kappa(s)} \right]^2 [t_m(s)]^{-4} \right)^{-\frac{1}{4}} \qquad [171]$$

The Jacobian factor $d\xi/ds$ for the path defined by these turning points is expressed in terms of the curvature and turning points by

$$d\xi/ds = \left\{ [1 - \bar{a}(s)]^2 + (d\bar{t}/ds)^2 \right\}^{\frac{1}{2}} \qquad [172]$$

where

$$\bar{a} = |\kappa(s)\, \bar{t}(s)| \qquad [173]$$

This expression has a singularity when the turning point is equal to the radius of curvature and is unphysical for values that are larger; i.e., $\bar{t} \geq 1/\kappa$. The problem can be solved by using an exponential form, in which case the effective mass for the SCT method is written as

$$\mu_{eff}^{SC}/\mu = \min \begin{cases} \exp\left\{-2\bar{a}(s) - [\bar{a}(s)]^2 + (d\bar{t}/ds)^2\right\} \\ 1 \end{cases} \qquad [174]$$

From the above expression, it is clear that $\mu_{eff}^{SC} \leq \mu$, and therefore, the transmission coefficients obtained by the small-curvature approximation are always equal to or larger than the zero-curvature transmission factors. As shown, if

the curvature along the reaction path is small or intermediate, it is possible to treat tunneling, without explicit evaluation of the tunneling path, by using an effective mass, which is a function of the reaction path curvature.

Large Curvature Transmission Coefficient

The SCT method is appropriate for use in reactions with small reaction path curvature. For systems with intermediate to large tunneling, the large-curvature tunneling methods[1,3,7,91,105–110,120,121] have been developed that build on the adiabatic approach, but they go beyond it to include important features affecting tunneling in large-curvature systems. The first important feature is that the tunneling paths are straight-line paths that connect the reactant and the product valleys of the reaction. A straight-line path is the shortest possible path between turning points in the reactant and product valleys, but the effective potential along this path is no longer the adiabatic potential and it can have a maximum that is larger than the adiabatic barrier maximum. Shortening the path decreases the tunneling integral, thus increasing the tunneling probability, while increasing the potential does the opposite. The optimal tunneling paths for large-curvature systems are often straight-line paths because the effect of shortening the tunneling path dominates for these systems. The second important feature is nonadiabatic tunneling, which is the possibility of tunneling into excited states for exoergic reactions or the possibility of tunneling from excited states for endoergic reactions. Finally, the straight-line tunneling paths go through regions of the PES, which are far from the MEP. We call this region the reaction swath. In this section, we start by describing the large-curvature tunneling method for systems dominated by tunneling from/to the ground vibrational states of reactants/products. We then describe how vibrationally excited states are included in the calculations and the general procedure to evaluate the LCG4 tunneling probabilities.[110] Finally, we describe how to carry out these calculations by sampling the reaction swath efficiently.[120,121]

At this point, it may be helpful to make some comments about how excited states enter the tunneling calculations. First consider the zero-curvature approximation. Here both the transverse vibrational and the rotational quantum numbers are conserved in the tunneling region, and the process is vibrationally adiabatic.[54] Next consider the small-curvature approximation. This is not really adiabatic because the tunneling path is affected by reaction path curvature, which is a manifestation of coupling to transverse modes.[116] Nevertheless, when we calculate a ground-state-to-ground-state process by the SCT approximation, we do not actually assume that the reactants and products are in the ground states.[122] What we assume is that the system tunnels in the ground level of the quantized transition state.[123] Outside the tunneling region, the transverse quantum numbers may be vibrationally adiabatic, and probably they are vibrationally nonadiabatic whenever there are

low-frequency modes; in addition, the process is probably usually rotationally nonadiabatic.[122,123] But in the dynamical bottleneck region where tunneling occurs, the transverse modes conserve their quantum number, or at least they are assumed to do so.

Next consider the large-curvature approximation. Here one cannot even assume that the transverse quantum numbers of high-frequency modes are conserved even during the tunneling process itself.[124] One cannot describe the wave function in the strong-interaction region, where tunneling occurs, in terms of asymptotic or adiabatic modes; instead one uses a diabatic representation in which all nonadiabaticity is associated with a single diabatic mode, which correlates more than one asymptotic mode of the product. This yields a recipe for calculating a realistic tunneling probability. To explain the algorithm, we will first consider the case where all quantum numbers are considered, even for this one diabatic mode; this case is treated in the Subsection below. Then we consider the case where tunneling proceeds in part into vibrationally excited levels of the product.

Large-Curvature Tunneling Without Vibrational Excitations

As stated, the large-curvature tunneling (LCT) methods use the ground-state vibrationally adiabatic potential to define classical reaction-coordinate turning points for a total energy E by inverting the equation

$$V_a^G(s_i) = E, i = 0, 1 \qquad [175]$$

to obtain $s_0(E)$ and $s_1(E)$, which are the turning points in the reactant and product valleys, respectively. One major departure from the adiabatic theory is that tunneling at total energy E is not initiated just from the reactant classical turning points at $s_0(E)$, but it occurs all along the entrance channel up to the turning point. Another departure is that tunneling occurs along straight-line tunneling paths connecting the reactant and product valleys, rather than the curvilinear path defined by the reaction path, vibrational turning points, and curvature couplings. Finally, tunneling is assumed to be initiated by vibrational motions perpendicular to the reaction coordinate rather than motion along the reaction coordinate.

The end points of the tunneling paths in the reactant and product valleys are defined as $\tilde{s}_0$ and $\tilde{s}_1$, and they obey the resonance condition

$$V_a^G(\tilde{s}_0) = V_a^G(\tilde{s}_1) \qquad [176]$$

This expression provides a relationship between $\tilde{s}_0$ and $\tilde{s}_1$ so that either one or the other is an independent variable. Unless stated otherwise, we use $\tilde{s}_0$ as the independent variable, and when $\tilde{s}_1$ appears, its dependence on $\tilde{s}_0$ is implicit. The tunneling path is a straight-line path in mass-scaled Cartesian coordinates defined by

$$\mathbf{x}(\xi, \tilde{s}_0) = \mathbf{x}_{RP}(\tilde{s}_0) + \xi\, \hat{\boldsymbol{\eta}}(\tilde{s}_0) \qquad [177]$$

where ξ denotes the progress variable along the linear path. The unit vector along the tunneling path is defined by

$$\hat{\boldsymbol{\eta}}(\tilde{s}_0) = \frac{\mathbf{x}_{RP}(\tilde{s}_1) - \mathbf{x}_{RP}(\tilde{s}_0)}{\xi_P} \qquad [178]$$

where $\mathbf{x}_{RP}(\tilde{s}_0)$ and $\mathbf{x}_{RP}(\tilde{s}_1)$ are mass-weighted Cartesian coordinates at the termini of the tunneling path, which lie on the reaction path at $\tilde{s}_0$ and $\tilde{s}_1$, respectively, and ξ_P is the length of the path

$$\xi_P = |\mathbf{x}_{RP}(\tilde{s}_1) - \mathbf{x}_{RP}(\tilde{s}_0)| \qquad [179]$$

so that ξ equals the distance from $\mathbf{x}_{RP}(\tilde{s}_0)$ along the path. For simplicity of notation, we do not explicitly show the dependence of ξ_P on $\tilde{s}_0$. To avoid confusion with coordinates along the straight-line tunneling paths, $\mathbf{x}(\xi, \tilde{s}_0)$, we use the notation $\mathbf{x}_{RP}(s)$ to denote mass-weighted Cartesian coordinates along the reaction path. The reaction path can be either the MEP or the variational reaction path.

The total tunneling amplitude along the incoming trajectory at energy E includes contributions from all tunneling paths initiated in the reactant valley

$$T_0(E) = \int_{-\infty}^{s_0(E)} d\tilde{s}_0 \, v_R^{-1}(E, \tilde{s}_0)\tau^{-1}(\tilde{s}_0)T_{tun}(\tilde{s}_0)\left|\sin\chi[\tilde{s}_0, \hat{\boldsymbol{\eta}}(\tilde{s}_0)]\right| \qquad [180]$$

The tunneling amplitude $T_{tun}(\tilde{s}_0)$ is weighted by the classical probability density $d\tilde{s}_0/v_R(E, \tilde{s}_0)$, which is proportional to the time spent between $\tilde{s}_0$ and $\tilde{s}_0 + d\tilde{s}_0$, by the number of collisions per unit time with the vibrational turning point in the tunneling direction, $\tau^{-1}(\tilde{s}_0)$, and by the sine of the angle $\chi[\tilde{s}_0, \hat{\boldsymbol{\eta}}(\tilde{s}_0)]$ between the vector tangent to the reaction path at $\tilde{s}_0$ and $\hat{\boldsymbol{\eta}}(\tilde{s}_0)$, which is a measure of how effectively the perpendicular vibrations initiate motion along the tunneling path. Tunneling can occur during the incoming and outgoing trajectory, so the total tunneling amplitude should be $2T_0(E)$. However, to enforce microscopic reversibility, the total tunneling amplitude is given by

$$T(E) = T_0(E) + T_1(E) \qquad [181]$$

where $T_1(E)$ is the tunneling amplitude for the outgoing trajectory in the product channel. The expression for $T_1(E)$ is similar to Eq. [180] except that we use $\tilde{s}_1$ as the independent variable instead of $\tilde{s}_0$ and the quantities $v_R(E, \tilde{s}_1)$, $\tau^{-1}(\tilde{s}_1)$, and $\chi[\tilde{s}_1, \hat{\boldsymbol{\eta}}(\tilde{s}_1)]$ are evaluated at locations along the reaction path in the product channel. The integrals in Eq. [180] and the analogous equation for $T_1(E)$ extend out to $s = \pm\infty$, but quantities along the reaction coordinate needed to evaluate the integrand are available on a grid that extends to finite values of s. Calculations of the tunneling amplitudes need to be converged with respect to the limits of the grid.

The local velocity for a point $\tilde{s}_i$ in the reactant channel ($i = 0$) or product channel ($i = 1$) is given by

$$v_R(E, \tilde{s}_i) = \left\{ \frac{2}{\mu} \left[E - V_a^G(\tilde{s}_i) \right] \right\}^{\frac{1}{2}}, i = 0, 1 \qquad [182]$$

The general expression for the angle $\chi[s, \hat{\eta}(\tilde{s}_i)]$ between the unit vector $\hat{\eta}(\tilde{s}_i)$ and the unit vector tangent to the reaction path at s is

$$\cos \chi[s, \hat{\eta}(\tilde{s}_i)] = \hat{\eta}(\tilde{s}_i) \cdot \frac{dx_{RP}/ds}{|dx_{RP}/ds|}, i = 0, 1 \qquad [183]$$

where $\chi[\tilde{s}_i, \hat{\eta}(\tilde{s}_i)]$, which is needed in the expressions for $T_0(E)$ and $T_1(E)$, is obtained by evaluating this expression at $s = \tilde{s}_i$. The vibrational period $\tau(\tilde{s}_i)$ is evaluated for the effective vibrational potential along the tunneling path. This effective potential is obtained by projecting the tunneling path onto the $(F - 1)$ vibrational modes perpendicular to the reaction path at $\tilde{s}_0$ and computing the potential along this projected straight-line path. In the harmonic approximation, the vibrational period reduces to

$$\tau(\tilde{s}_i) = \frac{2\pi}{\omega_\perp(\tilde{s}_i)}, i = 0, 1 \qquad [184]$$

where the harmonic frequency is expressed as

$$\omega_\perp(\tilde{s}_i) = \left\{ \sum_{m=1}^{F-1} [\omega_m(\tilde{s}_i) q_m(\tilde{s}_i)]^2 \right\}^{1/2}, i = 0, 1 \qquad [185]$$

and the components of unit vector along the projected path are given by

$$q_m(\tilde{s}_i) = \frac{\hat{\eta}(\tilde{s}_i) \cdot \mathbf{L}_m^{GT}(\tilde{s}_i)}{\left\{ \sum_{m'=1}^{F-1} \left[\hat{\eta}(\tilde{s}_i) \cdot \mathbf{L}_m^{GT}(\tilde{s}_i) \right]^2 \right\}^{\frac{1}{2}}}, i = 0, 1 \qquad [186]$$

where the eigenvectors are defined in Eq. [92]. Again, the sign of q_m depends on the "sign" of the vector $\mathbf{L}_m^{GT}$, but it is not an issue because we use the harmonic approximation.

The tunneling amplitude for each straight-line path is approximated using a primitive semiclassical expression

$$T_{tun}(\tilde{s}_0) = T_{tun}(\tilde{s}_1) = \exp[-\theta(\tilde{s}_0)], i = 0, 1 \qquad [187]$$

where the action integral along the linear path is

$$\theta(\tilde{s}_0) = \frac{(2\mu)^{\frac{1}{2}}}{\hbar}\left(\int_0^{\xi_I} d\xi\left\{V_a^G[s_I(\xi,\tilde{s}_0)] - V_a^G(\tilde{s}_0)\right\}^{\frac{1}{2}} \cos\chi[s_I(\xi,\tilde{s}_0),\hat{\boldsymbol{\eta}}(\tilde{s}_0)]\right.$$
$$+\int_{\xi_I}^{\xi_{III}} d\xi\,\left[V_{eff}^{II}(\xi,\tilde{s}_0) - V_a^G(\tilde{s}_0)\right]^{\frac{1}{2}}$$
$$\left.+\int_{\xi_{III}}^{\xi_P} d\xi\left\{V_a^G[s_{III}(\xi,\tilde{s}_0)] - V_a^G(\tilde{s}_0)\right\}^{\frac{1}{2}} \cos\chi\left[s_{III}(\xi,\tilde{s}_0),\hat{\boldsymbol{\eta}}(\tilde{s}_0)\right]\right) \qquad [188]$$

where for simplicity the dependence of the integration limits on $\tilde{s}_0$ are not explicitly shown. The intervals $[0, \xi_I]$ and $[\xi_{III}, \xi_P]$ along the tunneling path indicate the reactants region (labeled as I) and the products region (labeled as III), respectively. Regions I and III are called adiabatic because contributions to the action integral can be constructed from the information along the reaction path and the adiabatic potential. In these adiabatic regions, the system tunnels through the adiabatic barrier and the tunneling direction is along the reaction coordinate. Therefore, the contribution to the action integral in these regions is weighted by projections of the tunneling path along the reaction path, which are given by the cos χ factors. In the nonadiabatic region $[\xi_I, \xi_{III}]$, the tunneling is along the straight-line tunneling path and uses an effective potential, which is described below, in calculation of the contribution from this region to the action integral.

The vibrational adiabatic potential that enters Eq. [188] requires determination of s for geometry $\mathbf{x}(\xi,\tilde{s}_0)$ along the tunneling path. The value of s is defined such that the vector between the geometry along the reaction path $\mathbf{x}_{RP}(s)$ and the geometry along the linear tunneling path $\mathbf{x}(\xi,\tilde{s}_0)$ is perpendicular to the gradient at that s value:

$$[\mathbf{x}(\xi,\tilde{s}_0) - \mathbf{x}_{RP}(s)]\cdot\frac{d\mathbf{x}_{RP}}{ds} = 0 \qquad [189]$$

However, this equation may have multiple solutions. We are interested in two sets of solutions that make s a continuous function of ξ. The first solution $s_I(\xi,\tilde{s}_0)$ is obtained by starting in reactants with $\xi = 0$, where $s_I(\xi = 0, \tilde{s}_0) = \tilde{s}_0$, and then performing a root search for s at $\Delta\xi$, with $s_I(\xi = 0,\tilde{s}_0)$ as the initial guess for the root search. The procedure is iterated for $\xi + \Delta\xi$ using $s_I(\xi,\tilde{s}_0)$ as the initial guess for the root search to construct a single-valued and continuous function $s_I(\xi,\tilde{s}_0)$. A second solution $s_{III}(\xi,\tilde{s}_0)$ is found by starting in products with $\xi = \xi_P$, where $s_{III}(\xi = \xi_P,\tilde{s}_0) = \tilde{s}_1$ and iteratively decreasing ξ to find a solution starting from the product channel. Once the value of s is

found, it is possible to define the generalized normal mode coordinates $Q_m[s_i(\xi,\tilde{s}_0)], i = \text{I or III}$, by the relation

$$Q_m[s_i(\xi,\tilde{s}_0)] = \{\mathbf{x}(\xi,\tilde{s}_0) - \mathbf{x}_{RP}[s_i(\xi,\tilde{s}_0)]\} \cdot \mathbf{L}_m^{GT}[s_i(\xi,\tilde{s}_0)], i = \text{I or III} \quad [190]$$

and therefore, at every point along the linear path located in regions I or III, it is possible to assign a unique set of local normal modes.

Next we discuss how the boundaries between the adiabatic and nonadiabatic regions are determined. We begin by defining a zeroth-order estimate of the boundaries on the reactant side, ξ_I^0. A given geometry $\mathbf{x}(\xi,\tilde{s}_0)$ lies within this boundary (i.e., $\xi < \xi_I^0$) if all three of the following conditions are met: (1) The value of $s_I(\xi,\tilde{s}_0)$ calculated by Eq. [189] has to be smaller than $\tilde{s}_1$:

$$s_I(\xi,\tilde{s}_0) < \tilde{s}_1 \text{ for } \xi < \xi_I^0 \quad [191]$$

(2) All generalized normal mode coordinates are within their vibrational turning points

$$\left|Q_m[s_I(\xi,\tilde{s}_0)]\right| \leq \left|t_m[s_I(\xi,\tilde{s}_0)]\right| \text{ for } \xi < \xi_I^0 \quad [192]$$

where the turning points are defined in Eq. [167] but taking $n_m = 0$.
(3) The geometry $\mathbf{x}(\xi,\tilde{s}_0)$ lies within a single-valued region of the curvilinear coordinates; i.e.,

$$-\sum_{m=1}^{F-1} B_{mF}[s_I(\xi,\tilde{s}_0)]Q_m[s_I(\xi,\tilde{s}_0)] < 1 \text{ for } \xi < \xi_I^0 \quad [193]$$

where the curvature components are defined in Eq. [164]. Note that $\mathbf{L}_m^{GT}$ occurs in the definition of both B_{mF} and Q_m so the sign cancels out and we don't have to worry about it here. Similarly, we define a zeroth-order estimate of boundaries on the product side, ξ_{III}^0, by the conditions:

$$s_{III}(\xi,\tilde{s}_0) > \tilde{s}_0 \text{ for } \xi > \xi_{III}^0 \quad [194]$$

$$\left|Q_m[s_{III}(\xi,\tilde{s}_0)]\right| \leq \left|t_m[s_{III}(\xi,\tilde{s}_0)]\right| \text{ for } \xi > \xi_{III}^0 \quad [195]$$

$$-\sum_{m=1}^{F-1} B_{mF}[s_{III}(\xi,\tilde{s}_0)]Q_m[s_{III}(\xi,\tilde{s}_0)] < 1 \text{ for } \xi < \xi_{III}^0 \quad [196]$$

The values of the zeroth-order boundaries are now used to determine the boundaries, ξ_I and ξ_{III}, in Eq. [188]. Two cases can arise, $\xi_I^0 < \xi_{III}^0$, in which the effective potential in Eq. [188] needs to be specified for the nonadiabatic region, and $\xi_I^0 \geq \xi_{III}^0$, in which the adiabatic regions overlap and the

nonadiabatic region does not exist. We discuss the latter case first. When the adiabatic regions overlap, the adiabatic potential in the interval $[\xi_{III}, \xi_I]$ is calculated as

$$\min\left\{V_a^G[s_I(\xi, \tilde{s}_0)], V_a^G[s_{III}(\xi, \tilde{s}_0)]\right\} \qquad [197]$$

For the case $\xi_I^0 < \xi_{III}^0$, we define a zeroth-order effective potential for region II

$$\begin{aligned} V_{eff}^{II,0}(\xi, \tilde{s}_0) = {} & V[\mathbf{x}(\xi, \tilde{s}_0)] + V_{corr}^{I}(\xi_I^0, \tilde{s}_0) \\ & + \frac{\xi - \xi_I^0}{\xi_{III}^0 - \xi_I^0}\left[V_{corr}^{III}(\xi_{III}^0, \tilde{s}_0) - V_{corr}^{I}(\xi_I^0, \tilde{s}_0)\right] \end{aligned} \qquad [198]$$

where the first term is the actual potential along the straight-line tunneling path. The other terms correct for zero-point energy in modes that are within their turning points at the boundaries. Within the harmonic approximation, they are given by

$$V_{corr}^{i}(\xi_i^0, \tilde{s}_0) = \frac{1}{2}\sum_{m=1}^{F-1}\left[\hbar\omega_m(s) - \mu\omega_m^2(s)Q_m^2(s)\right]_{s=s_i(\xi_i^0, \tilde{s}_0)}, i = \text{I or III} \qquad [199]$$

This zeroth-order effective potential is not guaranteed to match up smoothly with the adiabatic potential at the boundaries. To correct for this deficiency, another requirement is added to the three conditions above, namely, (4) the adiabatic potential should be greater than or equal to the zeroth-order effective potential at the boundary. The boundaries ξ_I and ξ_{III} of the nonadiabatic region (labeled as II in Figure 4) are thus defined by

$$\xi_i = \xi_i^0 \text{ if } V_a^G[s_i(\xi_i^0, \tilde{s}_0)] \geq V_{eff}^{II,0}(\xi_i^0, \tilde{s}_0), i = \text{I or III} \qquad [200]$$

otherwise the value of ξ_i is defined implicitly by extending the nonadiabatic region until

$$\begin{aligned} & V_a^G[s_i(\xi_i, \tilde{s}_0)] = V_{eff}^{II,0}(\xi_i, \tilde{s}_0) \\ & \text{for } V_a^G[s_i(\xi_i^0, \tilde{s}_0)] < V_{eff}^{II,0}(\xi_i^0, \tilde{s}_0),\ i = \text{I or III} \end{aligned} \qquad [201]$$

For the case where the adiabatic potential is larger than the effective potential, another correction is made to the effective potential. The difference in energy between the boundaries is due to anharmonicity, and therefore, we introduce nonquadratic corrections of the type

$$V_{anh}^{i}(\tilde{s}_0) = V_a^G[s_i(\xi_i, \tilde{s}_0)] - V_{eff}^{II,0}(\xi_i, \tilde{s}_0), i = \text{I or III} \qquad [202]$$

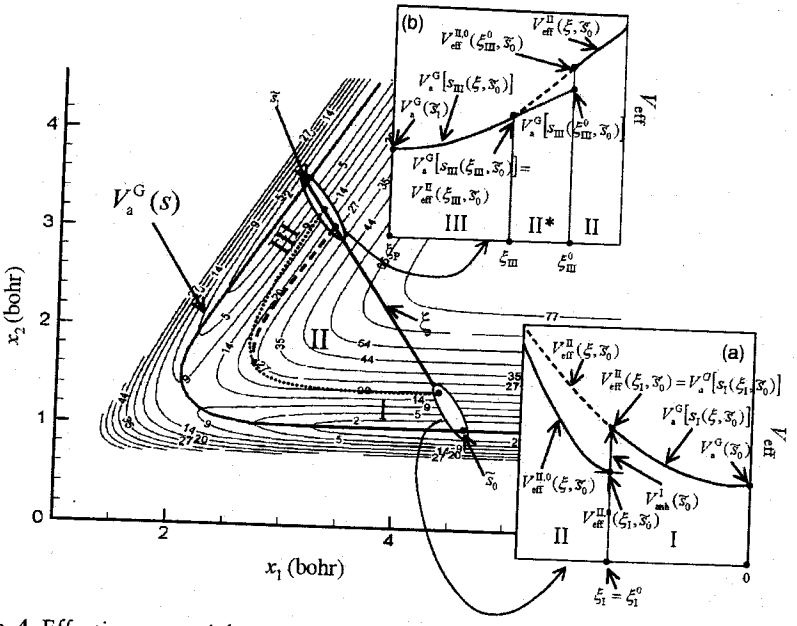

Figure 4 Effective potential contour plot of a reaction that illustrates some features of the LCG4 method for the evaluation of a linear path at a given tunneling energy. The linear path has a length ξ_P between the two classical turning points $\tilde{s}_0$ and $\tilde{s}_1$, and here we consider $n_p = 0$. The adiabatic region in the reactant side is labeled as I, the nonadiabatic LCG3 region is labeled as II, the nonadiabatic region that includes the condition given by Eq. [201] is labeled as II*, and the adiabatic region in the product side is labeled as III. The boundaries of the adiabatic region are indicated by a dotted line. The boundaries between the adiabatic and the nonadiabatic regions for the plotted linear path are zoomed in the squares labeled as (a) and (b). In the reactants side, we consider the case in which $V_a^G[s_I(\xi_I^0, \tilde{s}_0)] > V_{eff}^{II,0}(\xi_I, \tilde{s}_0)$, and in the products side, the opposite case is considered; i.e., $V_a^G[s_{III}(\xi_{III}^0, \tilde{s}_0)] > V_{eff}^{II,0}(\xi_{III}, \tilde{s}_0)$.

for the reactant channel ($i = I$) and for the product channel ($i = III$). With this correction, the effective potential is given by

$$V_{eff}^{II}(\xi, \tilde{s}_0) = V[\mathbf{x}(\xi, \tilde{s}_0)] + V_{corr}^{I}(\xi_I, \tilde{s}_0) + V_{anh}^{I}(\tilde{s}_0) + \frac{\xi - \xi_I}{\xi_{III} - \xi_I}\left[V_{corr}^{III}(\xi_{III}, \tilde{s}_0) - V_{corr}^{I}(\xi_I, \tilde{s}_0) + V_{anh}^{III}(\tilde{s}_0) - V_{anh}^{I}(\tilde{s}_0)\right] \quad [203]$$

Using the original boundaries ξ_I^0 and ξ_{III}^0 and zeroth-order effective potential $V_{eff}^{II,0}(\xi, \tilde{s}_0)$ and not imposing the addition condition (4) results in the LCG3 method,[3] whereas the use of the improved boundaries ξ_I and ξ_{III} and effective potential $V_{eff}^{II}(\xi, \tilde{s}_0)$ results in the LCG4 method.[110]

The tunneling amplitude $T(E)$ accounts for tunneling initiated by vibrational motion perpendicular to the reaction coordinate along the incoming and outgoing trajectories. There is also the probability that motion along the reaction coordinate can initiate tunneling at the classical turning point s_0 for the reaction coordinate motion. The amplitude for this tunneling contribution is $\exp\{-\theta[s_0(E)]\}\cos\chi\{s_0(E), \hat{\boldsymbol{\eta}}[s_0(E)]\}$ and for the reverse direction is $\exp\{-\theta[s_0(E)]\}\cos\chi\{s_1(E), \hat{\boldsymbol{\eta}}[s_0(E)]\}$. The total probability then becomes

$$P_{\text{prim}}^{\text{LCG4}}(E) = |T(E)|^2 + \left(\frac{\cos\chi\{s_0(E), \hat{\boldsymbol{\eta}}[s_0(E)]\} + \cos\chi\{s_1(E), \hat{\boldsymbol{\eta}}[s_0(E)]\}}{2}\right)^2 \times \exp\{-2\theta[s_0(E)]\} \quad [204]$$

This primitive probability can be greater than one because of the integration of the amplitudes over the incoming and outgoing trajectories. Within the uniform semiclassical approximation, the probability should go to 1/2 at the barrier maximum and we enforce this by the uniform expression in Eq. [205] for $E \leq V_a^{AG}$.[109]

$$P^{\text{LCG4}}(E) = \left\{1 + \frac{1}{2}\frac{\left[P_{\text{prim}}^{\text{LCG4}}(V_a^{AG})\right]^{-1} - 1}{P_{\text{prim}}^{\text{LCG4}}(V_a^{AG})} P_{\text{prim}}^{\text{LCG4}}(E)\right\} \times \frac{1}{1 + \left[P_{\text{prim}}^{\text{LCG4}}(E)\right]^{-1}} \quad [205]$$

This expression reduces to the primitive probability $P_{\text{prim}}^{\text{LCG4}}$ when it is sufficiently small and goes to 1/2 at the barrier maximum, V_a^{AG}. We use an expression analogous to Eq. [153] to extend the uniform probabilities to energies above the barrier.

Large-Curvature Tunneling with Vibrational Excitations

As we mentioned, exoergic reactions can have tunneling into excited states and endoergic reactions can have tunneling from excited states. To simplify the description of the LCG4 tunneling method, we only consider calculations of the tunneling correction factor for the exoergic direction. However, we construct the tunneling correction factor to obey detailed balance, so the tunneling correction factor for the endoergic reaction is the same. Tunneling is assumed to populate excited states of a single receptor mode p in the product channel. The p mode is a linear combination of the generalized transition-state vibrational modes along the reaction coordinate. We provide a description of how this mode is defined below. The primitive probability is obtained by summing over final states with the vibrational quantum number n_p of the LCG4 receptor vibrational mode

$$P_{n_{\max}}^{\text{LCG4}}(E) = \sum_{n_p=0}^{n_{\max}} P_{\text{prim}}^{\text{LCG4}}(E, n_p) \quad [206]$$

where n_{max} is the maximum value of n_p for which the primitive probabilities are included in the sum. $P^{LCG4}_{n_{max}}(E)$ is calculated for values of n_{max} from 0 to $N_p^{max}(E)$, which is defined below, and used in an expression similar to Eq. [205] to obtain a uniform expression for each n_{max}. Although $P^{LCG4}_{n_{max}}(E)$ increases monotonically with increasing n_{max}, the uniform expression may not, and so we choose the value of n_{max} that gives the maximum value:

$$P^{LCG4}(E) = \max_{n_{max}} \left\{ 1 + \frac{1}{2} \frac{\left[P^{LCG4}_{n_{max}}(V_a^{AG})\right]^{-1} - 1}{P^{LCG4}_{n_{max}}(V_a^{AG})} P^{LCG4}_{n_{max}}(E) \right\} \times \frac{1}{1 + \left[P^{LCG4}_{n_{max}}(E)\right]^{-1}} \quad [207]$$

Details of the methods for calculating $P^{LCG4}_{prim}(E, n_p)$ for $n_p = 0$ are described above. Calculation of $P^{LCG4}_{prim}(E, n_p)$ for excited states requires (1) definition of the p mode, (2) definition of $N_p^{max}(E)$, and (3) description of how calculation of the primitive tunneling probability is modified for $n_p \neq 0$.

Mode p, also called the quasiadibatic or receptor mode, is given by the projection of the $F-1$ normal modes on the straight-line tunneling path. Recall that for $n_p = 0$, a unique tunneling path is defined for each starting point for tunneling in the reactant channel, $\tilde{s}_0$. The tunneling vector given by Eq. [178] and the ending point for tunneling in the product channel, $\tilde{s}_1(\tilde{s}_0)$, is determined by the resonance condition in Eq. [176], where we now explicitly show the dependence of $\tilde{s}_1$ on $\tilde{s}_0$. For excited states, $n_p \neq 0$, the ending point of the tunneling path in the product channel depends on n_p; that is, $\tilde{s}_1(\tilde{s}_0)$ is replaced by $\tilde{s}_1(\tilde{s}_0, n_p)$. The resonance condition defining $\tilde{s}_1(\tilde{s}_0, n_p)$ requires calculation of the adiabatic potential with excitation in the p mode, which in turn requires definition of the p mode. We start by defining the p mode for an arbitrary straight line path connecting a geometry along the reaction path at $\tilde{s}_0$ in the reactant region, $\mathbf{x}_{RP}(\tilde{s}_0)$, with a geometry along the reaction path at an arbitrary location s along the reaction path in the product channel, $\mathbf{x}_{RP}(s)$. The vector connecting these two points is

$$\mathbf{E}(\tilde{s}_0, s) = \mathbf{x}_{RP}(s) - \mathbf{x}_{RP}(\tilde{s}_0) \quad [208]$$

The normalized projection of this vector onto the normal modes at location s along the reaction coordinate defines the p mode for this straight-line path and is given by

$$q_{p,m}(s; \tilde{s}_0) = \frac{\mathbf{E}(\tilde{s}_0, s) \cdot \mathbf{L}_m^{GT}(s)}{\left\{ \sum_{m=1}^{F-1} \left[\mathbf{E}(\tilde{s}_0, s) \cdot \mathbf{L}_m^{GT}(s)\right]^2 \right\}^{\frac{1}{2}}} \quad [209]$$

The harmonic frequency for the p mode can be calculated as

$$\omega_p(s;\tilde{s}_0) = \left\{ \sum_{m=1}^{F-1} \left[\omega_m(s) q_{p,m}(s;\tilde{s}_0) \right]^2 \right\}^{\frac{1}{2}} \qquad [210]$$

This procedure is equivalent to orthogonalizing $\mathrm{E}(\tilde{s}_0, s)$ to the tangent to the reaction path at s and computing the harmonic frequency along the resulting direction decoupled from the other modes.

The ground-state adiabatic potential is used in the reactant channel for values of s up to the location s_*^{AG} of the maximum in the ground-state adiabatic potential curve. The classical turning point in the reactant channel for energy E, $s_0(E)$, is still defined by Eq. [175]. In the product channel, we define the excited-state vibrationally adiabatic potential curve with quantum number n_p for each initiation point $\tilde{s}_0$ by

$$V_{\mathrm{a}}^{\mathrm{g}}(n_p, s; \tilde{s}_0) = V_{\mathrm{a}}^{\mathrm{G}}(s) + n_p \hbar \omega_p(s; \tilde{s}_0) \qquad [211]$$

The product-side endpoint $\tilde{s}_1(\tilde{s}_0, n_p)$ of the tunneling path initiated at $\tilde{s}_0$ is defined by the resonance condition

$$V_{\mathrm{a}}^{\mathrm{g}}\left[n_p, \tilde{s}_1(\tilde{s}_0, n_p); \tilde{s}_0\right] = V_{\mathrm{a}}^{\mathrm{G}}(\tilde{s}_0) \qquad [212]$$

The classical turning point at energy E on the product side is then given by

$$s_1(E, n_p) = \tilde{s}_1\left[s_0(E), n_p\right] \qquad [213]$$

There can be more than one solution to these two equations. The functions $\tilde{s}_1(\tilde{s}_0, n_p)$ and $s_1(E, n_p)$ are defined as the largest of these solutions.

The integer $N_p^{\max}$ is the largest value of n_p that allows tunneling at energy E. As mentioned, the quantities needed in the LCG4 calculations are stored on a grid of s values ranging from s_- in reactants to s_+ in products. The smallest initiation point in the reactant channel for a tunneling path with excited state n_p in products is defined by

$$\tilde{s}_{0,\min}(n_p) = \max\left[s_-, s_{\min 1}(n_p)\right] \qquad [214]$$

where $s_{\min 1}(n_p)$ is the value of the initiation point in the reactant channel that connects to the last point on the grid:

$$s_+ = \tilde{s}_1\left[s_{\min 1}(n_p), n_p\right] \qquad [215]$$

With these definitions, $N_p^{\max}(E)$ is defined as the largest integer value of n_p that satisfies

$$V_a^g\left\{n_p, \tilde{s}_1\left[\tilde{s}_{0,\min}(n_p), n_p\right]; \tilde{s}_{0,\min}(n_p)\right\} \leq E \qquad [216]$$

This definition assumes that the excited-state adiabatic potential for values of s greater than $\tilde{s}_1[\tilde{s}_{0,\min}(n_p), n_p]$ are smaller than the adiabatic potential at this s value.

Calculation of the primitive probabilities for each value of n_p follows the same procedure as outlined in the previous section. A major difference arises because the straight-line tunneling paths are different for each excited state. Generalizations of Eqs. [177]–[179] are as follows:

$$\mathbf{x}(\xi, \tilde{s}_0, n_p) = \mathbf{x}_{RP}(\tilde{s}_0) + \xi\, \hat{\boldsymbol{\eta}}(\tilde{s}_0, n_p) \qquad [217]$$

$$\hat{\boldsymbol{\eta}}(\tilde{s}_0, n_p) = \frac{\mathbf{x}_{RP}[\tilde{s}_1(\tilde{s}_0, n_p)] - \mathbf{x}_{RP}(\tilde{s}_0)}{\xi_P(\tilde{s}_0, n_p)} \qquad [218]$$

$$\xi_P(\tilde{s}_0, n_p) = \left|\mathbf{x}_{RP}[\tilde{s}_1(\tilde{s}_0, n_p)] - \mathbf{x}_{RP}(\tilde{s}_0)\right| \qquad [219]$$

The expression for tunneling amplitude $T_0(E, n_p)$ has the same form as Eq. [180], with the terms in the integrand modified appropriately to include the dependence on n_p. The expression for $\nu_R(E, \tilde{s}_0)$ remains unchanged, whereas those for $\tau^{-1}(\tilde{s}_0, n_p)$ and $\chi[\tilde{s}_0, \hat{\boldsymbol{\eta}}(\tilde{s}_0, n_p)]$ are modified only because of the change in the angle between the tunneling path and the reaction path. Changes to $T_{tun}(\tilde{s}_0, n_p)$ are more substantial and are discussed in more detail below. The expression for the reverse amplitude $T_1(E, n_p)$ takes the form

$$T_1(E, n_p) = \int_{\tilde{s}_1(E,n_p)}^{\infty} d\tilde{s}_1\, \nu_R^{-1}(E, \tilde{s}_1, n_p)\tau^{-1}(\tilde{s}_1, n_p)T_{tun}[\tilde{s}_1, n_p]\left|\sin\chi[\tilde{s}_1, \hat{\boldsymbol{\eta}}(\tilde{s}_1)]\right| \qquad [220]$$

where we use $\tilde{s}_1$ as the independent variable in this case and the reactant side terminus of the tunneling path, $\tilde{s}_0(\tilde{s}_1, n_p)$, is defined by

$$V_a^g[n_p, \tilde{s}_1; \tilde{s}_0(\tilde{s}_1, n_p)] = V_a^G[\tilde{s}_0(\tilde{s}_1, n_p)] \qquad [221]$$

The product-channel velocity term has an explicit dependence on n_p because the excited-state adiabatic potential is used in its evaluation:

$$\nu_R(E, \tilde{s}_1, n_p) = \left(\frac{2}{\mu}\left\{E - V_a^g[n_p, \tilde{s}_1; \tilde{s}_0(\tilde{s}_1, n_p)]\right\}\right)^{\frac{1}{2}} \qquad [222]$$

As in the expression for $T_0(E, n_p)$, the quantities $\tau^{-1}(\tilde{s}_1, n_p)$ and $\chi[\tilde{s}_1, \hat{\boldsymbol{\eta}}(\tilde{s}_1, n_p)]$ are modified only because of the change in the angle between the tunneling

path and the reaction path. Finally, the tunneling amplitudes in the expressions for $T_0(E, n_p)$ and $T_1(E, n_p)$ are related by

$$T_{\text{tun}}(\tilde{s}_1, n_p) = T_{\text{tun}}[\tilde{s}_0(\tilde{s}_1, n_p), n_p] \tag{223}$$

so all that remains is a description of the modifications needed in calculating $T_{\text{tun}}(\tilde{s}_0, n_p)$.

The tunneling amplitude takes the form

$$T_{\text{tun}}(\tilde{s}_0, n_p) = \exp[-\theta(\tilde{s}_0, n_p)] \tag{224}$$

where the action integral in Eq. [188] is modified to read as

$$\begin{aligned}\theta(\tilde{s}_0, n_p) = \frac{(2\mu)^{\frac{1}{2}}}{\hbar}\Bigg(&\int_0^{\xi_{\text{I}}(\tilde{s}_0, n_p)} d\xi \left\{ V_{\text{a}}^{\text{G}}[s_{\text{I}}(\xi, \tilde{s}_0, n_p)] - V_{\text{a}}^{\text{G}}(\tilde{s}_0) \right\}^{\frac{1}{2}} \\ &\times \cos\chi\left[s_{\text{I}}(\xi, \tilde{s}_0, n_p), \hat{\boldsymbol{\eta}}(\tilde{s}_0, n_p)\right] \\ &+ \int_{\xi_{\text{I}}(\tilde{s}_0, n_p)}^{\xi_{\text{III}}(\tilde{s}_0, n_p)} d\xi \left[V_{\text{eff}}^{\text{II}}(\xi, \tilde{s}_0, n_p) - V_{\text{a}}^{\text{G}}(\tilde{s}_0) \right]^{\frac{1}{2}} \\ &+ \int_{\xi_{\text{III}}(\tilde{s}_0, n_p)}^{\xi_{\text{P}}(\tilde{s}_0, n_p)} d\xi \left\{ V_{\text{a}}^{\text{g}}[n_p, s_{\text{III}}(\xi, \tilde{s}_0, n_p); \tilde{s}_0] - V_{\text{a}}^{\text{G}}(\tilde{s}_0) \right\}^{\frac{1}{2}} \\ &\times \cos\chi[s_{\text{III}}(\xi, \tilde{s}_0, n_p), \hat{\boldsymbol{\eta}}(\tilde{s}_0, n_p)]\Bigg)\end{aligned} \tag{225}$$

where for clarity we explicitly show the dependence of the integration limits on $\tilde{s}_0$ and n_p. The major change for the action integral with an excited state in the product region is that the excited-state adiabatic potential is used in the product adiabatic region. Note that the resonance condition in Eq. [212] allows us to replace $V_{\text{a}}^{\text{G}}(\tilde{s}_0)$ by $V_{\text{a}}^{\text{g}}[n_p, \tilde{s}_1(\tilde{s}_0, n_p); \tilde{s}_0]$ if it is more convenient computationally. Evaluation of $s_i(\xi, \tilde{s}_0, n_p)$ proceeds by finding the solution to Eq. [189], as described in the previous section, except that the geometry along the straight-line tunneling path is replaced by $\mathbf{x}(\xi, \tilde{s}_0, n_p)$ as defined in Eq. [217].

Determination of the zeroth-order boundary $\xi_{\text{I}}^0(\tilde{s}_0, n_p)$ between adiabatic region I and the nonadiabatic region uses the same procedure as outlined in the three conditions provided in Eqs. [191]–[193], with appropriate modifications to include the n_p-dependence of the straight-line path. Determination of the zeroth-order boundary $\xi_{\text{III}}^0(\tilde{s}_0, n_p)$ between adiabatic region I and the nonadiabatic region uses Eqs. [194]–[195], with one further modification beyond the one to include the n_p-dependence of the straight-line path. The turning points for the vibrational modes in the product region should include the effect of the excitation in the p mode. The excitation energy $n_p\hbar\omega_p(s; \tilde{s}_0)$ in Eq. [211]

is partitioned into all $F-1$ normal modes. Each of the m modes gets an energy that is given by

$$\Delta E_m(s;\tilde{s}_0,n_p) = n_p\hbar\omega_p(s;\tilde{s}_0)\frac{[\omega_m(s)q_{p,m}(s;\tilde{s}_0)]^2}{[\omega_p(s;\tilde{s}_0)]^2} \qquad [226]$$

so the energy of the generalized normal mode m is given by

$$E_m(s;\tilde{s}_0,n_p) = \frac{1}{2}\hbar\omega_m(s) + \Delta E_m(s;\tilde{s}_0,n_p) \qquad [227]$$

The harmonic turning point needed in the modified version of Eq. [195] is evaluated at $s = s_{III}(\xi,\tilde{s}_0,n_p)$ and is given by

$$t_{p,m}[s_{III}(\xi,\tilde{s}_0,n_p);\tilde{s}_0,n_p] = \pm\left(\frac{\hbar}{\mu\omega_m[s_{III}(\xi,\tilde{s}_0,n_p)]} + 2\frac{\Delta E_m[s_{III}(\xi,\tilde{s}_0,n_p);\tilde{s}_0,n_p]}{\{\mu\omega_m[s_{III}(\xi,\tilde{s}_0,n_p)]\}^2}\right)^{\frac{1}{2}} \qquad [228]$$

Once the values for $\xi_I^0(\tilde{s}_0,n_p)$ and $\xi_{III}^0(\tilde{s}_0,n_p)$ are determined for a given $\tilde{s}_0$ and n_p, they are used in the definition of $\xi_I(\tilde{s}_0,n_p)$ and $\xi_{III}(\tilde{s}_0,n_p)$ using the general approach described in Eqs. [197]–[201]. For the case that the adiabatic regions overlap, i.e., $\xi_I^0(\tilde{s}_0,n_p) \geq \xi_{III}^0(\tilde{s}_0,n_p)$, we set the adiabatic potential in the interval $[\xi_{III}(\tilde{s}_0,n_p),\xi_I(\tilde{s}_0,n_p)]$ as

$$\min\left\{V_a^G[s_I(\xi,\tilde{s}_0,n_p)],V_a^g[n_p,s_{III}(\xi,\tilde{s}_0,n_p);\tilde{s}_0]\right\} \qquad [229]$$

For the case that $\xi_I^0(\tilde{s}_0,n_p) < \xi_{III}^0(\tilde{s}_0,n_p)$, we define the zeroth-order effective potential $V_{eff}^{II,0}(\xi,\tilde{s}_0,n_p)$ by the same form as Eq. [198], with modification to include the n_p-dependence of the tunneling path. $V_{corr}^I(\xi_I^0,\tilde{s}_0,n_p)$ is given by Eq. [199] noting that the right-hand side is evaluated at $s_I(\xi,\tilde{s}_0,n_p)$ and the correction potential at the region III boundary is now given by

$$V_{corr}^{III}(\xi_{III}^0,\tilde{s}_0,n_p) = \sum_{m=1}^{F-1}\left[E_m(s;\tilde{s}_0,n_p) - \frac{1}{2}\mu\omega_m^2(s)Q_m^2(s)\right]_{s=s_{III}(\xi_{III}^0,\tilde{s}_0,n_p)} \qquad [230]$$

The boundary $\xi_I(\tilde{s}_0,n_p)$ is defined by modified forms of Eqs. [200] and [201], whereas for $\xi_{III}(\tilde{s}_0,n_p)$, these conditions are modified to read as follows:

$$\xi_{III}(\tilde{s}_0,n_p) = \xi_{III}^0(\tilde{s}_0,n_p)$$
$$\text{for } V_a^g[n_p,s_{III}(\xi_{III}^0,\tilde{s}_0,n_p);\tilde{s}_0] \geq V_{eff}^{II,0}(\xi_{III}^0,\tilde{s}_0,n_p) \qquad [231]$$

and

$$V_a^g[n_p, s_{III}(\xi_{III}, \tilde{s}_0, n_p); \tilde{s}_0] = V_{eff}^{II,0}(\xi_{III}, \tilde{s}_0, n_p)$$
$$\text{for } V_a^g[n_p, s_{III}(\xi_{III}^0, \tilde{s}_0, n_p); \tilde{s}_0] < V_{eff}^{II,0}(\xi_{III}^0, \tilde{s}_0, n_p) \quad [232]$$

Once the boundaries $\xi_I(\tilde{s}_0, n_p)$ and $\xi_{III}(\tilde{s}_0, n_p)$ are determined, the effective potential is defined by modification to Eq. [203], where the anharmonic potential on the reactant side $V_{anh}^I(\tilde{s}_0, n_p)$ is given by modifying Eq. [202] to include n_p-dependence of the straight-line path and the n_p-dependent zeroth-order effective potential, and on the product side, it is replaced by

$$V_{anh}^{III}(\tilde{s}_0, n_p) = V_a^g[n_p, s_{III}(\xi_{III}, \tilde{s}_0, n_p); \tilde{s}_0] - V_{eff}^{II,0}(\xi_{III}, \tilde{s}_0, n_p) \quad [233]$$

One final modification is needed in the treatment of excited states in the LCG4 calculations. With $T_0(E, n_p)$ and $T_1(E, n_p)$ obtained with the procedures defined above, the primitive semiclassical probability for state n_p is given by the following modification to Eq. [204]:

$$P_{prim}^{LCG4}(E, n_p) = |T_0(E, n_p) + T_1(E, n_p)|^2 + \delta_{n_p,0}\left(\frac{\cos\chi\{s_0(E), \hat{\eta}[s_0(E), n_p]\} + \cos\chi\{s_1(E, n_p), \hat{\eta}[s_0(E), n_p]\}}{2}\right)^2 \times \exp\{-2\theta[s_0(E), n_p]\} \quad [234]$$

where the tunneling contribution from motion along the reaction coordinate initiated at the classical turning point, which is accounted for in the last term, is an adiabatic process and therefore only contributes to $n_p = 0$.

Practical Methods to Evaluate LCT Transmission Coefficients

The action integral in Eq. [225] can be evaluated by standard numerical integration procedures, and about 180 points along the linear path are needed to get full convergence in a typical case. Some of those points may correspond to the nonadiabatic region, for which information in the reaction swath is needed. In addition, calculation of the transmission coefficient with the above procedure has to be repeated at many tunneling energies, of the order of 80 energies, and it is not unusual to have to calculate several hundreds of energies along the linear path, which cannot be extrapolated from information about the MEP. These large numbers of single-point energy calculations can make evaluation of the LCT probabilities directly from ab initio data expensive.

One way of reducing the computational cost is to interpolate some of the energies along the linear path by a spline under tension rather than computing

them all directly. If at a given tunneling energy E_i we have to evaluate a set of energies along the linear path $\{\xi_1, \ldots, \xi_j, \ldots, \xi_{N_T}\}$, where N_T can be for instance 180, we may have a subset $\{\xi_I, \ldots, \xi_{III}\}$ of points in the nonadiabatic region, which points cannot be extrapolated from the MEP (in this section, we assume $n_p = 0$ for clarity). We can pick up a given number N_{na} of equally spaced points in this subset and calculate all others by spline under tension interpolation. This procedure can be repeated for each of the $\{E_1, \ldots, E_i, \ldots, E_{M_T}\}$ tunneling energies, with M_T being the total number of tunneling energies needed to evaluate the transmission factor (a common value is $M_T = 80$). This algorithm is called one-dimensional spline interpolation large curvature tunneling [ILCT(1D)], and in general, with a value of $N_{na} = 9$, it is possible to get converged transmission coefficients with an error smaller than 4%.[120] This algorithm reduces the computational cost of the LCT transmission coefficients by about a factor of 5.

Another possibility is to consider the $M_T \times N_T$ grid and to interpolate not only the points along the linear path but also the tunneling energies. Of the whole set of energies $\{E_1, \ldots, E_i, \ldots, E_{M_T}\}$, we take a subset $\{E_1, \ldots, E_i, \ldots, E_M\}$, where E_1 is the same in both sets, specifically the lowest energy at which tunneling is possible, and $E_{M_T} = E_M$ coincides with the top of the vibrationally adiabatic barrier V_a^{AG}. The difference is that the second subset includes only M equally spaced energies of the total M_T energies. At this particular set of energies, we also build a subset $\{\xi_1, \ldots, \xi_{j'}, \ldots, \xi_N\}$ of the $\{\xi_1, \ldots, \xi_j, \ldots, \xi_{M_T}\}$ original set of progress variables where ξ_1 is the same in both sets and $\xi_{N_T} = \xi_N = \xi_P$, but as before, the second subset includes only N equally spaced points instead of the total N_T points. The subsets are built in this way because when squared, the $M \times N$ and $M_T \times N_T$ grids have the same boundaries. In fact the $M \times N$ grid is transformed in a unitary square by performing the following scaling:

$$\bar{E}_{i'} = \frac{E_{i'} - E_1}{E_M - E_1} \quad \text{and} \quad \bar{\xi}_{j'} = \frac{\xi_{j'}}{\xi_{P,j'}} \tag{235}$$

where $i' = 1, \ldots, M$ and $j' = 1, \ldots, N$. The grid is interpolated using a two-dimensional spline under tension algorithm, and so this method is usually call ILCT(2D).[121] Any given geometry specified by (E_i, ξ_i) and that belongs to the $M_T \times N_T$ grid can be retrieved from the $M \times N$ grid by interpolation, because any geometry that belongs to the first grid belongs also to the second one. It has been shown for the reaction of the CF_3 radical with several hydrocarbons that the ILCT(2D) algorithm produces converged results with a relative error of less than 1% using a 9×11 grid with respect to the LCG4 full calculation (80×180 grid). Due to the good performance of the ILCT(2D) algorithm, we highly recommend its use for the evaluation of the LCG4 transmission factors.

The Microcanonically Optimized Transmission Coefficient

For a bimolecular reaction of the type A + BC → AB + C, where A, B, and C may be atoms or groups of atoms, the reaction path curvature is a function of the skew angle, which is the angle between the gradient of V along the reaction path in the product channel and the gradient of V along the reaction path in the reactant channel. If we consider isoinertial coordinates, the skew angle is defined by

$$\beta = \cos^{-1}\left(\frac{m_A m_C}{(m_A + m_B)(m_B + m_C)}\right)^{1/2} \qquad [236]$$

and it is related to the reaction path curvature by

$$\left[\int_{-\infty}^{+\infty} \kappa(s)ds\right] \cdot \frac{d\mathbf{x}^R}{ds} = \left(\frac{d\mathbf{x}^P}{ds} - \frac{d\mathbf{x}^R}{ds}\right) \cdot \frac{d\mathbf{x}^R}{ds} = -(1 + \cos\beta) \qquad [237]$$

where $\mathbf{x}^P$ and $\mathbf{x}^R$ are the geometries in the reactant and product valleys, respectively. The skew angle is close to $\pi/2$ when B has a much larger mass than A and C, and it is close to zero when B has a much smaller mass than A and C. Small skew angles lead to large curvature. In Figure 5, two examples illustrate the curvature of the reaction path. For the reaction $H + H_2 \rightarrow H_2 + H$, the skew angle is $\beta = 60$ degrees (Figure 5a), whereas for reaction $Cl + HCl \rightarrow ClH + Cl$, the skew angle is only $\beta = 14$ degrees (Figure 5b). In general, for a bimolecular reaction, the curvature of the reaction path is large when a light particle (like a proton) is being transferred between two heavy

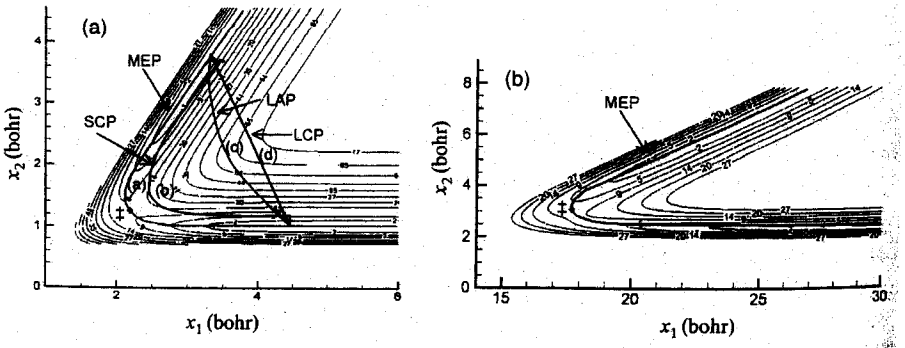

Figure 5 Contour plots in Jacobi coordinates for (a) $H + H_2 \rightarrow H_2 + H$ and (b) $Cl + HCl \rightarrow ClH + Cl$ reactions, respectively. The MEP is indicated in both figures to illustrate the larger curvature in the latter case. Figure (a) also shows other alternative tunneling paths (see text).

atoms, although this need not be the case for unimolecular reactions.[125] These systems are usually called heavy–light–heavy reactions, and we expect large tunneling effects in those cases. In fact, it is well known that the SC approximation may seriously underestimate tunneling for heavy–light–heavy systems, and therefore, we have to search for a better tunneling path.[102] Figure 5a shows a plot with four possible paths for a given tunneling energy E. The points on the MEP (labeled as $s_<$ and $s_>$) that correspond to a particular tunneling energy, in both the reactant and the product sides, are called classical turning points of reaction-coordinate motion, and they correspond to the limits of integration of Eq. [151]. The longest, but energetically more favorable path, is the MEP [labeled as (a) in Figure 5a], whereas the shortest path, but with the highest energy, corresponds to the straight-line path [labeled as (d) in Figure 5a]. In between there are an infinite number of paths that connect reactants to products at that particular tunneling energy (among them is the SC path, which is labeled as (b) in Figure 5a). Among all the possible paths, we have to find the one that has the largest tunneling probability, which is equivalent to finding the path that, for the correct boundary conditions, minimizes the action [labeled as (c)], i.e., the so-called least-action path (LAP).[102,124,126,127] Tunneling calculations based on the LAP are called least-action tunneling (LAT). Some approximate methods try to find the LAP without its explicit evaluation,[128] because the search for the LAP is often unaffordable or not worth the cost for polyatomic systems. One way to circumvent this problem is to evaluate the probability along the straight-line path, which is the kind of path[3,108,129–131] that dominates in the large-curvature limit and is usually called the large-curvature path (LCP). We can compute both the SCT and the LCT (the T in the acronym stands for tunneling) probabilities, the first being accurate for small-to-intermediate curvature, whereas the second is accurate for intermediate-to-large curvature (and also often reasonably accurate even for small-curvature). As the objective is to find the tunneling mechanism with the largest tunneling probability, an alternative to searching for the LAP is to choose between the maximum of the SCT and LCT probabilities. This new probability is called the microcanonically optimized multidimensional tunneling probability, $P^{\mu OMT}$, and it is given by[91]

$$P^{\mu OMT} = \max_E \begin{Bmatrix} P^{SCT}(E) \\ P^{LCT}(E) \end{Bmatrix} \qquad [238]$$

It has been shown that the μOMT transmission coefficients are comparable in accuracy with the LAT transmission coefficients for atom–diatom reactions.[103] Often we just say OMT without including the microcanonical specification in the algorithm (OMT can also mean canonical OMT in which we first thermally average the SCT and LCT probabilities and then choose the larger transmission coefficient). The resulting VTST/OMT rate constants

have been tested carefully against accurate quantum dynamics,[103,111,112] and the accuracy has been found to be very good.

Sometimes we just say VTST/MT. The MT acronym ("multi-dimensional tunneling") can denote ZCT, SCT, LCT, or OMT, all of which are multidimensional, but we usually use SCT or OMT when we carry out MT calculations.

BUILDING THE PES FROM ELECTRONIC STRUCTURE CALCULATION

For the vast majority of chemically interesting systems, a potential energy surface (PES) is not available. When this is the case, there are two options: Create an analytic potential energy function (PEF), or use direct dynamics.[62,118,132] The traditional route of creating an analytic high-level PEF requires considerable data (from electronic structure or experiment) and human development time. A new method called multiconfiguration molecular mechanics (MCMM),[133–135] which allows more straightforward creation of a PES from limited data, has recently been developed and is described below. For small to moderately sized systems where electronic structure gradients and Hessians are not overly expensive, direct dynamics is typically the method of choice.

Direct dynamics has been defined as "the calculation of rates or other dynamical observables directly from electronic structure information, without the intermediacy of fitting the electronic energies in the form of a potential energy function."[132] In this method, information about the PES is calculated by electronic structure methods as it is needed, i.e., "on the fly." For example, consider the calculation of the MEP using the steepest descent method. A Hessian calculation is done by electronic structure theory at the saddle point, and a step is taken in the direction of the imaginary frequency. At this new geometry, a gradient is requested, which is then calculated using electronic structure theory. That information is passed back to the MEP calculation, a step is taken in the direction of the gradient, and once again a gradient is requested at the new geometry. This iterative process continues until the MEP reaches the desired length, and then it is repeated for the other side of the MEP. In a CVT calculation, Hessians must also be calculated at several points along the path to determine the vibrationally adiabatic ground-state potential energy curve and free energy of activation profile for each value of s.

Achieving chemical accuracy by electronic structure calculations is computationally expensive, and the time required calculating a rate constant is governed almost entirely by the time spent calculating the gradients and Hessians. In addition, the accuracy of the rate constant depends on the accuracy of the electronic structure method. Therefore, the user must make judicious decisions about the length of the MEP, how often Hessians are calculated, whether to use options like LCT that require extra information about the PES, and which electronic structure method to use.

Direct dynamics calculations can be carried out by interfacing an electronic structure package with POLYRATE, and several such interfaces are available, including MORATE,[4,109,136] GAUSSRATE,[137] GAMESSPLUSRATE,[138] MULTILEVELRATE,[139] MC-TINKERATE,[140] and CHARMMRATE.[141]

A key point to be emphasized here is that using so-called "straight direct dynamics" may not be the most efficient approach.[142] In straight direct dynamics, whenever the dynamical algorithm requires a potential energy, a gradient, or a Hessian, it is calculated by a full electronic structure calculation. Such algorithmic purity provides one extreme on the spectrum that spans the range from straight direct dynamics to fitting a global potential energy function. However, there are several intermediate possibilities in this spectrum, corresponding to more economical ways of combining electronic structure theory and dynamics. As these algorithmic possibilities are fleshed out, it is not always possible to distinguish whether a calculation should be classified as fitting, as local interpolation (a form of direct dynamics), or as direct.[143] In fact, such classification is less important than the ability of the algorithm to reduce the cost for given level of accuracy and size of system, to allow for a given level of accuracy to be applied with affordable cost to larger systems, or to allow more complete dynamical treatments such as large-curvature tunneling, a more expensive treatment of anharmonicity, or a trajectory-based estimate of recrossing. This section will consider interpolation schemes as well as straight direct dynamics.

Direct Dynamics with Specific Reaction Parameters

Direct dynamics with specific reaction parameters (SRPs)[132] involves the use of an electronic structure method that has been adjusted to reproduce important data for a specific reaction, followed by determining the reaction rate using direct dynamics. The adjusted method is typically parameterized to agree with the correct forward barrier height and possibly also with one experimental or high-level energy of reaction, but it may actually be parameterized for any property that is important for the specific reaction, for example, the potential energy profile along the reaction path.[144]

When using experimental data, the barrier height is sometimes approximated by the activation energy, although this is not recommended because they may differ by several kcal/mol. High-level frequency calculations may be carried out for reactants and products, yielding an approximation to their zero-point energy and heat capacity, and these data may be used in combination with the experimental enthalpy of reaction to calculate a good approximation to estimate the Born–Oppenheimer energy of reaction. Alternatively, the barrier height and energy of reaction may be calculated from high-level electronic structure methods, such as a correlated wave function theory or density functional theory. Unfortunately such calculations, although often affordable for stationary points, may become prohibitively expensive

for direct dynamics due to the large number of gradients and Hessians required.

In the original application,[132] the SRP method was applied to the following reaction:

$$Cl^-(H_2O)_n + CH_3Cl' \rightarrow CH_3Cl + Cl'^-(H_2O)_n, \quad n = 0, 1, \text{ or } 2 \qquad [239]$$

In this particular example, a neglect of the diatomic differential overlap (NDDO)[145,146] method was created based on semiempirical molecular orbital theory, namely AM1.[147,148] The resulting method was referred to as NDDO-SRP. The adjusted parameters were the one-center, one-electron energies, $U_{\mu\mu}^X$, which were adjusted to achieve the correct electron affinity for Cl and the correct barrier height for the $n = 0$ reaction. The NDDO-SRP rate constants were compared with those calculated using an accurate PES; the errors for the CVT/SCT rate constants ranged from 39% at 200 K to 30% at 1000 K for the unsolvated complex. When considering the enormous amount of time required to create an accurate PES compared with the relatively fast SRP direct dynamics calculation, these results are very encouraging. The method also gave good results for the solvated reactions of Eq. [239], where $n = 1$ and $n = 2$.

Interpolated VTST

MCMM

Multiconfigurational molecular mechanics (MCMM)[133–135] is an algorithm that approximates a global PES by combining molecular mechanics (MM) with a limited number of energies, gradients, and Hessians based on quantum mechanics. (This is a special case of a dual-level strategy in which one combines a lower and a higher level.) MCMM is an extension of conventional MM (which is only applicable to nonreactive systems) to describe reaction potential energy surfaces. It extends the empirical valence bond method[149] so that it becomes a systematically improvable fitting scheme. This is accomplished by combining the rectilinear Taylor series method of Chang, Minichino, and Miller[150,151] for estimating V_{12} in the local region around a given geometry with the use of redundant internal coordinates[71,72] for the low-order expansion of the PES and the Shepard interpolation method.[152,153] The key to MCMM is the limited number of high-level quantum mechanical data required, because, whether or not one uses interpolation or MCMM, the vast majority of time required to calculate a rate constant is consumed by the electronic structure calculations. It has been shown that potential energy surfaces created using 13 or fewer Hessians can yield accurate rate constants.[134] Even greater efficiency can be achieved if one is certain that large-curvature tunneling paths need not be explored and/or if one uses partial high-level Hessians.[135]

In MCMM, the Born–Oppenheimer PES is estimated as being the lowest eigenvalue of the 2×2 potential matrix **V**:

$$\begin{vmatrix} V_{11} - V & V_{12} \\ V_{12} & V_{22} - V \end{vmatrix} = 0 \qquad [240]$$

where V_{11} corresponds to the molecular mechanics potential function associated with the well on the reactant side, V_{22} corresponds to the molecular mechanics potential function associated with the well on the product side, and V_{12} corresponds to resonance energy function or resonance integral.

The lowest eigenvalue $V(\mathbf{q})$ of the matrix in Eq. [240] at a given geometry, $\mathbf{q}$, is given by

$$V(\mathbf{q}) = \frac{1}{2}\left\{(V_{11}(\mathbf{q}) + V_{22}(\mathbf{q})) - \left[(V_{11}(\mathbf{q}) + V_{22}(\mathbf{q}))^2 + 4V_{12}(\mathbf{q})^2\right]^{\frac{1}{2}}\right\} \qquad [241]$$

where V_{11} and V_{22} are calculated by molecular mechanics using the connectivity of reactants and products, respectively, and where $\mathbf{q}$ denotes either the $\mathbf{R}$ or $\mathbf{x}$ coordinate set of Eq. [36] or a set of valence internal coordinates,[28,68–72] such as stretch, bend, and torsion coordinates. Therefore

$$V_{12}(\mathbf{q})^2 = [V_{11}(\mathbf{q}) - V(\mathbf{q})][V_{22}(\mathbf{q}) - V(\mathbf{q})] \qquad [242]$$

Using a suitable quantum mechanical electronic structure method, the energy, gradient, and Hessian can be calculated at an arbitrary geometry, $\mathbf{q}^{(k)}$, which is called an interpolation point or a Shepard point. Near $\mathbf{q}^{(k)}$, $V_{11}(\mathbf{q})$, $V(\mathbf{q})$, and $V_{22}(\mathbf{q})$ may be expanded as a Taylor series, yielding

$$V(\mathbf{q}; k) \cong V^{(k)} + \mathbf{g}^{(k)\dagger} \cdot \Delta\mathbf{q}^{(k)} + \frac{1}{2}\Delta\mathbf{q}^{(k)\dagger} \cdot \mathbf{f}^{(k)} \cdot \Delta\mathbf{q}^{(k)} \qquad [243]$$

where

$$\Delta\mathbf{q}^{(k)} = \mathbf{q} - \mathbf{q}^{(k)} \qquad [244]$$

In Eq. [243], $V^{(k)}$, $\mathbf{g}^{(k)}$, and $\mathbf{f}^{(k)}$ are the energy, gradient, and Hessian, respectively, at reference point $\mathbf{q}^{(k)}$. The diagonal elements of V_{nn} can be expanded around reference point $\mathbf{q}^{(k)}$, yielding

$$V_{nn}(\mathbf{q}; k) \cong V_n^{(k)} + \mathbf{g}_n^{(k)\dagger} \cdot \Delta\mathbf{q}^{(k)} + \frac{1}{2}\Delta\mathbf{q}^{\dagger(k)} \cdot \mathbf{f}^{(k)} \cdot \Delta\mathbf{q}^{(k)} \qquad [245]$$

where

$$V_n^{(k)} = V_{nn}(\mathbf{q}^{(k)}), \mathbf{g}_n^{(k)} = \left(\frac{\partial V_{nn}}{\partial \mathbf{q}}\right)_{\mathbf{q}=\mathbf{q}^{(k)}}, \mathbf{f}_n^{(k)} = \left(\frac{\partial^2 V_{nn}}{\partial \mathbf{q}\partial \mathbf{q}}\right)_{\mathbf{q}=\mathbf{q}^{(k)}} \qquad [246]$$

Substituting these expressions into Eq. [242] yields an analytic expression for $V_{12}(\mathbf{q})$ in the vicinity of reference point $\mathbf{q}^{(k)}$, given by

$$\begin{aligned} V_{12}(\mathbf{q};k)^2 \cong & \left(V_1^{(k)}-V^{(k)}\right)\left(V_2^{(k)}-V^{(k)}\right)+\left(V_2^{(k)}-V^{(k)}\right)\left(\mathbf{g}_1^{(k)}-\mathbf{g}^{(k)}\right)^{\dagger}\Delta\mathbf{q}^{(k)} \\ & +\left(V_1^{(k)}-V^{(k)}\right)\left(\mathbf{g}_2^{(k)}-\mathbf{g}^{(k)}\right)^{\dagger}\Delta\mathbf{q}^{(k)}+\frac{1}{2}\left(V_2^{(k)}-V^{(k)}\right)\Delta\mathbf{q}^{\dagger(k)}\left(\mathbf{f}_1^{(k)}-\mathbf{f}^{(k)}\right) \\ & \times\Delta\mathbf{q}^{(k)}+\frac{1}{2}\left(V_1^{(k)}-V^{(k)}\right)\Delta\mathbf{q}^{\dagger(k)}\left(\mathbf{f}_2^{(k)}-\mathbf{f}^{(k)}\right)\Delta\mathbf{q}^{(k)}+\left[\left(\mathbf{g}_1^{(k)}-\mathbf{g}^{(k)}\right)^{\dagger}\Delta\mathbf{q}^{(k)}\right] \\ & \times\left[\left(\mathbf{g}_2^{(k)}-\mathbf{g}^{(k)}\right)^{\dagger}\Delta\mathbf{q}^{(k)}\right] \end{aligned} \quad [247]$$

Now that expressions for $V_{11}(\mathbf{q})$, $V_{12}(\mathbf{q})$, and $V_{22}(\mathbf{q})$ are available in the vicinity of $\mathbf{q}^{(k)}$, an expression must be derived for $V(\mathbf{q})$ that is globally smooth as $\mathbf{q}$ approaches different reference points on the PES. In MCMM, this is done using a Shepard interpolation.[152,153] Suppose that a collection of M "Shepard points" is available, for which there are ab initio energies $V^{(k)}$, gradients $\mathbf{g}^{(k)}$, and Hessians $\mathbf{f}^{(k)}$. By using the Shepard interpolation method, the resonance energy function is given by

$$V_{12}^{S}(\mathbf{q})=\sum_{k=1}^{M} W_k(\mathbf{q})\,V'_{12}(\mathbf{q};k) \quad [248]$$

where the normalized weight is given by

$$W_k(\mathbf{q})=\frac{w_k(\mathbf{q})}{w(\mathbf{q})} \quad [249]$$

in terms of unnormalized weights w_k (discussed below) and in terms of the normalization constant

$$w(\mathbf{q})=\sum_{l=1}^{M+2} w_l(\mathbf{q}) \quad [250]$$

where the upper limit of the sum is now greater than in Eq. [248] because this sum also includes van der Waals minima (for biomolecular reagents) or chemical minima (for unimolecular reagents) corresponding to the two molecular mechanics structures; the resonance integral is zero by definition at these two structures.

In Eq. [248], V'_{12} is a modified quadratic function given by

$$[V'_{12}(\mathbf{q};k)]^2=[V_{12}(\mathbf{q};k)]^2 u(\mathbf{q};k) \quad [251]$$

where u is a modifier given by

$$u(\mathbf{q};k)=\begin{cases}\exp\left(\dfrac{-\delta}{[V_{12}(\mathbf{q};k)]^2}\right), & [V_{12}(\mathbf{q};k)]^2>0\\ 0, & [V_{12}(\mathbf{q};k)]^2\le 0\end{cases} \quad [252]$$

where δ is $10^{-8}\ E_h^2$, and E_h is one hartree. In practice, the expression for $V_{12}(\mathbf{q};k)$ is given by

$$[V_{12}(\mathbf{q};k)]^2 = D^{(k)}\left[1 + \mathbf{b}^{(k)\dagger}\left(\mathbf{q}-\mathbf{q}^{(k)}\right) + \frac{1}{2}\left(\mathbf{q}-\mathbf{q}^{(k)}\right)^{\dagger}\mathbf{C}^{(k)}\left(\mathbf{q}-\mathbf{q}^{(k)}\right)\right] \quad [253]$$

Choosing constants in Eq. [253] such that Eq. [243] is reproduced when Eq. [251] is substituted into Eq. [241] yields

$$D^{(k)} = \Delta V_1^{(k)} \Delta V_2^{(k)} \quad [254]$$

$$\mathbf{b}^{(k)\dagger} = \frac{\mathbf{g}_1^{(k)} - \mathbf{g}^{(k)}}{\Delta V_1^{(k)}} + \frac{\mathbf{g}_2^{(k)} - \mathbf{g}^{(k)}}{\Delta V_2^{(k)}} \quad [255]$$

$$\mathbf{C}^{(k)} = \frac{1}{D^{(k)}}\left[(\mathbf{g}_1^{(k)} - \mathbf{g}^{(k)})(\mathbf{g}_2^{(k)} - \mathbf{g}^{(k)})^{\dagger} + (\mathbf{g}_2^{(k)} - \mathbf{g}^{(k)}) \times (\mathbf{g}_1^{(k)} - \mathbf{g}^{(k)})^{\dagger}\right] + \frac{\mathbf{f}_1^{(k)} - \mathbf{f}^{(k)}}{\Delta V_1^{(k)}} + \frac{\mathbf{f}_2^{(k)} - \mathbf{f}^{(k)}}{\Delta V_2^{(k)}} \quad [256]$$

$$\Delta V_n^{(k)} = V_n^{(k)} - V^{(k)} \quad [257]$$

We can recap this procedure as follows: Electronic structure calculations are used to generate the Taylor series $V(\mathbf{q};k)$ of Eqs. [243] and [244] in the vicinity of point $\mathbf{q}^{(k)}$. This $V(\mathbf{q})$ and the Taylor series (Eqs. [245] and [246]) of the reactant and product MM potential energy surfaces are substituted into Eq. [242] to yield a Taylor series of V_{12} in the vicinity of $\mathbf{q}(k)$.

Next we will interpolate V_{12}, which is much smoother and easier to interpolate than the original V. As discussed further below, the interpolation of V_{12} is carried out in valence internal coordinates[28,68–72] to avoid the necessity of achieving a consistent molecular orientation, which would be required for interpolation in atomic Cartesians.

Finally, we must specify the weighting function $w_k(\mathbf{q})$ to be used for interpolation via Eqs. [248] through [252]. Several conditions should be met by the weight w_k associated with a particular geometry $\mathbf{q}^{(k)}$. These conditions involve the behavior of w_k near $\mathbf{q}^{(k)}$ and near the other interpolation points $q^{(k')}$ with $k' \neq k$. The conditions assure that w_k is smooth enough (zero first and second derivatives near all interpolation points) that the left-hand side of Eq. [248] has the same Taylor series, through quadratic terms, at $\mathbf{q}^{(k)}$ as that of $V'_{12}(\mathbf{q};k)$. The conditions are

$$w_k(\mathbf{q}^{(k)}) = 1, \quad \text{all } k \quad [258]$$

$$w_k(\mathbf{q}^{(k')}) << 1, \quad k' \neq k \quad [259]$$

$$\left.\frac{\partial w_k}{\partial \mathbf{q}}\right|_{\mathbf{q}=\mathbf{q}^{(k')}} \cong 0, \quad \text{all } k' \quad [260]$$

$$\left.\frac{\partial^2 w_k}{\partial \mathbf{q}^2}\right|_{\mathbf{q}=\mathbf{q}^{(k')}} \cong 0, \quad \text{all } k' \quad [261]$$

A variety of functional forms could be chosen for the weight function. A good choice is critical to the success and efficiency of the method. The choice made in Refs. 133 and 134 is

$$w_k(\mathbf{q}) = \frac{[d_k(\mathbf{q})]^{-4}}{\sum_{i=1}^{M+2} \frac{1}{[d_i(\mathbf{q})]^4}} \qquad [262]$$

where

$$d_k(\mathbf{q}) = \sqrt{\sum_{j=1}^{j_{max}} (q_j - q_j^{(k)})^2} \qquad [263]$$

Note that Eq. [262] is the smoothest possible function that satisfies Eqs. [258] to [261]. The recommended j_{max} for atom-transfer reactions is 3, where q_1, q_2, and q_3 are the forming bond distance, the making bond distance, and the nontransferring bond distance, respectively.

Although the PES is uniquely expressed in Cartesian coordinates, the Shepard interpolation is done using internal coordinates to avoid ambiguities relating to the orientation of the system. Therefore, the data are first transformed from Cartesians to internal coordinates, the Shepard interpolation is then completed, and the potential and derivatives are finally transformed back to Cartesians. For a detailed description of how this is accomplished, see Kim et al.[133]

A decision must now be made on where to locate the Shepard points. In addition to the three required Shepard points corresponding to the reactant well, transition state, and product well, other points can be added to improve the accuracy of the surface. A calculation with no additional points is referred to as MCMM-0. A systematic method for choosing the additional points has been presented by Albu, Corchado, and Truhlar.[134] The first supplementary point is placed on the dynamical bottleneck side of the MEP, where the energy is equal to one quarter the barrier height. This calculation with four Shepard points is referred to as MCMM-1. Additional Shepard points may be added systematically to yield a sequence of approximations MCCM-2,..., MCMM-*n*, where MCCM-*n* uses 10 nonstationary points. The user may specify as many additional points as needed to achieve the best accuracy for the PES. For a full discussion of the accuracy of rate calculations, see Ref. 134. Once six nonstationary points have been used in MCMM-6, CVT/SCT rates are typically within about 15% of the corresponding direct dynamics calculations. MCMM thus provides efficient calculations of reaction rates using only a small amount of high-level data.

IVTST-M

Interpolated variational transition state theory by mapping (IVTST-M)[154] is simpler than MCMM in that it does not involve molecular mechanics.

IVTST-M has two goals:

(1) to minimize the length of the path that must be calculated, and
(2) to minimize the number of Hessians that must be calculated.

The notation for an IVTST-M calculation is IVTST-M-*H*/*G*, where *H* and *G* indicate, respectively, the number of additional Hessians and gradients used.

Interpolation of V_{MEP} uses the $G + 3$ energies that are available. These energies include those of the stationary points corresponding to the reactant, transition state, and the product, and the gradients are the G nonstationary points that are situated along the reaction path. Because the reactants and products for a bimolecular reaction are at $s = -\infty$ and $s = +\infty$, respectively, and because interpolation over an infinite interval is less desirable than interpolation over a finite one, it is advisable to map the potential $V_{MEP}(s)$ onto a new function, $V_{MEP}(z)$, based on a new variable z:

$$z = \frac{2}{\pi}\arctan\left(\frac{s - s_0}{L}\right) \qquad [264]$$

where s_0 and L are parameters discussed in the next paragraph. This mapping changes the interval for the potential function from $(-\infty,+\infty)$ for $V_{MEP}(s)$ to $(-1,+1)$ for $V_{MEP}(z)$.

The interpolation is more efficient if one calculates s_0 such that the new function is centered where the important changes are occurring as the reaction takes place. A simple approach is to set s_A^0 and s_B^0 to the values of s where the potential on the reaction path is equal to half the barrier height (measured from reactants and products respectively) and then to set s_0 equal to the mean of s_A^0 and s_B^0, but this may cause unphysical values of s_0 for very exothermic or endothermic reactions. Therefore, it is recommended that s_0 should be calculated using s_A and s_B defined as

$$s_A = -\min\left(|s_A^0|, 2s_B^0\right) \qquad [265]$$

$$s_B = \min\left(|s_A^0|, s_B^0\right) \qquad [266]$$

where

$$s_A^0 = -\sqrt{\frac{V_{MEP}(s=0) - V_{MEP}(s_R)}{|\omega^\ddagger|^2\mu}} \qquad [267]$$

$$s_B^0 = \sqrt{\frac{V_{MEP}(s=0) - V_{MEP}(s_P)}{|\omega^\ddagger|^2\mu}} \qquad [268]$$

in which μ is the reduced mass used to scale the coordinates of the system in Eq. [36], $\omega^\ddagger$ is the imaginary frequency of the transition state, and s_R and s_P

correspond to the values of s at the reactants and products, respectively. Once s_A and s_B have been determined, s_0 is calculated using the arithmetic mean:

$$s_0 = \frac{(s_A + s_B)}{2} \qquad [269]$$

The range parameter L is estimated from the width of the reaction path:

$$L = \frac{(-|s_A| + s_B)}{2} \qquad [270]$$

$V_{MEP}(s)$ can now be successfully mapped to $V_{MEP}(z)$. Ten extra points are then placed between the last gradient on the reactant side and $z = -1$, and 10 extra points are placed between the last gradient on the product side and $z = 1$. These points, whose energies are calculated in the following steps, are used along with the gradient calculations to create a spline-under-tension potential energy function along the reaction path.

The energy of these 20 additional points is estimated using the Eckart potential in Eq. [271] whose terms are defined in Eqs. [272]–[276].

$$V_{MEP} = \frac{AY}{1+Y} + \frac{BY}{(1+Y)^2} + C \qquad [271]$$

$$Y = \exp\left(\frac{s - s_0^{Eck}}{L^{Eck}(s)}\right) \qquad [272]$$

$$A = V_{MEP}(s_P) - V_{MEP}(s_R) \qquad [273]$$

$$C = V_{MEP}(s_R) \qquad [274]$$

$$B = [2V_{MEP}(s=0) - A - 2C] \pm 2([V_{MEP}(s=0) - C] \times [V_{MEP}(s=0) - A - C])^{\frac{1}{2}} \qquad [275]$$

$$s_0^{Eck} = -L^{Eck}(s) \ln\left(\frac{A+B}{B-A}\right) \qquad [276]$$

where L^{Eck} is a new function. L^{Eck} is calculated for each nonstationary point s such that the Eckart potential goes through $V_{MEP}(s)$ at that s as well as at reactants, products, and saddle point. At the saddle point only, $L^{Eck}(s)$ is calculated using the imaginary frequency:

$$L^{Eck}(s=0) = \sqrt{\frac{2[V_{MEP}(s=0) - A]V_{MEP}(s=0)}{\mu|\omega^{\ddagger}|^2 B}} \qquad [277]$$

The $G + 1$ values of $L^{Eck}(s)$ are then mapped onto the $[-1,+1]$ interval using Eq. [264]. The values of $L^{Eck}(z = -1)$ and $L^{Eck}(z = +1)$ are approximated

using a quadratic polynomial that has been fitted to the last two G points on the reactant and product sides of the saddle point, respectively. The continuous function for $L^{\text{Eck}}(z)$ (from $z = -1$ to $z = +1$) can now be calculated using a spline under tension based on values of $L^{\text{Eck}}(z)$ and the saddle point, the G nonstationary points, and the approximated values at $z = -1$ and $z = +1$. At this time, the energies for the 10 extra points on each side of the saddle point are calculated using an Eckart potential of $L^{\text{Eck}}(z)$.

Finally, using the $G + 23$ energies between $z = -1$ and $z = +1$, $V_{\text{MEP}}(z)$ is calculated using a spline under tension. This provides an energy along the reaction path from $s = -\infty$ to $s = +\infty$. For more details about the minor adjustments to the theory needed to account for a unimolecular or association reaction rather than a bimolecular reaction with bimolecular products, see Ref. 154.

Once the MEP has been calculated, the moments of inertia $I(s)$ and the frequencies required to calculate the partition function must be determined. The determinant of the moment of inertia is calculated at the saddle point and the G nonstationary points. (The values of this determinant for bimolecular reactants and products are assumed to be infinity.) The $G + 3$ values of $I(s)$ are mapped using Eq. [264] to yield $I(z)$. Because the moment of inertia changes as the square of the geometry and to keep the interpolant in a convenient numerical range, one actually interpolates $(I(z^{\ddagger})/I(z))^{1/2}$ rather than $I(z)$ at the $G + 3$ points. Finally, a spline fit is created using this function to give $I(s)$ for any s.

Interpolation of the frequencies is likewise done using a spline fit; for each of the $F - 1$ bound modes, the frequency $\omega(s)$ is calculated at the location of each Hessian. These frequencies are then mapped using Eq. [264] and put in canonical order, such that any avoided crossing or symmetry constraints are ignored. Imaginary frequencies are treated as negative numbers. The canonical order is defined so that the real frequencies are first in order of decreasing magnitude, following by the imaginary frequencies in their order of increasing magnitude followed by the six (five for linear systems) frequencies of smallest magnitude regardless if they are real or imaginary.

The cost of using the IVTST-M algorithm is negligible compared with the cost of calculating high-level electronic structure gradients and Hessians. The method was developed to allow for a shorter sequence of reaction path data, but even if long reaction paths have already been calculated, it is advantageous to use IVTST-M to map out the remainder of the path rather than truncating it.

Dual-Level Dynamics

Dual-level dynamics[142,143,155,156] refers to dynamics calculations that use two levels of electronic structure theory or two PEFs of different quality. In the VTST/MT context, such methods use a low-level method to calculate the MEP and gather some information along it followed by using a smaller

number of high-level calculations to improve accuracy. Computing all of the necessary data with a high-level method may be prohibitively CPU-expensive; yet the low-level method may not provide the required accuracy; dual-level methods attempt to use both levels to obtain the highest possible accuracy at the lowest possible cost.

Interpolated Single-Point Energies

Variational transition state theory with interpolated single-point energies (VTST–ISPE), is a dual-level method[156] that uses high-level, single-point energies on a low-level MEP to correct the V_{MEP}. POLYRATE has implemented this by using a mapped coordinate as in the IVTST-M algorithm. The low-level MEP is first mapped to the interval from $z = -1$ to $z = +1$ using Eq. [264] as before. Wherever a high-level, single-point energy has been evaluated, ΔV is calculated as $\Delta V = V_{HL} - V_{LL}$, where the subscripts denote high level (HL) and low level (LL). Finally, the dual-level reaction path is evaluated using

$$V_{DL} = V_{LL} + V_{spline}(\Delta V, z) \qquad [278]$$

where $V_{spline}(\Delta V, z)$ is a spline-under-tension fit.

Interpolated Optimized Corrections

The interpolated optimized corrections (IOC) method[143,155] uses HL energies, gradients, and Hessians at the high-level stationary points to improve the quality of a V_{MEP} and of frequency and moment of inertia profiles originally calculated at LL.

We have proposed two dual-level schemes for V_{MEP}.[143,155] The dual-Eckart (DE) scheme is given by[143]

$$V_{MEP}^{DE} = V_{MEP}^{LL}(s) + \left[V_{Eck}^{HL}(s) - V_{Eck}^{LL}(s)\right] \qquad [279]$$

where

$$V_{Eck} = \frac{AY}{1+Y} + \frac{BY}{(1+Y)^2} + C \qquad [280]$$

$$Y = \exp\left(\frac{s - S_0}{L}\right) \qquad [281]$$

$$A = V_{MEP}(s = +\infty) - C \qquad [282]$$

$$C = V_{MEP}(s = -\infty) \qquad [283]$$

$$B = (2V^{\ddagger} - A - 2C) + 2\left[\left(V^{\ddagger} - C\right)\left(V^{\ddagger} - A - C\right)\right]^{\frac{1}{2}} \qquad [284]$$

$$S_0 = -L \ln\left(\frac{A+B}{B-A}\right) \qquad [285]$$

where $V^{\ddagger}$ is $V_{\mathrm{MEP}}(s=0)$, the range parameter for $V_{\mathrm{Eck}}^{\mathrm{HL}}(s)$ is given by

$$L^{\mathrm{HL}} = \left[-\frac{2V^{\ddagger}(V^{\ddagger} - A)}{\mu(\omega^{\ddagger})^2 B} \right]^{\frac{1}{2}} \qquad [286]$$

where all quantities on the right-hand side are calculated at the high level, and L^{LL} is determined by fitting the low-level V_{MEP} to an Eckart function at the three stationary points and at one additional point $s = s_{\mathrm{L}}$, where

$$V_{LL}^{\ddagger} - V_{\mathrm{MEP}}^{\mathrm{LL}}(s = s_{\mathrm{L}}) = \frac{1}{2}\left\{ V_{LL}^{\ddagger} - V_{\mathrm{MEP}}^{\mathrm{LL}}(s = sign(s_{\mathrm{L}})\infty) \right\} \qquad [287]$$

The sign of s_{L} is positive if A^{LL} is positive and negative if A^{LL} is negative.

The single-Eckart (SE) scheme for correcting V_{MEP} is[155]

$$V_{\mathrm{MEP}}^{\mathrm{SE}} = V_{\mathrm{MEP}}^{\mathrm{LL}}(s) + V_{\mathrm{Eck}}(s) \qquad [288]$$

with Eq. [281] for Y, where the parameters in the single-Eckart potential are given by

$$A = \Delta V(s = +\infty) - C \qquad [289]$$

$$C = \Delta V(s = -\infty) \qquad [290]$$

$$B = \left[(2\Delta V^{\ddagger} - A - C) \pm 2(\Delta V^{\ddagger} - C)(\Delta V^{\ddagger} - A - C) \right]^{1/2} \qquad [291]$$

along with Eq. [287] to determine L. In these equations, ΔV denotes the difference of V^{HL} from V^{LL}. Furthermore, we use the upper sign in Eq. [291] when $\Delta V^{\ddagger} > \Delta V(s = \pm\infty)$ and the lower sign otherwise. We have found that sometimes the DE scheme is preferred,[143] but on average, the SE scheme is better.[156]

In addition to correcting V_{MEP}, the frequencies and the determinant of the moment of inertia tensor are also corrected.

The formula for the interpolation of frequencies in the original method[155] allowed for the possibility of negative frequencies, which was problematic. Therefore, only the updated interpolation method[143] will be discussed. The $3N - 7$ real frequencies calculated using the lower level method are denoted as $\omega_m^{\mathrm{LL}}(s)$. The dual-level frequencies calculated using the high-level corrections are given by

$$\omega_m^{\mathrm{DL}} = \omega_m^{\mathrm{LL}}(s) \exp[f^{\mathrm{ICL}}(s)] \qquad [292]$$

where

$$f^{\mathrm{ICL}} = \frac{A_m Y}{1+Y} + \frac{B_m Y}{(1+Y)^2} + C_m \qquad [293]$$

$$Y = \exp\left(\frac{s - S_{0,m}}{L}\right) \qquad [294]$$

$$A_m = \ln\frac{\omega_m^{\mathrm{DL}}(s=+\infty)}{\omega_m^{\mathrm{LL}}(s=+\infty)} - C_m \qquad [295]$$

$$C_m = \ln\frac{\omega_m^{\mathrm{DL}}(s=-\infty)}{\omega_m^{\mathrm{LL}}(s=-\infty)} \qquad [296]$$

$$B = \left(2\ln\frac{\omega_m^{\mathrm{DL}}(s=0)}{\omega_m^{\mathrm{LL}}(s=0)} - A_m - 2C_m\right) \pm 2\left[\left(\ln\frac{\omega_m^{\mathrm{DL}}(s=0)}{\omega_m^{\mathrm{LL}}(s=0)} - C_m\right) \times \left(\ln\frac{\omega_m^{\mathrm{DL}}(s=0)}{\omega_m^{\mathrm{LL}}(s=0)} - A_m - C_m\right)\right]^{\frac{1}{2}} \qquad [297]$$

$$S_{0,m} = -L\ln\left(\frac{A_m + B_m}{B_m - A_m}\right) \qquad [298]$$

in which L is defined using Eq. [286]. The frequencies are matched in order of decreasing magnitude, disregarding symmetry and avoided crossings, and setting the leftover modes to zero at $s = \pm\infty$.

The determinant $I(s)$ of the moment of inertia tensor is corrected by

$$I_{\mathrm{HL}}(s) = \alpha I_{\mathrm{LL}}(s) \qquad [299]$$

where

$$\alpha = \frac{I_{\mathrm{HL}}(s=0)}{I_{\mathrm{LL}}(s=0)} \qquad [300]$$

This simple formula was chosen so that no difficulties would arise as $I(s)$ approaches infinity at reactant and product states.

IVTST–IOC can also be applied to reactions having reactant-side and/or product-side wells. Furthermore, the theory explained here is readily applied to VTST, ZCT, and SCT, but applying the theory to LCT requires additional steps, all of which are explained in Ref. 155.

Interpolated Optimized Energies

The interpolated optimized energies (IOE) scheme[156] is like the IOC scheme except that the frequencies are not corrected at the higher level. Although the IOE method only uses high-level data at the stationary points,

it is often more accurate than the ISPE method because it involves geometry optimization at the higher level.[155]

REACTIONS IN LIQUIDS

Variational transition state theory can also be applied to reactions in liquids when those reactions are not diffusion controlled. For instance, for a general reaction of the type:

$$A + B \underset{k_{-D}}{\overset{k_D}{\rightleftharpoons}} AB \xrightarrow{k_r} \text{Products} \qquad [301]$$

where AB is a complex formed by the two molecules before reaction, application of the steady-state approximation for the concentration of the complex gives the following rate constant:[157]

$$k = \frac{k_D k_r}{k_{-D} + k_r} \qquad [302]$$

If $k_r >> k_{-D}$, then $k \cong k_D$ and the reaction is controlled by diffusion. A typical value for k_D is $4 \times 10^9\ M^{-1}s^{-1}$. Conversely, when $k_r << k_{-D}$, the process is controlled by the chemical step, and we can use CVT to predict the thermal rate constants. Specifically, the CVT bimolecular rate constant can be written as

$$k^{CVT}(T) = \frac{1}{\beta h C^0} \exp\left\{-\left[G_T^0(CVT) - G_T^0(R)\right]\Big/RT\right\} \qquad [303]$$

where C^0 is the concentration corresponding to the standard state, $G_T^0(R)$ is the solution-phase standard-state free energy of reactants at temperature T, and $G_T^0(CVT)$ is the solution-phase standard-state free energy of activation[106,158–160] of the canonical variational transition state at temperature T. As for the gas-phase case, the variational free energy of activation is given by

$$G_T^0(CVT) = \max_s G_T^0(GT, s) \qquad [304]$$

where $G_T^0(GT, s)$ is the standard-state free energy of activation for a generalized transition state at a location s along the reaction path. The rate constant expression is similar for a unimolecular reaction, the difference being that C^0 is missing in Eq. [303].

The quantity $G_T^0(R)$ is a standard-state free energy in liquid solution, denoted $G_T^0(l)$, and it is obtained by treating the solute as a system interacting

with a thermal environment. The system is the solute (or the solute plus a few closely coupled solvent molecules), and the environment is the (rest of the) solvent. In the rest of this section, we will simply call the system the solute. The liquid-phase free energy of the solute is the solute's gas-phase free energy plus the free energy of solvation, which is defined by

$$\Delta G_S^0 = G_T^0(l) - G_T^0(g) \qquad [305]$$

In the Born–Oppenheimer approximation,

$$G_T^0(g) = E_E(g) + RT \ln d_E + G_{VRT}(T) \qquad [306]$$

where E_E is the ground-state electronic energy (including nuclear repulsion as usual) of the solute, d_E is the degeneracy of the ground electronic state, and $G_{VRT}(T)$ is the vibrational–rotational–translational free energy in the standard state. Many methods are available for approximating the standard-state free energy of solvation, but here we focus on those that use the SM*x* universal solvent models.[161–171] In these models

$$\Delta G_S^0 = \Delta G_{ENP}(T) + G_{CDS}(T) \qquad [307]$$

where ΔG_{ENP} is the bulk electrostatic component of the solvation free energy obtained by treating the environment as a homogeneous dielectric medium with properties of the neat solvent. When the solute is inserted in the solvent, the latter is polarized, and as a result, it exerts a field, called the reaction field, on the solute. ΔG_{ENP} is composed of (1) a polarization energy G_P, which represents the net free energy of inserting the solute in the solvent (accounts for favorable solute-solvent interactions and the energy cost of the solvent rearrangement), and (2) the distortion energy ΔE_{EN}, which represents the cost of distorting the solute geometry and electronic charge distribution to be self-consistent with the solvent reaction field; i.e.,

$$\Delta G_{ENP}(T) = G_P(T) + \Delta E_{EN}(T) \qquad [308]$$

Note that the solute electronic energy in the liquid phase is

$$E_{EN}(l, T) = E_{EN}(g) + \Delta E_{EN}(T) \qquad [309]$$

The term G_{CDS} accounts for the first-solvation-shell effects and is given by[163–166]

$$G_{CDS} = \sum_k \sigma_k^A(T) A_k\left(\left\{r_k; r_s^{CD}\right\}\right) + \sigma^{CS} A_k\left(\left\{r_k; r_s^{CS}\right\}\right) \qquad [310]$$

where k labels atoms, A_k is the exposed area of atom k, σ_k^A is a partial atomic surface tension for atom k, and $A_k(\{r_k; r_S^{CX}\})$, with $X = S$ or D is the

solvent-accessible surface area of atom k and is a function of a given set of effective solute radii $\{r_k\}$ and of effective solvent radii, r_S^{CS} and r_S^{CD}. Several solvation models, such as SM5.42, SM5.43, and SM6, have been created, and they have different values for these parameters. SM6 is recommended for most systems.

Equations [305]–[310] are strictly valid only for thermodynamic species, which are ordinarily associated with stationary points on the potential energy surface $V(\mathbf{R})$, where $\mathbf{R}$ denotes the full set of solute coordinates. However, we also use the SMx solvation models to calculate potentials of mean force,[172] which are called $W(\mathbf{R},T)$. The gradient of $W(\mathbf{R},T)$ gives the force on the solute molecule averaged over a canonical ensemble of solvent molecules and is a generalization of the one-dimensional radial potential of mean force that appears in Debye–Hückel theory. Thus, we write

$$W = V(\mathbf{R}) + \Delta G_S^0(\mathbf{R}, T) \qquad [311]$$

where $G_S^0(\mathbf{R}, T)$ is like $G_S^0(T)$ except that the nuclear coordinates of the solute are fixed at $\mathbf{R}$; thus, $\Delta E_{EN}(T)$ does not involve a change in the nuclei, and it may be written as $\Delta E_E(\mathbf{R},T)$.

The simplest way to implement Eq. [303] for the liquid-phase reaction rate is called separable equilibrium solvation or the SES approximation.[159] In this approximation, one optimizes the stationary points and calculates the reaction path and vibrational frequencies in the gas phase. Then, at every stationary-point and reaction path geometry, one replaces the potential energy V by the potential of mean force W. If one also replaced V by W in calculating partition functions, this would provide an exact expression for the flux through the generalized-transition-state dividing surface in a classical mechanical world, although one no longer can obtain the exact rate constant by varying the dividing surface because the dividing surface depends only on the subset $\mathbf{R}$ of the total set of solute and solvent coordinates. However, in the SES approximation, the partition functions are still calculated using V. Note that the location of the variational transition state along the reaction path may be different in the gas phase and in the SES approximation to the liquid-phase rate, even though the reaction path is unaltered.

The SES approximation also replaces V by W for the tunneling calculations, which is called the zero-order canonical-mean-shape approximation[173] (CMS-O). Note that the tunneling turning points and hence the tunneling paths may be different in the gas phase and in solution in the SES approximation, even though the reaction path is unaltered.

Algorithmically, because one only corrects the potential energy surface along the reaction path, the IVTST-M algorithm can be (and is) used for SES calculations where W plays the role of the high-level surface and V plays the role of the low-level surface.

Because the transition state geometry optimized in solution and the solution-path reacton path may be very different from the gas-phase saddle point and the gas-phase reaction path, it is better to follow the reaction path given by the steepest-descents-path computed from the potential of mean force. This approach is called the equilibrium solvation path (ESP) approximation. In the ESP method, one also substitutes W for V in computing the partition functions. In the ESP approximation, the solvent coordinates are not involved in the definition of the generalized-transition-state dividing surface, and hence, they are not involved in the definition of the reaction coordinate, which is normal to that surface. One says physically that the solvent does not participate in the reaction coordinate. That is the hallmark of equilibrium solvation.

A third approach is to incorporate nonequilibrium solvent (NES) effects. In POLYRATE, this is accomplished by replacing the many degrees of freedom of the solvent with a single collective solvent coordinate.[174] Further discussion of equilibrium and nonequilibrium solvation effects on liquid-phase reactions is provided elsewhere.[33,162,167,169]

ENSEMBLE-AVERAGED VARIATIONAL TRANSITION STATE THEORY

The concept of reaction coordinate plays an important role in VTST. In fact, there is more than one reaction coordinate. Globally the reaction coordinate is defined as the distance s along the reaction path, and this coordinate plays a critical role in tunneling calculations. Locally the reaction coordinate is the degree of freedom (sometimes called z, but often also called s) that is missing in the generalized transition state.

The treatment of VTST given so far is well suited for bimolecular reactions with tight transition states and simple barrier potentials. In such cases, it has been shown that the variational transition state can be found by optimization of a one-parameter (s) or few-parameter (s and orientation of the dividing surface) sequence of dividing surfaces orthogonal to the reaction path, where the reaction path is defined as the minimum energy path through isoinertial coordinates. (See also Refs. 76, 77, and 81–89 for extensions to gas-phase systems with loose transition states, where more general reaction coordinates are considered.) In this section, we discuss the extension of VTST for condensed-phase reactions to allow the generalized-transition-state dividing surface to depend on more than just the solute coordinates; for example, it can depend on the solvent, or for an enzyme-catalyzed reaction, it can depend on protein coordinates. To include these different kinds of cases in a single formalism, we generalize the solute/solvent or system/environment separation, and we speak of a primary subsystem (or primary zone) instead of a solute or system and a secondary subsystem (or secondary zone) instead of a solvent or environment. As the reaction coordinate is the degree of freedom that is normal to the

generalized transition state, allowing the generalized-transition-state definition to depend on secondary-subsystem coordinates is equivalent to allowing the definition of the reaction coordinate to depend on secondary-subsystem coordinates, that is, to allowing the secondary subsystem to participate in the reaction coordinate. Thus, this extension of VTST allows one, for example, to include protein motions in the reaction coordinate for enzyme-catalyzed reactions. This is accomplished by ensemble averaging,[175–180] and the extension is called ensemble-averaged variational transition state theory (EA-VTST); although it is more general than just for enzyme-catalyzed reactions, EA-VTST will be explained here mainly in the enzyme context.

For simple reactions, all, or almost all, of the reaction flux (at least in the absence of large-curvature tunneling) passes through the TS in a quasi-harmonic valley centered on a single reaction path passing through a single saddle point. EA-VTST is designed for applications to complex reactions in the condensed phase where an appropriate reaction coordinate may be very complicated, and where reaction proceeds through a large number of reaction paths, each passing through a different saddle point. These saddle points might differ trivially (for example, by a torsion around a far away hydrogen bond) or they might differ more substantially. But the essence of a liquid-phase reaction is that the number of saddle points is so numerous that they must be treated by statistical mechanical theories of liquids. This means, algorithmically, that we must sample rather than examine all contributing configurations. As for the single-reaction coordinate version of VSTS described in the previous sections, EA-VTST may be combined with multidimensional tunneling or optimized multidimensional tunneling, using the canonical mean-shape approximation, but now in an ensemble-averaged extension.

When applying EA-VTST to enzyme reactions, another kind of system/environment separation is made. Here the reactive system is considered to be the substrate and perhaps part of the enzyme or coenzyme (and perhaps including one or two closely coupled water molecules), and the environment is the rest of the substrate–coenzyme–enzyme complex plus the (rest of the) surrounding water. In what follows we will sometimes call the reactive system the "primary subsystem" and the environment as the "secondary subsystem." For the treatment of reactions in liquids that was presented earlier, the solvent was replaced by a homogeneous dielectric medium, which greatly simplifies the calculation. For enzyme-catalyzed reactions, we treat the environment explicitly at the atomic level of detail.

For enzyme-catalyzed reactions, we consider the unimolecular rate constant for the chemical step, which is the reaction of the Michaelis complex. The EA-VTST/OMT method involves a two-stage or three-stage procedure, where the third stage is optional. In stage one, a user-defined, physically meaningful reaction coordinate is used to calculate a one-dimensional potential of mean force. This provides a classical mechanical free energy of activation along that coordinate that is used to identify a transition state ensemble. In

stage two, the transition state ensemble is used to sample a set of transition pathways (reaction paths) to determine the transmission coefficient and the quantum mechanical tunneling contributions. The reaction coordinate for stage 1 is called a "distinguished reaction coordinate," (DRC) which is the generally accepted name for a coordinate that has been "picked out" or assigned to serve as a reaction progress variable.[64,181–183]

In the first step of stage 1, all atoms (5000–25000 atoms for a typical application to an enzyme-catalyzed reaction) are treated on the same footing. In this step, one calculates a one-dimensional potential of mean force (PMF) as a function of the distinguished reaction coordinate z by a classical molecular dynamics simulation. Any method for calculating classical mechanical PMFs could be used; for example, one can use the CHARMM program[184] to carry out this step by employing molecular dynamics simulation with umbrella sampling.[185–187] As discussed below, this provides an approximation to the free energy of activation profile for generalized transition states (i.e., transition state dividing surfaces) orthogonal to this reaction coordinate.[32] The umbrella sampling method involves several "windows," which are sampled separately, and then the results from all the windows are merged. During the umbrella sampling calculations, configurations are saved at regular intervals; these saved configurations are sorted into bins based on their value of z and are later used at selected values of z in the second step of stage 1 and the first step of stage 2 described below. (Windows and bins are both spaced out along the reaction coordinate. Windows overlap, but bins do not. Bins are spaced more closely than windows.)

Stage 1 is the calculation of the PMF along the distingished reaction coordinate and various types of reaction coordinates can be used, for example, proton and hydride transfer reactions could be evaluated with a geometry-based distinguished reaction coordinate described by the difference between the breaking and forming bond distances as

$$z = r_{HD} - r_{HA} \qquad [312]$$

where r_{HD} is the distance of the proton or hydride atom that is being transferred to the donor atom and r_{HA} is its distance to the acceptor atom. Selecting a different reaction coordinate should not, in principle, change the final calculated rate constants significantly because stage 2, which uses the transition state ensemble of stage 1 to sample a set of reaction paths and uses an ensemble of more optimal reaction coordinates to calculate the rate constants.

The first step of stage 2 treats the system and its environment together, without distinction, as a supersystem. In all subsequent steps (that is, in step two of stage 1 and in stage 2 as well as the optional stage 3), the N-atom system is divided into two subsystems, a primary subsystem with N_1 atoms and secondary subsystem with N_2 atoms, such that

$$N = N_1 + N_2 \qquad [313]$$

Typically N_1 ranges from 25 to 43 atoms.

In the second step of stage 1, vibrational quantization effects are included in the vibrational free energy,[188] where the number of vibrations treated quantum mechanically is

$$M_* = 3N_1 - 7 \qquad [314]$$

This is done for each z bin by computing the frequencies by using a rectilinear projection operator to remove the reaction-coordinate motion from instantaneous normal mode analyses at the sampled points. Second, the vibrational frequencies are averaged over an ensemble of sampled points in a given bin, and the vibrational free energy is calculated from the average frequencies by both the quantized and the classical formulas for the free energy of a collection of harmonic oscillators. Because the sampled points have been sampled at various distances from the bed of the reaction valley, this analysis implicitly includes anharmonicity. The difference of the quantized and classical calculations is added to the classical PMF, and the resulting adjusted PMF, called the quasi-classical PMF, corresponds to the M_* nuclear motions being quantized, with the remaining motion being classical. At the end of the first stage, the rate constant is given by

$$k^{(1)} = \frac{1}{\beta h} \exp\left[-\Delta G_T^{(1)}/RT\right] \qquad [315]$$

where

$$\Delta G_T^{(1)} = W^{\mathrm{CM}}(T,z_*) + \Delta W_{\mathrm{vib}}^{(M)}(T,z_*) + C(T,z_*) - \left[W^{\mathrm{CM}}(T,z_{\mathrm{R}}) + W_{\mathrm{R},T,F}^{\mathrm{CM}} + \Delta W_{\mathrm{vib}}^{(3N_1-6)}(T,z_{\mathrm{R}})\right] \qquad [316]$$

in which $W^{\mathrm{CM}}(T,z)$ is the classical mechanical PMF of stage 1–step 1, z_* is value of z that maximizes the right-hand side of Eq. [316], z_{R} is value of z where $W^{\mathrm{CM}}(T,z)$ has a minimum corresponding to reactants, $\Delta W_{\mathrm{vib}}^{(M_*)}(T,z')$ is the ensemble-averaged correction to the vibrational free energy for quantizing the M_* highest frequencies at $z = z'$, $C(T,z)$ is the correction[32] for a curvilinear z, and $W_{\mathrm{R},T,F}^{\mathrm{CM}}$ is the nonseparable vibrational free energy of the reaction coordinate at $z = z_{\mathrm{R}}$. Equation [315] is a quasi-classical rate constant because it includes quantization in transverse vibrational coordinates but not in the reaction coordinate (but it is not the final quasi-classical rate constant of the EA-VTST treatment). Equation [316] can also be written as

$$\Delta G_T^{(1)} = \Delta^* W^{\mathrm{CM}}(Y,z) + W_{\mathrm{corr}}(T) \qquad [317]$$

where

$$\Delta^* W^{\mathrm{CM}}(T,z) \equiv W^{\mathrm{CM}}(T,z_*) - W^{\mathrm{CM}}(T,z_{\mathrm{R}}) \qquad [318]$$

and

$$W_{\mathrm{corr}}(T) \equiv -W^{\mathrm{CM}}_{\mathrm{R},T,M_{\mathrm{R}}} + C(T,z_*) + \Delta W^{(M_*)}_{\mathrm{vib}}(T,z_*) - \Delta W^{(M_{\mathrm{R}})}_{\mathrm{vib}}(T,z_{\mathrm{R}}) \qquad [319]$$

where

$$M_{\mathrm{R}} = F = M_* + 1 \qquad [320]$$

The vibrational frequencies ω^*_m at $z = z_*$ are calculated from a Hessian that has the reaction coordinate projected out, but the reactant frequencies ω^{R}_m are calculated without projection.

In the second stage, a transition state ensemble is selected. This ensemble is defined as the set $\{i = 1,2,\ldots,I\}$ of I saved configurations from the umbrella sampling that have z nearest to z_*. The individual values of z for these ensemble members are called $z_{*,i}$. For each of these geometries, the primary system is optimized to the nearest saddle point, with fixed coordinates for the secondary zone. An isoinertial MEP of the primary system is then computed, again with the secondary zone fixed. Note that each value of i corresponds to a different secondary zone and, hence, a different saddle point. Each MEP ($i = 1,2,\ldots,I$) corresponds to a different valley through the supersystem consisting of the reactive system plus its environment. Furthermore, because each MEP has a different reaction coordinate corresponding to a different set of coordinates for the secondary zone, the reaction coordinate depends on the coordinates of the secondary zone. In this way the entire supersystem (including the enzyme and solvent) participates in the definition of the reaction coordinate.

For each MEP, VTST and VTST/OMT calculations are carried out using the progress variable s_i along MEP i as the optimized reaction coordinate. (Note that s_i is the variable s for ensemble member i.) The improved reaction coordinate for ensemble member i yields a recrossing transmission coefficient Γ_i, given by

$$\Gamma^{(2)}_i = \exp\left\{\left[\Delta G^{\mathrm{CVT,o}}_T\left(s_{*,i}\right) - \Delta G^{\mathrm{GT,o}}_T\left(s_{0,i}\right)\right]\Big/RT\right\} \qquad [321]$$

where $s_{*,i}$ is the location of maximum free energy of activation for ensemble member i along its own reaction coordinate s_i and $s_{0,i}$ is the value of s_i for which $z = z_{*,i}$. These recrossing transmission coefficients are averaged over the I members of the TS ensemble. The actual calculation of $\Delta G^{\mathrm{CVT,o}}(s_{*,i})$ and $\Delta G^{\mathrm{GT,o}}(s_{0,i})$ for the embedded primary system of transition ensemble

member i is carried out with the CHARMMRATE module of CHARMM. (Note that CHARMMRATE is based on POLYRATE.) The transmission coefficient calculated from this step of stage 2 is

$$\Gamma^{(2)} = \langle \Gamma_i^{(2)} \rangle \qquad [322]$$

where $< \ldots >$ denotes an ensemble average ($i = 1, 2, \ldots, I$). The resulting rate constant is

$$k^{\text{EA-VTST}} = \Gamma^{(2)}(T) k^{(1)}(T) \qquad [323]$$

This stage-2, step-1 rate expression $k^{\text{EA-VTST}}$ is the final quasi-classical rate constant of the two-state process. Equation [323] has sometimes been called the static-secondary-zone rate constant without tunneling, but this term is deceptive because the secondary zone changes from one ensemble member to another and, hence, is not really static.

At this point one can include optimized multidimensional tunneling in each ($i = 1, 2, \ldots, I$) of the VTST calculations. The tunneling transmission coefficient of stage 2 for ensemble member i is called $\kappa_i^{(2)}$ and is evaluated by treating the primary zone in the "ground-state" approximation (see the section titled "Quantum Effects on Reaction Coordinate Motion") and the secondary zone in the zero-order canonical mean shape approximation explained in the section titled "Reactions in Liquids", to give an improved transmission coefficient that includes tunneling:

$$\gamma^{(2)} = \langle \kappa_i^{(2)} \Gamma_i^{(2)} \rangle \qquad [324]$$

with the final stage-2 rate constant being

$$k^{\text{EA-VTST/OMT}} = \gamma^{(2)}(T) k^{(1)}(T) \qquad [325]$$

The procedure just discussed for stage 2 includes the thermal energy and entropy of secondary-zone atoms in $k^{(1)}(T)$ and in the determination of each $s_{0,i}$ that is used in stage 2, but the s dependence of these contributions is not included in each MEP. Optionally these effects could be included in a third stage. However, when secondary-zone dynamics are slow on the time scale over which s crosses the barrier[189] (or on the time scale of a wave packet traversing the tunneling segment of the reaction path), one is in what Hynes has called the "nonadiabatic solvation limit."[190–192] In this limit, the transition state passage occurs with an ensemble average of essentially fixed secondary-zone configurations[190–192] because the secondary zone cannot respond to the reaction coordinate motion to provide equilibrium solvation; in such a case, allowing the secondary zone to relax could provide less accurate results

than stopping after stage 2. Contrarily, if the adjustment of the secondary zone is rapid on the time scale of barrier passage, one can improve the result by adding a third stage,[175,178] which we call the equilibrium secondary zone approximation. If invoked, this stage uses free energy perturbation theory all along each MEP to calculate the change in secondary-zone free energy as a function of each s_i. That change is added to the generalized transition state theory free energy of activation profile for the calculation of both the quasiclassical CVT rate constant and the quantum effects on the reaction coordinate.

GAS-PHASE EXAMPLE: $H + CH_4$

In this section, CVT/μOMT theory is applied to the $H + CH_4 \rightarrow H_2 + CH_3$ reaction by using the Jordan–Gilbert[193] (JG) potential energy surface. We select this example because it is one of the few polyatomic systems for which accurate quantum dynamics calculations are available.[194–196] (By accurate quantum dynamics, we mean that the nuclear quantum dynamics are converged for a given potential energy surface.) All the VTST calculations have been carried out with POLYRATE–version 9.3.1, and the calculations discussed here reproduce the CVT/μOMT rate constants obtained previously by Pu et al.[111,112]

First, the reactants, products, and saddle point are optimized. The imaginary frequency at the saddle point of this example has a value of $1093i\ \text{cm}^{-1}$. The energies calculated at these points yield a classical barrier height of $V^{\ddagger} = 10.92$ kcal/mol and an energy of reaction, ΔE, of 2.77 kcal/mol. From the normal mode analyses performed at the stationary points, the vibrationally adiabatic ground-state barrier at the saddle point is calculated to be $\Delta V_a^{\ddagger G} = 10.11$ kcal/mol, where

$$\Delta V_a^{\ddagger G} = V_a^{\ddagger G} - V_a^G(s = -\infty) \qquad [326]$$

and the reaction, for the assumed potential energy surface, is slightly exothermic, $\Delta H_0^o = -0.01$ kcal/mol, where H is the enthalpy. Notice that $\Delta H_T^o = \Delta G_T^o$ at $T = 0$ K.

The MEP was followed over the interval $-2.50\,a_o \leq s \geq 2.50\,a_o$ by using the Page–McIver algorithm with a step size of 0.01 a_o, and curvilinear Hessian calculations were performed at every step. The scaling mass that transforms mass-weighted coordinates to mass-scaled coordinates has been set equal to 1 amu. The vibrationally adiabatic ground-state barrier is located at $s_*^{AG} = 0.182\ a_o$, and the vibrationally adiabatic ground-state barrier height is found to be $\Delta V_a^{AG} = 10.44$ kcal/mol. The meaning of Δ is that this is V_a^G at its maximum (denoted by A) relative to the value of V_a^G at reactants, whereas V_a^{AG} without Δ refers to V_a^G relative to the energy at the classical equilibriun

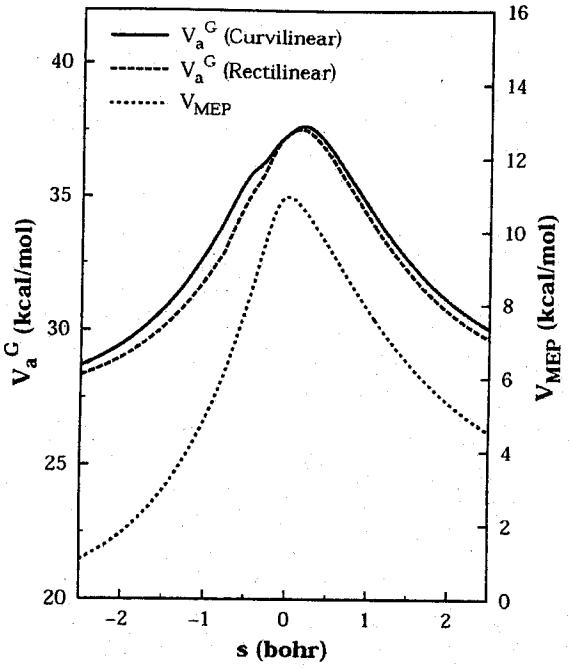

Figure 6 Plot of the MEP (dotted line) and the vibrationally adiabatic ground-state potential curve as calculated in curvilinear (solid line) and rectilinear (dashed line) coordinates for the H + CH_4 reaction.

structure of reactants; this is about 38 kcal/mol as shown in Figure 6. In Figure 6, we plot V_{MEP} and the vibrationally adiabatic potential with vibrations orthogonal to the reaction path treated in both curvilinear and rectilinear (Cartesian) coordinates. It should be noticed that both the MEP and the potential V_{MEP} along the MEP are the same in both systems of coordinates; however, the vibrationally adiabatic potential energy curves are different at nonstationary points because the vibrational frequencies at nonstationary points depend on the coordinate system. The values of the vibrational frequencies along the reaction path are more physical in curvilinear coordinates, as discussed.

Once the MEP and the frequencies along it have been calculated, one can calculate the generalized-transition-state-theory free energy profiles, as shown in Figure 7 for $T = 200, 300$, and 500 K. As indicated in Figure 3, the maximum V_a^{AG} of the adiabatic potential need not coincide with the maximum $\Delta G^{CVT,o}(T)$ of the free energy of activation profile at a given temperature. The values of $s_*^{CVT}(T)$ are 0.177, 0.171, and 0.152 a_o at $T = 200, 300$, and 500 K, respectively as shown in Figure 7. Thus, the CVT rate constant is lower than the conventional TST rate constant because the best dividing surface (the bottleneck) is located at $s \neq 0$. For instance, at $T = 300$ K, the value of the CVT rate constant is 2.2×10^{-20} cm^3 molecule^{-1} s^{-1}, whereas the conventional

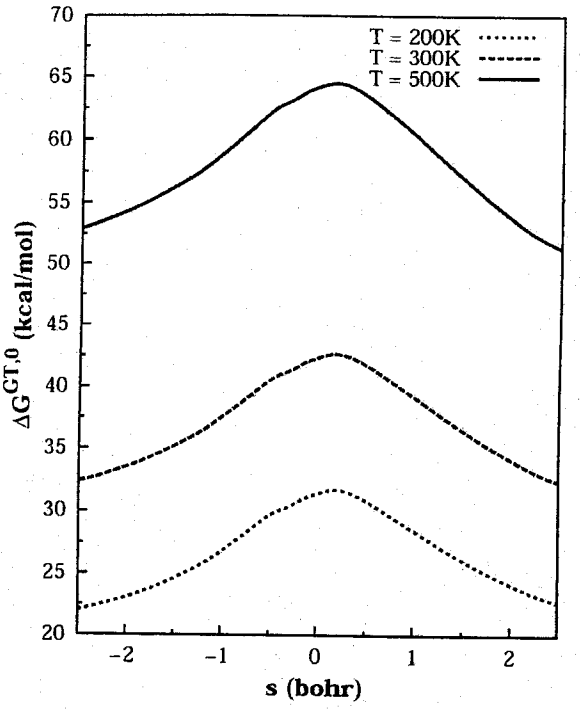

Figure 7 Generalized-transition-state free energy of activation along the MEP at three different temperatures for the $H + CH_4$ reaction.

TST rate constant is $3.6 \times 10^{-18}\,cm^3$ molecule$^{-1}\,s^{-1}$. These rate constants include quantum effects in all the $F - 1$ degrees of freedom perpendicular to the reaction coordinate, but the reaction-coordinate motion is classical; thus, we sometimes call these rate constants hybrid (in older papers) or quasi-classical (in more recent papers). The quantum effects on the reaction coordinate are incorporated by a transmission coefficient as described earlier. Because the maximum of the vibrationally adiabatic potential curve and the maximum of the free energy of activation profile at a given temperature do not coincide, one must employ the classical adiabatic ground-state CAG correction of Eq. [163] in the calculation of the CVT rate constant.

Tunneling effects are important at low temperatures for this reaction because a light particle is transferred. The curvature of the reaction path was calculated by Eq. [166], and it is plotted in Figure 8. The small-curvature approximation to the effective mass along the reaction path is calculated by Eq. [174], and its ratio to the scaling mass is also plotted in Figure 8, which shows how the effective mass is reduced along the reaction path. This reduction in the effective mass also reduces the imaginary action integral and therefore increases the tunneling probability. The ZCT transmission coefficients use

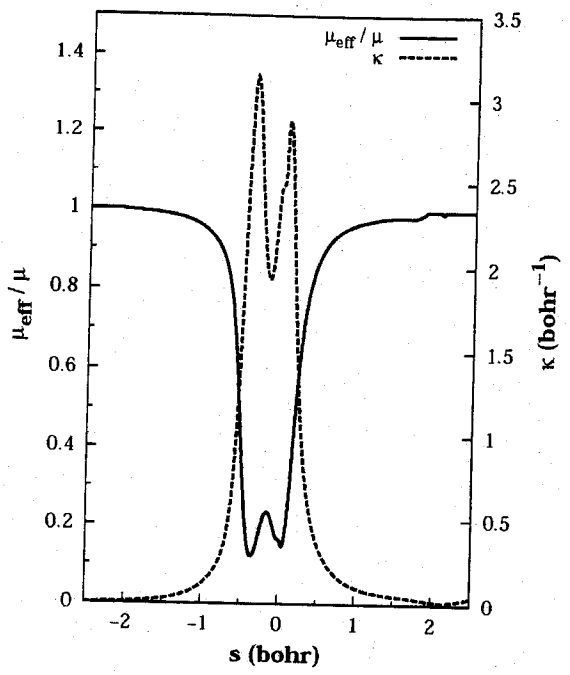

Figure 8 Plot of μ_{eff}/μ and the reaction path curvature κ along the MEP for the $H + CH_4$ reaction.

an effective mass that is always equal to the scaling mass, because the curvature along the reaction path is neglected in ZCT, and therefore, ZCT transmission coefficients always predict less tunneling than SCT transmission coefficients. The LCT transmission factors are calculated using the procedure described in the section entitled Large Curvature Transmission Coefficient. The larger of the SCT and LCT tunneling probabilities at each tunneling energy is the μOMT transmission probability. Thermally averaging these gives the μOMT transmission coefficient, which is is 18.7 at $T = 200$ K and 1.57 at $T = 500$ K.

The effect of tunneling on the reaction is further analyzed by finding the energy that contributes most to the ground-state transmission coefficient. Making a change of variable, i.e., letting $x = E - V_a^{AG}$, in Eq. [160] and by using Eqs. [162] and [163], then

$$k^{CVT/\mu OMT} = k^{CVT}(T)\beta\kappa^{CVT/CAG}(T)\left\{\int_{E_0 - V_a^{AG}}^{0} P(x)\exp(-\beta x)dx + \int_0^{\infty} P(x)\exp(-\beta x)dx\right\} \quad [327]$$

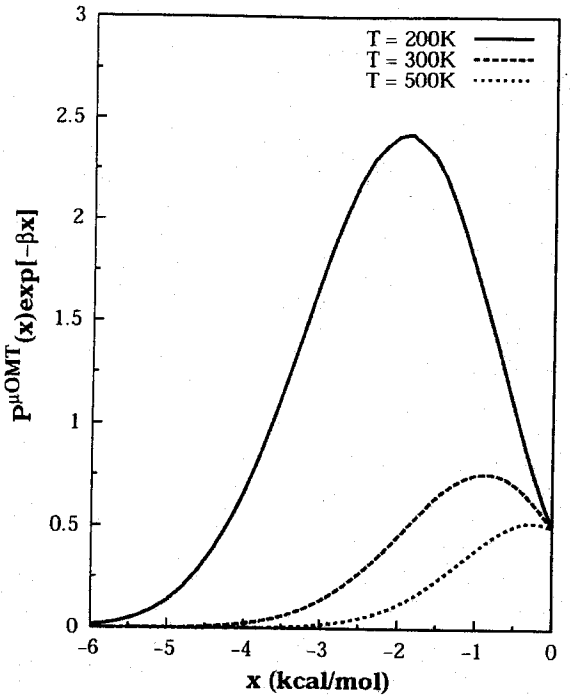

Figure 9 Plot of the first integrand of Eq. [327] versus $x = E - V_a^{AG}$ at three different energies for the $H + CH_4$ reaction. The maximum of the curves indicates the representative tunneling energy. The top of the barrier is located at $x = 0$.

The first integral yields the tunneling contribution to the transmission coefficient, and the integrand is plotted in Figure 9. The curves are the product of the tunneling probability multiplied by the Boltzmann factor. The energy at which this product has a maximum is called[119] the representative tunneling energy (RTE). At a given temperature, the RTE indicates the energy at which it is most probable for the particle to tunnel. For instance, at $T = 200\,K$ and $T = 500\,K$, the RTE is located 2.02 and 0.31 kcal/mol below the barrier top, respectively. The μOMT transmission factor is larger at lower temperatures because the area under the curve is larger.

The CVT/μOMT rate constants are 7.1×10^{-21} and 4.1×10^{-15} cm^3 molecule^{-1} s^{-1} at $T = 200$ and 500 K, respectively, whereas the accurate quantum calculations[194–196] are 9.0×10^{-21} and 3.8×10^{-15} cm^3 molecule^{-1} s^{-1} at those two temperatures. The average absolute deviation between the CVT/μOMT and the accurate rate constants is only 17% in the range 200–500 K. The performance of CVT/μOMT for this reaction is astonishing, considering that the quantum calculations for this system took several

months, whereas the VTST/μOMT results require only a few seconds of computer time. In particular, the calculations were carried out in less than 30 seconds on an old computer, including full LCT calculations without even using the faster spline algorithm. The calculations are so fast that the slowest part is setting up the input file.

LIQUID-PHASE EXAMPLE: MENSHUTKIN REACTION

In this section, VTST is applied to the bimolecular Menshutkin reaction in aqueous solution:[159]

$$ClCH_3 + NH_3 \rightarrow Cl^- + H_3CNH_3^+ \qquad [328]$$

An important difference of this example from that given earlier is that in this case no analytical potential energy surface was provided to the program. Instead, the electronic structure data needed for the dynamics were calculated "on the fly" by the MN-GSM[197] program; that is, direct dynamics was used. The gas-phase electronic structure calculations were carried out with the HF/6-31G(d) method, and the MEP was followed by using the Page–McIver algorithm with a step size of 0.01 a_o with analytical Hessian calculations every nine steps. Generalized normal modes were calculated using redundant curvilinear coordinates. The calculations in solution were performed with the program MN-GSM–version 5.2, which incorporates the SM5.42, SM5.43, and SM6 solvation models into *Gaussian* 98.[198] The dynamics calculations were carried out with GAUSSRATE–version 9.1, which in this case was modified to serve as an interface between the MN-GSM–v5.2 and POLYRATE–version 9.3.1 programs.

The SES calculations were carried out along the gas-phase MEP. In an SES calculation, the solvent is not considered when constructing the MEP, and solvent effects are added separately to create the potential of mean force using Eq. [311]. The solvation free energy was evaluated with the SM5.43 model, and therefore, the SES calculations are denoted as SM5.43/HF/6-31+G(d)//HF/6-31G(d) or simply as SM5.43/HF/6-31G(d)//*g*.

The ESP calculations, which include solvent effects when determining geometries of stationary points and points on the reaction path, are denoted as SM5.43/HF/6-31+G(d). The stationary points within the ESP approximation are optimized using the potential of mean force, where this potential has a minimum for reactants and products and a maximum for the transition state in solution. The reaction path was obtained by using the Page–McIver algorithm with a step size of 0.01 a_o. We evaluated numerical Hessians, including the effect of solvent, by central differences at every ninth step. Vibrational

Table 1 Bond Lengths of the Stationary Points in Å

	Gas Phase		ESP	
	R_{NC}	R_{CCl}	R_{NC}	R_{CCl}
Reactant	∞	1.785	∞	1.805
van der Waals complex	3.419	1.793	—	—
Saddle point	1.876	2.482	2.263	2.312
Ion pair	1.548	2.871	—	—
Products	1.507	∞	1.476	∞

frequencies were calculated in redundant curvilinear coordinates. In the ESP approach, we consider the liquid-phase saddle point on the potential of mean force surface of the solute as the dividing surface for the conventional transition state theory calculations.

For Reaction [328], the Cl, C, and N atoms are collinear. The bond lengths between these three atoms in the gas phase and in solution are listed in Table 1, and the energetics of the stationary points are listed in Table 2. For this reaction, solvent effects are very large for products. The aqueous solution stabilizes the charged products, as shown in Table 3. The gas-phase V_{MEP} and the SES canonical mean-shape potential $U(s|T)$ are plotted in Figure 10. Note that

$$U(s|T) = V_{MEP}(s) + \Delta G_S^0(\mathbf{R}(s), T) \qquad [329]$$

In the gas phase, a transition state exists for reaction only because there is a slightly stable ion-pair structure, which disappears when the geometry is optimized in solution. The maximum of $U(s|T)$ in the SES approximation is located at $s = -1.60\ a_0$. The maximum of $U(s|T)$ along the reaction path at the SM5.43//HF/6-31G(d) level is much closer to reactants than in the gas phase, which was expected, because in solution, products are much more stabilized.

Table 2 Zero-Order Mean Shape Potential of the Stationary Points Relative to Reactants (in kcal/mol)

	Gas[a]	SES[a]	ESP[a]
van der Waals complex	−2.0	−0.98	—
Saddle point	36.1	2.61	13.4
Ion pair	30.6	−27.5	—
Products	111.7	−38.6	−35.6

[a]Reactants absolute energy (in hartrees): −555.277509 (gas); −555.285927 (SES); −555.286366 (ESP).

Table 3 Standard-State Free Energies of Solvation of the Stationary Points in kcal/mol

Level	SES	ESP
NH_3	−4.6	−5.1
CH_3Cl	−0.7	1.4
$ClCH_3...NH_3$	−4.2	—
Transition state	−78.8	−20.1
$Cl^-...CH_3NH_3^+$	−78.9	—
Cl^-	−72.0	−72.0
$CH_3NH_3^+$	−83.6	−84.3

The potentials along the reaction paths in the SES and ESP approximations are plotted in Figure 11 using a common reaction coordinate consisting of the difference between the breaking and the forming bonds along the path involving the breaking and forming bond distance in the gas-phase transition state (this reaction coordinate is used only for plotting the two cases on a common scale; the actual reaction coordinates are distance along the gas-phase MEP for the SES cases and along the liquid-phase MEP for ESP). The SES and ESP potentials show similar profiles and therefore similar rate constants at room

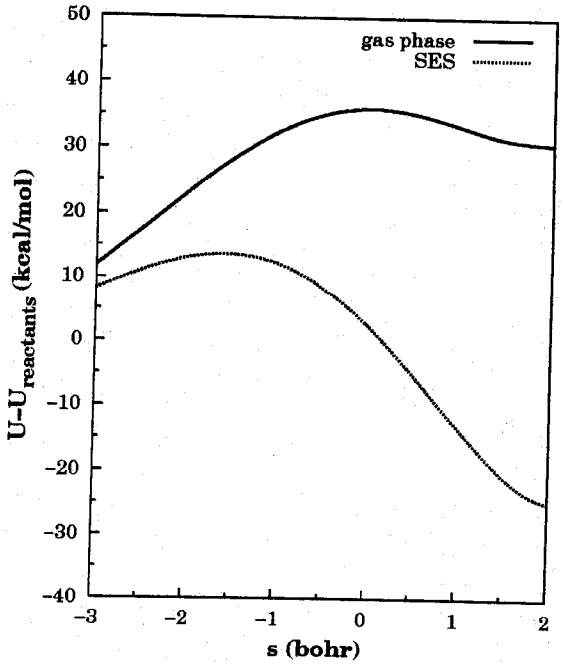

Figure 10 Zero-order canonical mean shape potential U for reaction [328] calculated at the HF/6-31 G(d) (gas phase) and SM5.43//HF/6-31G(d) (SES) levels as functions of the reaction coordinate s for the Menshutkin reaction.

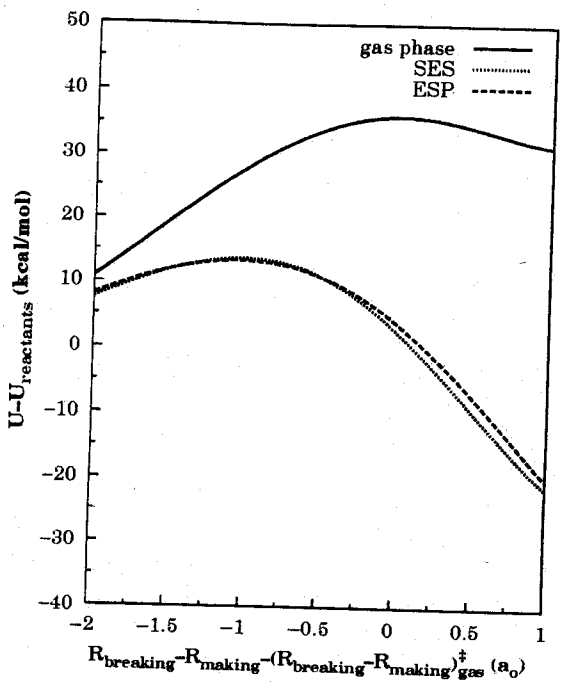

Figure 11 Zero-order canonical mean shape potential U for reaction [328] calculated at the HF/6-31G(d) (gas phase), SM5.43//HF/6-31G(d) (SES), and SM5.43/HF/6-31G(d) (ESP) levels as functions for the Menshutkin reaction.

temperature (see Table 4). The exception is the conventional TST rate constant in the SES approach, which is about six orders of magnitude higher than the CVT rate constant. This is caused by the very different location of the maximum of the potential in liquid-phase solution as compared with the gas phase. As expected, tunneling is not very important for this reaction, and therefore, the SCT approach for tunneling suffices for this case.

Although the above reaction is quite simple, the similarity between the SES and the ESP profiles is stunning if we consider the great difference between the gas-phase and liquid-phase potentials. From this example, we can conclude that, although the ESP allows a more reliable description of the reaction in solution, the SES approach is an inexpensive approach that can sometimes provide a reasonably accurate alternative to the ESP method.

Table 4 Rate Constants in cm^3 molecule^{-1} s^{-1}

k	SES	ESP
TST	3.7×10^{-18}	3.7×10^{-25}
CVT	2.0×10^{-25}	1.9×10^{-25}
CVT/SCT	2.9×10^{-25}	2.6×10^{-25}

CONCLUDING REMARKS

Transition state theory is based on the assumption of a dynamical bottleneck. The dynamical bottleneck assumption would be perfect, at least in classical mechanics, if the reaction coordinate were separable. Then one could find a dividing surface separating reactants from products that is not recrossed by any trajectories in phase space. Conventional transition state theory assumes that the unbound normal mode of the saddle point provides such a separable reaction coordinate, but dividing surfaces defined with this assumption often have significant recrossing corrections. Variational transition state theory corrects this problem, eliminating most of the recrossing.

Variational transition state theory has proved itself to be a flexible and practical tool for finding better transition state dividing surfaces in both simple and complex systems. Such dividing surfaces are called generalized transition states, and the optimum or optimized generalized transition states are called variational transition states. Real chemical reactions involve reactants with quantized vibrations, and this feature must be included in realistic rate constant calculations. Much more accurate rate constants are obtained if vibrations are treated as quantized both in the generalized transition state dividing surface and in the reactants. The reaction-coordinate motion, which is unbound for bimolecular reactions and therefore does not have quantized vibrations, also exhibits quantum effects, especially tunneling and nonclassical reflection. For thermal reactions that involve significant tunneling contributions, it is necessary to treat the overbarrier and tunneling processes in a consistent framework because the fraction of reaction that occurs by a tunneling mechanism tends to decrease gradually as the temperature is increased; this consistency can only be achieved in general if a variational criterion is used to optimize the overbarrier contribution; after such optimization is carried out, the ground-state transmission coefficient approximation and the canonical-mean-shape approximation provide ways of consistently incorporating tunneling effects into variational transition state theory for gas-phase and liquid-phase reactions, respectively.

For simple reactions, one needs to consider only a single reaction coordinate, and the isoinertial minimum energy path provides a good choice that is often sufficient. Early work took the transition state dividing surfaces to be hyperplanes perpendicular to the isoinertial minimum energy path and optimized the location of such hyperplanes along this path. The next generation of algorithms either optimized the orientation of hyperplanes or used curvilinear coordinates to define more physical dividing surfaces. The most complete algorithms consider an ensemble of reaction paths. In this way one can account, at least in part, for recrossing the dividing surface defined by a single reaction coordinate.

It is not sufficient to merely treat tunneling consistently with overbarrier processes; it must be treated accurately. For overbarrier processes,

the nonseparability of the reaction coordinate shows up as recrossing, and the nonseparability of the reaction coordinate is even more important for tunneling than for overbarrier processes. Two kinds of nonseparability are recognized. First, the effective barrier along the tunneling coordinate depends on all other degrees of freedom. Second, the tunneling paths themselves tend to be shorter than the minimum energy path, and this path shortening, called corner cutting, depends on the multidimensional shape of the potential energy surface. For small curvature of the minimum energy path in isoinertial coordinates, the effective potential may be calculated vibrationally adiabatically, and tunneling-path shortening may be calculated to a good approximation from the reaction-path curvature. For large curvature of the minimum energy path in isoinertial coordinates, the effective potential is vibrationally nonadiabatic, and one must average over a set of nearly straight tunneling paths that usually cannot be represented in coordinate systems based on the minimum-energy path; special procedures called large-curvature tunneling approximations have been worked out to treat such tunneling consistently with variational transition state theory.

This chapter has included a discussion of algorithms for treating all these issues, especially as they are incorporated in the POLYRATE computer program. The POLYRATE program requires information about the potential energy surface, and this can be included in a variety of ways. These include global analytical potential energy surfaces and direct dynamics. In direct dynamics, the energies, gradients, and Hessians required by the algorithms are computed "on the fly" by electronic structure calculations whenever the algorithms call for them. This is called direct dynamics. POLYRATE also includes several interpolation schemes in which the needed energies, gradients, and Hessians are locally interpolated from a small dataset of electronic structure calculations; this is a particularly efficient form of direct dynamics.

ACKNOWLEDGMENTS

This work was supported in part by the U.S. Department of Energy (DOE), Office of Basic Energy Sciences (BES), under Grant DE-FG02-86ER13579 and by the Air Force Office of Scientific Research by a Small Business Technology Transfer grant to Scientific Applications and Research Assoc., Inc. A.F.R. thanks the Ministerio de Educación y Ciencia of Spain for a Ramón y Cajal research contract and for Project #BQU2003-01639. B.C.G. acknowledges BES support at Pacific Northwest National Laboratory (PNNL). Battelle operates PNNL for DOE.

REFERENCES

1. D. G. Truhlar, A. D. Isaacson, and B. C. Garrett, in *Theory of Chemical Reaction Dynamics*, Vol. 3, M. Baer, ed., CRC Press, Boca Raton, FL, 1985, pp. 65–137. Generalized Transition State Theory.

2. A. D. Isaacson, D. G. Truhlar, S. N. Rai, R. Steckler, G. C. Hancock, B. C. Garrett, and M. J. Redmon, *Comput. Phys. Commun.*, 47, 91 (1987). POLYRATE: A General Computer Program for Variational Transition State Theory and Semiclassical Tunneling Calculations of Chemical Reaction Rates.

3. D.-h. Lu, T. N. Truong, V. S. Melissas, G. C. Lynch, Y.-P. Liu, B. C. Garrett, R. Steckler, A. D. Isaacson, S. N. Rai, G. C. Hancock, J. G. Lauderdale, T. Joseph, and D. G. Truhlar, *Comput. Phys. Commun.*, 71, 235 (1992). POLYRATE 4: A New Version of a Computer Program for the Calculation of Chemical Reaction Rates for Polyatomics.

4. W.-P. Hu, R. Steckler, G. C. Lynch, Y.-P. Liu, B. C. Garrett, A. D. Isaacson, D.-h. Lu, V. S. Melissas, I. Rossi, J. J. P. Stewart, and D. G. Truhlar, *QCPE Bull.*, 15,32 (1995). POLYRATE -version 6.5 and MORATE -version 6.5/P6.5-M5.05. Two Computer Programs for the Calculation of Chemical Reaction Rates.

5. R. Steckler, W.-P. Hu, Y.-P. Liu, G. C. Lynch, B. C. Garrett, A. D. Isaacson, V. S. Melissas, D.-h. Lu, T. N. Truong, S. N. Rai, G. C. Hancock, J. G. Lauderdale, T. Joseph, and D. G. Truhlar, *Comput. Phys. Commun.*, 88, 341 (1995). POLYRATE 6.5: A New Version of a Computer Program for the Calculation of Reaction Rates for Polyatomics.

6. J. C. Corchado, Y.-Y. Chuang, P. L. Fast, W.-P. Hu, Y.-P. Liu, G. C. Lynch, K. A. Nguyen, C. F. Jackels, A. Fernandez-Ramos, B. A. Ellingson, B. J. Lynch, V. S. Melissas, J. Villà, I. Rossi, E. L. Coitiño, J. Pu, T. V. Albu, R. Steckler, B. C. Garrett, A. D. Isaacson, and D. G. Truhlar, POLYRATE - version 9.4.3. University of Minnesota, Minneapolis, Minnesota, 2006. Available: http://comp.chem.umn.edu/polyrate.

7. S. C. Tucker and D. G. Truhlar, in *New Theoretical Concepts for Understanding Organic Reactions*, J. Bertrán and I. G. Csizmadia, Eds., Kluwer, Dordrecht, The Netherlands, 1989, pp. 291–346. [NATO ASI Ser. C 267, 291–346 (1989)]. Dynamical Formulation of Transition State Theory: Variational Transition States and Semiclassical Tunneling.

8. H. Eyring, *J. Chem. Phys.*, 3, 107 (1935). The Activated Complex in Chemical Reactions.

9. M. G. Evans and M. Polanyi, *Trans. Faraday Soc.*, 31, 875 (1935). Some Applications of the Transition State Method to the Calculation of Reaction Velocities, Especially in Solution.

10. W. F. K. Wynne-Jones and H. Eyring, *J. Chem. Phys.*, 3, 492 (1935). The Absolute Rate of Reactions in Condensed Phases.

11. R. H. Fowler, *Trans. Faraday Soc.*, 34, 124 (1938). General Discussion.

12. R. K. Boyd, *Chem. Rev.*, 77, 93 (1977). Macroscopic and Microscopic Restrictions on Chemical Kinetics.

13. C. Lim and D. G. Truhlar, *J. Phys. Chem.*, 89, 5 (1985). Internal-State Nonequilibrium Effects for a Fast, Second-Order Reaction.

14. C. Lim and D. G. Truhlar, *J. Phys. Chem.*, 90, 2616 (1986). The Effect of Vibrational-Rotational Disequilibrium on the Rate Constant for an Atom-Transfer Reaction.

15. H. Teitelbaum, *J. Phys. Chem.*, 94, 3328 (1990). Nonequilibrium Kinetics of Bimolecular Exchange Reactions. 3. Application to Some Combustion Reactions.

16. C. Bowes, N. Mina, and H. Teitelbaum, *J. Chem. Soc., Faraday Trans.*, 87, 229 (1991). Non-Equilibrium Kinetics of Bimolecular Exchange Reactions. 2. Improved Formalism and Applications to Hydrogen Atom + Hydrogen Molecule → Hydrogen Molecule + Hydrogen drogen Atom and its Isotopic Variants.

17. H. Teitelbaum, *Chem. Phys.*, 173, 91 (1993). Non-Equlibrium Kinetics of Bimolecular Reactions. IV. Experimental Prediction of the Breakdown of the Kinetic Mass-Action Law.

18. H. Teitelbaum, *Chem. Phys. Lett.*, 202, 242 (1993). Non-Equilibrium Kinetics of Bimolecular Reactions. Effect of Anharmonicity on the Rate Law.

19. P. Pechukas, *Annu. Rev. Phys. Chem.*, 32, 159 (1981). Transition State Theory.

20. B. C. Garrett and D. G. Truhlar, *J. Phys. Chem.*, 83, 1052 (1979); Erratum: 87, 4553 (1983). Generalized Transition State Theory. Classical Mechanical Theory and Applications to Collinear Reactions of Hydrogen Molecules.

21. E. Wigner, *J. Chem. Phys.*, 5, 720 (1937). Calculation of the Rate of Elementary Association Reactions.
22. J. Horiuti, *Bull. Chem. Soc. Jpn.*, 13, 210 (1938). On the Statistical Mechanical Treatment of the Absolute Rates of Chemical Reactions.
23. J. C. Keck, *J. Chem. Phys.*, 32, 1035 (1960). Variational Theory of Chemical Reaction Rates Applied to Three-Body Recombinations.
24. J. C. Keck, *Adv. Chem. Phys.*, 13, 85 (1967). Variational Theory of Reaction Rates.
25. R. L. Jaffe, J. M. Henry, and J. B. Anderson, *J. Chem. Phys.*, 59, 1128 (1973). Variational Theory of Reaction Rates: Application to $F+H_2 \leftrightarrow HF+H$.
26. W. H. Miller, *J. Chem. Phys.*, 61, 1823 (1974). Quantum Mechanical Transition State Theory and a New Semiclassical Model for Reaction Rate Constants.
27. B. C. Garrett and D. G. Truhlar, *J. Chem. Phys.*, 70, 1593 (1979). Criterion of Minimum State Density in the Transition State Theory of Bimolecular Reactions.
28. E. B. Wilson, Jr., J. C. Decius, and P. C. Cross, *Molecular Vibrations*, Dover Publications, Inc., New York, 1955.
29. R. A. Marcus, *Discuss. Faraday Soc.*, 44, 7 (1967). Analytical Mechanics and Almost Vibrationally Adiabatic Chemical Reactions.
30. B. C. Garrett and D. G. Truhlar, *J. Phys. Chem.*, 83, 1079 (1979); Erratum: 87, 4553 (1983). Generalized Transition State Theory. Quantum Effects for Collinear Reactions of Hydrogen Molecules and Isotopically Substituted Hydrogen Molecules.
31. K. Fukui, in *The World of Quantum Chemi*stry, R. Daudel and B. Pullman, Eds., D. Reidel, Dordrecht, The Netherlands, 1974, pp. 113. The Charge and Spin Transfers in Chemical Reaction Paths.
32. G. K. Schenter, B. C. Garrett, and D. G. Truhlar, *J. Chem. Phys.*, 119, 5828 (2003). Generalized Transition State Theory in Terms of the Potential of Mean Force.
33. G. K. Schenter, B. C. Garrett, and D. G. Truhlar, *J. Phys. Chem. B*, 105, 9672 (2001). The Role of Collective Solvent Coordinates and Nonequilibrium Solvation in Charge-Transfer Reactions.
34. P. L. Fast and D. G. Truhlar, *J. Chem. Phys.*, 109, 3721 (1998). Variational Reaction Path Algorithm.
35. B. C. Garrett and D. G. Truhlar, *J. Am. Chem. 50c*, 101, 4534 (1979). Generalized Transition State Theory. Bond Energy–Bond Order Method for Canonical Variational Calculations with Application to Hydrogen Atom Transfer Reactions.
36. A. Tweedale and K. J. Laidler, *J. Chem. Phys.*, 53, 2045 (1970). Vibrationally Adiabatic Model for the Dyamics of $H + H_2$ Systems.
37. J. C. Keck, *Adv. Chem. Phys.*, 13, 85 (1967). Variational Theory of Reaction Rates.
38. E. Wigner, *Z. Physik Chem. B*, B19, 203 (1932). On the Penetration of Potential Energy Barriers in Chemical Reactions.
39. M. A. Eliason and J. O. Hirschfelder, *J. Chem. Phys.*, 30, 1426 (1956). General Collision Theory Treatment for the Rate of Bimolecular, Gas Phase Reactions.
40. C. Steel and K. J. Laidler, *J. Chem. Phys.*, 34, 1827 (1961). High Frequency Factors in Unimolecular Reactions.
41. B. C. Garrett, D. G. Truhlar, R. S. Grev, and A. W. Magnuson, *J. Phys. Chem.*, 84, 1730 (1980). Improved Treatment of Threshold Contributions in Variational Transition-State Theory.
42. J. O. Hirschfelder and E. Wigner, *J. Chem. Phys.*, 7, 616 (1939). Some Quantum-Mechanical Considerations in the Theory of Reactions Involving an Activation Energy.
43. W. H. Miller, *J. Chem. Phys.*, 65, 2216 (1976). Unified Statistical Model for "Complex" and "Direct" Reaction Mechanisms.
44. B. C. Garrett and D. G. Truhlar, *J. Chem. Phys.*, 76, 1853 (1982). Canonical Unified Statistical Model. Classical Mechanical Theory and Applications to Collinear Reactions.

45. D. G. Truhlar and B. C. Garrett, *J. Phys. Chem. A*, 107, 4006 (2003). Reduced Mass in the One-Dimensional Treatment of Tunneling.

46. G. Gamow, *Z. Phys.*, 51, 204 (1928). Quantum Theory of the Atomic Nucleus.

47. E. C. Kemble, *The Fundamental Principles of Quantum Mechanics With Elementary Applications*, Dover Publications, New York, 1937.

48. R. P. Bell, *Proc. Royal Soc. A*, 139, 466 (1933). The Application of Quantum Mechanics to Chemical Kinetics.

49. R. P. Bell, *Trans. Faraday Soc.*, 55, 1 (1959). The Tunnel Effect Correction for Parabolic Potential Barriers.

50. R. T. Skodje and D. G. Truhlar, *J. Phys. Chem.*, 85, 624 (1981). Parabolic Tunneling Calculations.

51. C. Eckart, *Phys. Rev.*, 35, 1303 (1930). The Penetration of a Potential Barrier by Electrons.

52. R. A. Marcus, *J. Chem. Phys.*, 49, 2617 (1968). Analytical Mechanics of Chemical Reactions. IV. Classical Mechanics of Reactions in Two Dimensions.

53. I. Shavitt, *J. Chem. Phys.*, 49, 4048 (1968). Correlation of Experimental Rate Constants of the Hydrogen Exchange Reactions with a Theoretical H_3 Potential Surface, Using Transition-State Theory.

54. D. G. Truhlar and A. Kuppermann, *J. Am. Chem. Soc.*, 93, 1840 (1971). Exact Tunneling Calculations.

55. K. Fukui, S. Kato, and H. Fujimoto, *J. Am. Chem. Soc.*, 97, 1 (1975). Constituent Analysis of the Potential Gradient Along a Reaction Coordinate. Method and an Application to Methane + Tritium Reaction.

56. M. C. Flanigan, A. Komornicki, and J. W. McIver, Jr. In *Semiempirical Methods of Electronic Structure Calculation, Part B: Applications*, G. A. Segal, Ed., Plenum, New York, 1977, pp. 1–47.

57. C. Peng, P. Y. Ayala, H. B. Schlegel, and M. J. Frisch, *J. Comput. Chem.*, 17, 49 (1996). Using Redundant Internal Coordinates to Optimize Equilibrium Geometries and Transition States.

58. P. Y. Ayala and H. B. Schlegel, *J. Chem. Phys.*, 107, 375 (1997). A Combined Method for Determining Reaction Paths, Minima, and Transition State Geometries.

59. V. S. Melissas, D. G. Truhlar, and B. C. Garrett, *J. Chem. Phys.*, 96, 5758 (1992). Optimized Calculations of Reaction Paths and Reaction-Path Functions for Chemical Reactions.

60. M. W. Schmidt, M. S. Gordon, and M. Dupuis, *J. Am. Chem. Soc.*, 107, 2585 (1985). The Intrinsic Reaction Coordinate and the Rotational Barrier in Silaethylene.

61. B. C. Garrett, M. J. Redmon, R. Steckler, D. G. Truhlar, K. K. Baldridge, D. Bartol, M. W. Schmidt, and M. S. Gordon, *J. Phys. Chem.*, 92, 1476 (1988). Algorithms and Accuracy Requirements for Computing Reaction Paths by the Method of Steepest Descent.

62. K. K. Baldridge, M. S. Gordon, R. Steckler, and D. G. Truhlar, *J. Phys. Chem.*, 93, 5107 (1989). Ab Initio Reaction Paths and Direct Dynamics Calculations.

63. M. Page and J. W. McIver, Jr., *J. Chem. Phys.*, 88, 922 (1988). On Evaluating the Reaction Path Hamiltonian.

64. J. Villà and D. G. Truhlar, *Theor. Chem. Acc.*, 97, 317 (1997). Variational Transition State Theory Without the Minimum-Energy Path.

65. W. H. Miller, N. C. Handy, and J. E. Adams, *J. Chem. Phys.*, 72, 99 (1980). Reaction Path Hamiltonian for Polyatomic Molecules.

66. G. A. Natanson, *Mol. Phys.*, 46, 481 (1982). Internal Motion of a Nonrigid Molecule and its Relation to the Reaction Path.

67. G. A. Natanson, B. C. Garrett, T. N. Truong, T. Joseph, and D. G. Truhlar, *J. Chem. Phys.*, 94, 7875 (1991). The Definition of Reaction Coordinates for Reaction-Path Dynamics.

68. C. F. Jackels, Z. Gu, and D. G. Truhlar, *J. Chem. Phys.*, 102, 3188 (1995). Reaction-Path Potential and Vibrational Frequencies in Terms of Curvilinear Internal Coordinates.

69. G. Herzberg, *Molecular Spectra and Molecular Structure. II. Infrared and Raman Spectra of Polyatomic Molecules*, D. Van Nostrand, Princeton, New Jersey, 1945.

70. A. D. Isaacson, D. G. Truhlar, K. Scanlon, and J. Overend, *J. Chem. Phys.*, 75, 3017 (1981). Tests of Approximation Schemes for Vibrational Energy Levels and Partition Functions for Triatomics: H_2O and SO_2.

71. P. Pulay and G. Fogarasi, *J. Chem. Phys.*, 96, 2856 (1992). Geometry Optimization in Redundant Internal Coordinates.

72. Y.-Y. Chuang and D. G. Truhlar, *J. Phys. Chem. A*, 102, 242 (1998). Reaction-Path Dynamics in Redundant Internal Coordinates.

73. D. F. McIntosh and K. H. Michelian, *Can. J. Spectrosc.*, 24, 1 (1979). The Wilson GF Matrix Method of Vibrational Analysis. Part I: General Theory.

74. D. F. McIntosh and K. H. Michelian, *Can. J. Spectrosc.*, 24, 35 (1979). The Wilson GF Matrix Method of Vibrational Analysis. Part II. Theory and Worked Examples of the Construction of the B Matrix.

75. D. F. McIntosh and K. H. Michelian, *Can. J. Spectrosc.*, 24, 65 (1979). The Wilson GF Matrix Method of Vibrational Analysis. Part III: Worked Examples of The Vibrational Analysis of Carbon Dioxide and Water.

76. S. J. Klippenstein, *J. Chem. Phys.*, 94, 6469 (1991). A Bond Length Reaction Coordinate for Unimolecular Reactions. II. Microcanonical and Canonical Implementations with Application to the Dissociation of NCNO.

77. S. J. Klippenstein, *J. Chem. Phys.*, 96, 367 (1992); Erratum: 96, 5558 (1992). Variational Optimizations in the Rice–Ramsperger–Kassel–Marcus Theory Calculations For Unimolecular Dissociations With No Reverse Barrier.

78. J. Villà, A. González-Lafont, J. M. Lluch, and D. G. Truhlar, *J. Am. Chem. Soc.*, 120, 5559 (1998). Entropic Effects on the Dynamical Bottleneck Location and Tunneling Contributions for $C_2H_4 + H \rightarrow C_2H_5$. Variable Scaling of External Correlation Energy for Association Reactions.

79. J. Villà, J. C. Corchado, A. González-Lafont, J. M. Lluch, and D. G. Truhlar, *J. Am. Chem. Soc.*, 120, 12141 (1998). Explanation of Deuterium and Muonium Kinetic Isotope Effects for Hydrogen Atom Addition to an Olefin.

80. J. Villà, J. C. Corchado, A. González-Lafont, J. M. Lluch, and D. G. Truhlar, *J. Phys. Chem. A*, 103, 5061 (1999). Variational Transition State Theory with Optimized Orientation of the Dividing Surface and Semiclassical Tunneling Calculations for Deuterium and Muonium Kinetic Isotope Effects in the Free Radical Association Reaction $H + C_2H_4 \rightarrow C_2H_5$.

81. D. A. Wardlaw and R. A. Marcus, *J. Chem. Phys.* 83, 3462 (1985). Unimolecular Reaction Rate Theory for Transition States of Partial Looseness. II. Implementation and Analysis with Applications to NO_2 and C_2H_6 Dissociations.

82. D. M. Wardlaw and R. A. Marcus, *Adv. Chem. Phys.* 107, 9776 (1988). On the Statistical Theory of Unimolecular Processes.

83. S. J. Klippenstein, *J. Phys. Chem.* 98, 11459 (1994). An Efficient Procedure for Evaluating the Number of Available States within a Variably Defined Reaction Coordinate Framework.

84. M. Pesa, M. J. Pilling, S. H. Robertson, and D. M. Wardlaw, *J. Phys. Chem. A*, 102, 8526 (1998). Application of the Canonical Flexible Transition State Theory to CH_3, CF_3, and CCl_3 Recombination Reactions.

85. S. C. Smith, *J. Chem. Phys.*, 111, 1830 (1999). Classical Flux Integrals in Transition State Theory: Generalized Reaction Coordinates.

86. S. Robertson, A. F. Wagner, and D. M. Wardlaw, *J. Phys. Chem. A*, 106, 2598 (2002). Flexible Transition State Theory for a Variable Reaction Coordinate: Analytical Expressions and an Application.

87. Y. Georgievskii and S. J. Klippenstein, *J. Chem. Phys.*, 118, 5442 (2003). Variable Reaction Coordinate Transition State Theory: Analytic Results and Application to the $C_2H_3 + H \rightarrow C_2H_4$ Reaction.

88. Y. Georgievskii and S. J. Klippenstein, *J. Phys. Chem. A*, **107**, 9776 (2003). Transition State Theory for Multichannel Addition Reactions: Multifaceted Dividing Surfaces.

89. Y. Georgievskii and S. J. Klippenstein, *J. Chem. Phys.*, **122**, 194103 (2005). Long-Range Transition State Theory.

90. Y.-Y. Chuang and D. G. Truhlar, *J. Chem. Phys.*, **112**, 1221 (2000); Erratum: **124**, 179903 (2006). Statistical Thermodynamics of Bond Torsional Modes.

91. Y.-P. Liu, D.-h. Lu, A. González-Lafont, D. G. Truhlar, and B. C. Garrett, *J. Am. Chem. Soc.*, **115**, 7806 (1993). Direct Dynamics Calculation of the Kinetic Isotope Effect for an Organic Hydrogen-Transfer Reaction, Including Corner-Cutting Tunneling in 21 Dimensions.

92. K. S. Pitzer and W. D. Gwinn, *J. Chem. Phys.*, **10**, 428 (1942). Energy Levels and Thermodynamic Function for Molecules with Internal Rotation.

93. K. S. Pitzer, *J. Chem. Phys.*, **14**, 239 (1946). Energy Levels and Thermodynamic Functions for Molecules with Internal Rotation: II. Unsymmetrical Tops Attached to a Rigid Frame.

94. D. G. Truhlar, *J. Comput. Chem.*, **12**, 266 (1991). A Simple Approximation for the Vibrational Partition Function of a Hindered Internal Rotation.

95. B. A. Ellingson, V. A. Lynch, S. L. Mielke, and D. G. Truhlar, *J. Chem. Phys.*, **125**, 84305 (2006). Statistical Thermodynamics of Bond Torsional Modes. Tests of Separable, Almost-Separable, and Improved Pitzer–Gwinn Approximations.

96. G. Herzberg, *Molecular Spectra and Molecular Structure. I. Spectra of Diatomic Molecules*, Van Nostrand Reinhold, Princeton, New Jersey, 1950.

97. A. D. Isaacson and D. G. Truhlar, *J. Chem. Phys.*, **76**, 1380 (1982). Polyatomic Canonical Variational Theory for Chemical Reaction Rates. Separable-mode Formalism With Application to Hydroxyl Radical + Diatomic Hydrogen → Water + Atomic Hydrogen.

98. D. G. Truhlar, *J. Mol. Spect.*, **38**, 415 (1971). Oscillators with Quartic Anharmonicity: Approximate Energy Levels.

99. B. C. Garrett and D. G. Truhlar, *J. Phys. Chem.*, **83**, 1915 (1979). Importance of Quartic Anharmonicity for Bending Partition Functions in Transition-State Theory.

100. K. A. Nguyen, C. F. Jackels, and D. G. Truhlar, *J. Chem. Phys.*, **104**, 6491 (1996). Reaction-Path Dynamics in Curvilinear Internal Coordinates Including Torsions.

101. Y.-Y. Chuang and D. G. Truhlar, *J. Chem. Phys.*, **107**, 83 (1997). Reaction-Path Dynamics with Harmonic Vibration Frequencies in Curvilinear Internal Coordinates: H + *trans*-N_2H_2 → NH_2 + H_2.

102. B. C. Garrett and D. G. Truhlar, *J. Chem. Phys.*, **79**, 4931 (1983). A Least-Action Variational Method for Calculating Multidimensional Tunneling Probabilities for Chemical Reactions.

103. T. C. Allison and D. G. Truhlar, in *Modern Methods for Multidimensional Dynamics Computations in Chemistry*, D. L. Thompson, Ed., World Scientific, Singapore, 1998, pp. 618–712. Testing the Accuracy of Practical Semiclassical Methods: Variational Transition State Theory With Optimized Multidimensional Tunneling.

104. Y.-P. Liu, G. C. Lynch, T. N. Truong, D.-h. Lu, D. G. Truhlar, and B. C. Garrett, *J. Am. Chem. Soc.*, **115**, 2408 (1993). Molecular Modeling of the Kinetic Isotope Effect for the [1,5]-Sigmatropic Rearrangement of *cis*-1,3-Pentadiene.

105. D. G. Truhlar and B. C. Garrett, in *Annual Review of Physical Chemistry*, Vol. 35, B. S. Rabinovitch, J. M. Schurr, and H. L. Strauss, Eds., Annual Reviews, Inc., Palo Alto, California, 1984, pp. 159–189. Variational Transition State Theory.

106. M. M. Kreevoy and D. G. Truhlar, in *Investigation of Rates and Mechanisms of Reactions*, Fourth edition, Part 1, C. F. Bernasconi, Ed., Wiley, New York, 1986, pp. 13-95. Transition State Theory.

107. D. G. Truhlar and B. C. Garrett, *Journal de Chimie Physique*, **84**, 365 (1987). Dynamical Bottlenecks and Semiclassical Tunneling Paths for Chemical Reactions.

108. B. C. Garrett, T. Joseph, T. N. Truong, and D. G. Truhlar, *Chem. Phys.*, 136, 271 (1989). Application of the Large-Curvature Tunneling Approximation to Polyatomic Molecules: Abstraction of H or D by Methyl Radical.

109. T. N. Truong, D.-h. Lu, G. C. Lynch, Y.-P. Liu, V. S. Melissas, J. J. P. Stewart, R. Steckler, B. C. Garrett, A. D. Isaacson, A. González-Lafont, S. N. Rai, G. C. Hancock, T. Joseph, and D. G. Truhlar, *Comput. Phys. Commun.*, 75, 143 (1993). MORATE: A Program for Direct Dynamics Calculations of Chemical Reaction Rates by Semiempirical Molecular Orbital Theory.

110. A. Fernandez-Ramos and D. G. Truhlar, *J. Chem. Phys.*, 114, 1491 (2001). Improved Algorithm for Corner-Cutting Tunneling Calculations.

111. J. Pu, J. C. Corchado, and D. G. Truhlar, *J. Chem. Phys.*, 115, 6266 (2001). Test of Variational Transition State Theory With Multidimensional Tunneling Contributions Against an Accurate Full-Dimensional Rate Constant Calculation for a Six-Atom System.

112. J. Pu and D. G. Truhlar, *J. Chem. Phys.*, 117, 1479 (2002). Validation of Variational Transition State Theory with Multidimensional Tunneling Contributions Against Accurate Quantum Mechanical Dynamics for $H + CH_4 \rightarrow H_2 + CH_3$ in an Extended Temperature Interval.

113. R. A. Marcus, *J. Chem. Phys.*, 45, 4493 (1966). On the Analytical Mechanics of Chemical Reactions. Quantum Mechanics of Linear Collisions.

114. A. Kuppermann, J. T. Adams, and D. G. Truhlar, in *Abstractions of Papers, VIII ICPEAC, Beograd, 1973*, B. C. Cubic and M. V. Kurepa, Eds., Institute of Physics, Belgrade, Serbia. 1973 pp. 149–150.

115. R. A. Marcus and M. E. Coltrin, *J. Chem. Phys.*, 67, 2609 (1977). A New Tunneling Path for Reactions Such as $H+H_2 \rightarrow H_2+H$.

116. R. T. Skodje, D. G. Truhlar, and B. C. Garrett, *J. Chem. Phys.*, 77, 5955 (1982). Vibrationally Adiabatic Models for Reactive Tunneling.

117. M. M. Kreevoy, D. Ostovic, D. G. Truhlar, and B. C. Garrett, *J. Phys. Chem.*, 90, 3766 (1986). Phenomenological Manifestations of Large-Curvature Tunneling in Hydride Transfer Reactions.

118. D. G. Truhlar and M. S. Gordon, *Science*, 249, 491 (1990). From Force Fields to Dynamics: Classical and Quantal Paths.

119. Y. Kim, D. G. Truhlar, and M. M. Kreevoy, *J. Am. Chem. Soc.*, 113, 7837 (1991). An Experimentally Based Family of Potential Energy Surfaces for Hydride Transfer Between NAD^+ Analogues.

120. A. Fernandez-Ramos, D. G. Truhlar, J. C. Corchado, and J. Espinosa-Garcia, *J. Phys. Chem. A*, 106, 4957 (2002). Interpolated Algorithm for Large-Curvature Tunneling Calculations of Transmission Coefficients for Variational Transition State Theory Calculations of Reaction Rates.

121. A. Fernandez-Ramos and D. G. Truhlar, *J. Chem. Theory Comput.*, 1, 1063 (2005). A New Algorithm for Efficient Direct Dynamics Calculations of Large-Curvature Tunneling and its Application to Radical Reactions with 9–15 Atoms.

122. G. C. Lynch, P. Halvick, D. G. Truhlar, B. C. Garrett, D. W. Schwenke, and D. J. Kouri, *Z. Naturforsch.*, 44a, 427 (1989). Semiclassical and Quantum Mechanical Calculations of Isotopic Kinetic Branching Ratios for the Reaction of $O(^3P)$ with HD.

123. D. C. Chatfield, R. S. Friedman, D. G. Truhlar, and D. W. Schwenke, *Faraday Discuss. Chem. Soc.*, 91, 289 (1991). Quantum-Dynamical Characterization of Reactive Transition States.

124. B. C. Garrett, N. Abusalbi, D. J. Kouri, and D. G. Truhlar, *J. Chem. Phys.*, 83, 2252 (1985). Test of Variational Transition State Theory and the Least-Action Approximation for Multidimensional Tunneling Probabilities Against Accurate Quantal Rate Constants for a Collinear Reaction Involving Tunneling into an Excited State.

125. D. G. Truhlar, *J. Chem. Soc. Faraday Trans.*, 90, 1740 (1994). General Discussion.

126. B. C. Garrett and D. G. Truhlar, *J. Phys. Chem.*, 89, 2204 (1985). Generalized Transition State Theory and Least-Action Tunneling Calculations for the Reaction Rates of Atomic

Hydrogen(Deuterium) + Molecular Hydrogen ($n = 1$)→ Molecular Hydrogen(Hydrogen Deuteride) + Atomic Hydrogen.

127. S. C. Tucker, D. G. Truhlar, B. C. Garrett, and A. D. Isaacson, *J. Chem. Phys.*, 82, 4102 (1985). Variational Transition State Theory With Least-Action Tunneling Calculations for the Kinetic Isotope Effects in the Atomic Chlorine + Molecular Hydrogen Reaction: Tests of Extended-LEPS, Information-Theoretic, and Diatomics-in-Molecules Potential Energy Surfaces.

128. A. Fernandez-Ramos, Z. Smedarchina, M. Zgierski, W. Siebrand, and M. A. Rios, *J. Am. Chem. Soc.*, 121, 6280 (1999). Direct-Dynamics Approaches to Proton Tunneling Rate Constants. A Comparative Test for Molecular Inversions and Application to 7-Azaindole.

129. M. Y. Ovchinnikova, *Chem. Phys.*, 36, 85 (1979). The Tunneling Dynamics of the Low-Temperature Hydrogen Atom Exchange Reactions.

130. V. K. Babamov and R. A. Marcus, *J. Chem. Phys.*, 74, 1790 (1981). Dynamics of Hydrogen Atom and Proton Transfer Reactions. Symmetric Case.

131. D. K. Bondi, J. N. L. Connor, B. C. Garrett, and D. G. Truhlar, *J. Chem. Phys.*, 78, 5981 (1983). Test of Variational Transition State Theory with a Large-Curvature Tunneling Approximation Against Accurate Quantal Reaction Probabilities and Rate Coefficients for Three Collinear Reactions with Large Reaction-Path Curvature: Atomic Chlorine + Hydrogen Chloride, Atomic Chlorine + Deuterium Chloride, and Atomic Chlorine + MuCl.

132. A. González-Lafont, T. N. Truong, and D. G. Truhlar, *J. Phys. Chem.*, 95, 4618 (1991). Direct Dynamics Calculations with NDDO (Neglect of Diatomic Differential Overlap) Molecular Orbital Theory with Specific Reaction Parameters.

133. Y. Kim, J. C. Corchado, J. Villà, J. Xing, and D. G. Truhlar, *J. Chem. Phys.*, 112, 2718 (2000). Multiconfiguration Molecular Mechanics Algorithm for Potential Energy Surfaces of Chemical Reactions.

134. T. V. Albu, J. C. Corchado, and D. G. Truhlar, *J. Phys. Chem. A*, 105, 8465 (2001). Molecular Mechanics for Chemical Reactions: A Standard Strategy for Using Multiconfiguration Molecular Mechanics for Variational Transition State Theory with Optimized Multidimensional Tunneling.

135. H. Lin, J. Pu, T. V. Albu, and D. G. Truhlar, *J. Phys. Chem. A*, 108, 4112 (2004). Efficient Molecular Mechanics for Chemical Reactions Using Partial Electronic Structure Hessians.

136. Y.-Y. Chuang, P. L. Fast, W.-P. Hu, G. C. Lynch, Y.-P. Liu, and D. G. Truhlar, MORATE—version 8.5. Available: http://comp.chem.umn.edu/morate.

137. J. C. Corchado, Y.-Y. Chuang, E. L. Coitiño, and D. G. Truhlar, GAUSSRATE—version 9.4. Available: http://comp.chem.umn.edu/gaussrate.

138. Y.-Y. Chuang, J. C. Corchado, J. Pu, and D. G. Truhlar, GAMESSPLUSRATE—version 9.3. Available: http://comp.chem.umn.edu/gamessplusrate.

139. J. Pu, J. C. Corchado, B. J. Lynch, P. L. Fast and D. G. Truhlar, MULTILEVELRATE—version 9.3. Available: http://comp.chem.umn.edu/multilevelrate.

140. T. V. Albu, J. C. Corchado, Y. Kim, J. Villà, J. Xing, H. Lin, and D. G. Truhlar, MC-TINKERATE—version 9.1. Available: http://comp.chem.umn.edu/mc-tinkerate.

141. M. Garcia-Viloca, C. Alhambra, J. Corchado, M. Luz Sánchez, J. Villà, J. Gao, and D. G. Truhlar, CRATE—version 9.0. Available: http://comp.chem.umn.edu/crate.

142. D. G. Truhlar, in *The Reaction Path in Chemistry: Current Approaches and Perspectives*, D. Heidrich, Ed., Kluwer, Dordrecht, The Netherlands, 1995, pp. 229-255. Direct Dynamics Method for Calculations of Reaction Rates.

143. Y.-Y. Chuang, and D. G. Truhlar, *J. Phys. Chem. A*, 101, 3808, 8741(E) (1997). Improved Dual-Level Direct Dynamics Method for Reaction Rate Calculations with Inclusion of Multidimensional Tunneling Effects and Validation for the Reaction of H with *trans*-N_2H_2.

144. I. Rossi and D. G. Truhlar, *Chem. Phys. Lett.* 223, 231 (1995). Parameterization of NDDO Wavefunctions using Genetic Algorithms: An Evolutionary Approach to Parameterizing Potential Energy Surfaces and Direct Dynamics Calculations for Organic Reactions.

145. J. A. Pople, D. P. Santry, and G. A. Segal, *J. Chem. Phys.*, 43, S129 (1965). Approximate Self-Consistent Molecular Orbital Theory. I. Invariant Procedures.

146. J. A. Pople and D. J. Beveridge, *Approximate Molecular Orbital Theory*, McGraw-Hill, New York, 1970.

147. M. J. S. Dewar, E. G. Zoebisch, E. F. Healy, and J. J. P. Stewart, *J. Am. Chem. Soc.*, 107, 3902 (1985). Development and Use of Quantum Mechanical Molecular Models. 76. AM1: A New General Purpose Quantum Mechanical Molecular Model.

148. M. J. S. Dewar and E. G. Zoebisch, *J. Mol. Struct. (THEOCHEM)*, 180, 1 (1988). Extension of AM1 to the Halogens.

149. A. Warshel and R. M. Weiss, *J. Am. Chem. Soc.*, 102, 6218 (1980). An Empirical Valence Bond Approach for Comparing Reactions in Solutions and in Enzymes.

150. Y. T. Chang and W. H. Miller, *J. Phys. Chem.*, 94, 5884 (1990). An Empirical Valence Bond Model for Constructing Global Potential Energy Surfaces for Chemical Reactions of Polyatomic Molecular Systems.

151. Y. T. Chang, C. Minichino, and W. H. Miller, *J. Chem. Phys.*, 96, 4341 (1992). Classical Trajectory Studies of the Molecular Dissociation Dynamics of Formaldehyde: $H_2CO \rightarrow H_2 + CO$.

152. J. Ischtwan and M. A. Collins, *J. Chem. Phys.*, 100, 8080 (1994). Molecular Potential Energy Surfaces by Interpolation.

153. K. A. Nguyen, I. Rossi, and D. G. Truhlar, *J. Chem. Phys.*, 103, 5222 (1995). A Dual-Level Shepard Interpolation Method for Generating Potential Energy Surfaces for Dynamics Calculations.

154. J. C. Corchado, E. L. Coitiño, Y.-Y. Chuang, P. L. Fast, and D. G. Truhlar, *J. Phys. Chem. A*, 102, 2424 (1998). Interpolated Variational Transition-State Theory by Mapping.

155. W.-P. Hu, Y.-P. Liu, and D. G. Truhlar, *J. Chem. Soc., Faraday Trans.*, 90, 1715 (1994). Variational Transition-State Theory and Semiclassical Tunneling Calculations With Interpolated Corrections: A New Approach to Interfacing Electronic Structure Theory and Dynamics for Organic Reactions.

156. Y.-Y. Chuang, J. C. Corchado, and D. G. Truhlar, *J. Phys. Chem. A*, 103, 1140 (1999). Mapped Interpolation Scheme for Single-Point Energy Corrections in Reaction Rate Calculations and a Critical Evaluation of Dual-Level Reaction Path Dynamics Methods.

157. D. G. Truhlar, *J. Chem. Educ.*, 62, 104 (1985). Nearly Encounter-Controlled Reactions: The Equivalence of the Steady-State and Diffusional Viewpoints.

158. K. A. Connors, *Chemical Kinetics: The Study of Reaction Rates in Solution*; VCH Publishers, New York, 1990, pp. 207–208.

159. Y.-Y. Chuang, C. J. Cramer, and D. G. Truhlar, *Int. J. Quantum Chem.*, 70, 887 (1998). Interface of Electronic Structure and Dynamics for Reactions in Solution.

160. M. J. Pilling and P. W. Seakins, *Reaction Kinetics*, Oxford University Press, Oxford, United Kingdom, 1995, pp. 155–156.

161. C. J. Cramer and D. G. Truhlar, in *Reviews in Computational Chemistry*, Vol. 6, K. B. Lipkowitz and D. B. Boyd, Eds., VCH Publishers, New York, 1995, pp. 1–72. Continuum Solvation Models: Classical and Quantum Mechanical Implementations.

162. C. J. Cramer and D. G. Truhlar, in *Solvent Effects and Chemical Reactivity*, O. Tapia and J. Bertrán, Eds., Kluwer, Dordrecht, The Netherlands, 1996, pp. 1–80. [Understanding Chem. React. 17, 1–80 (1996).] Continuum Solvation Models.

163. D. J. Giesen, C. C. Chambers, G. D. Hawkins, C. J. Cramer, and D. G. Truhlar, in *Computational Thermochemistry*, K. Irikura and D. J. Frurip, Eds., American Chemical Society Symposium Series Volume 677, Washington, D.C., 1998, pp. 285–300. Modeling Free Energies of Solvation and Transfer.

164. G. D. Hawkins, T. Zhu, J. Li, C. C. Chambers, D. J. Giesen, D. A. Liotard, C. J. Cramer, and D. G. Truhlar, in *Combined Quantum Mechanical and Molecular Mechanical Methods*, J. Gao and M. A. Thompson, Eds., American Chemical Society Symposium Series Volume 712, Washington, D.C., 1998, pp. 201–219. Universal Solvation Models.

165. J. Li, G. D. Hawkins, C. J. Cramer, and D. G. Truhlar, *Chem. Phys. Lett.*, 288, 293 (1998). Universal Reaction Field Model Based on Ab Initio Hartree-Fock Theory.

166. T. Zhu, J. Li, G. D. Hawkins, C. J. Cramer, and D. G. Truhlar, *J. Chem. Phys.*, 109, 9117 (1998). Density Functional Solvation Model Based on CM2 Atomic Charges.

167. C. J. Cramer and D. G. Truhlar, *Chem. Rev.*, 99, 2161 (1999). Implicit Solvation Models: Equilibria, Structure, Spectra, and Dynamics.

168. J. Li, T. Zhu, G. D. Hawkins, P. Winget, D. A. Liotard, C. J. Cramer, and D. G. Truhlar, *Theor. Chem. Acc.*, 103, 9 (1999). Extension of the Platform of Applicability of the SM5.42R Universal Solvation Model.

169. C. J. Cramer and D. G. Truhlar, in *Free Energy Calculations in Rational Drug Design*, M. R. Reddy and M. D. Erion, Eds., Kluwer Academic/Plenum, New York, 2001, pp. 63–95. Solvation Thermodynamics and the Treatment of Equilibrium and Nonequilibrium Solvation Effects by Models Based on Collective Solvent Coordinates.

170. J. D. Thompson, C. J. Cramer, and D. G. Truhlar, *J. Phys. Chem. A*, 108, 6532 (2004). New Universal Solvation Model and Comparison of the Accuracy of Three Continuum Solvation Models, SM5.42R, SM5.43R, and C-PCM, in Aqueous Solution and Organic Solvents and for Vapor Pressures.

171. C. P. Kelly, C. J. Cramer, and D. G. Truhlar, *J. Chem. Theory Comput.*, 1, 1133 (2005). SM6: A Density Functional Theory Continuum Solvation Model for Calculating Aqueous Solvation Free Energies of Neutrals, Ions, and Solute-Water Clusters.

172. D. A. McQuarrie, *Statistical Mechanics*, Harper & Row, New York, 1976, pp. 266.

173. D. G. Truhlar, Y.-P. Liu, G. K. Schenter, and B. C. Garrett, *J. Phys. Chem.*, 98, 8396 (1994). Tunneling in the Presence of a Bath: A Generalized Transition State Theory Approach.

174. Y.-Y. Chuang, and D. G. Truhlar, *J. Am. Chem. Soc.*, 121, 10157 (1999). Nonequilibrium Solvation Effects for a Polyatomic Reaction in Solution.

175. C. Alhambra, J. Corchado, M. L. Sánchez, M. Garcia-Viloca, J. Gao, and D. G. Truhlar, *J. Phys. Chem. B*, 105, 11326 (2001). Canonical Variational Theory for Enzyme Kinetics with the Protein Mean Force and Multidimensional Quantum Mechanical Tunneling Dynamics. Theory and Application to Liver Alcohol Dehydrogenase.

176. D. G. Truhlar, J. Gao, C. Alhambra, M. Garcia-Viloca, J. Corchado, M. L. Sánchez, and J. Villà, *Acc. Chem. Res.*, 35, 341 (2002). The Incorporation of Quantum Effects in Enzyme Kinetics Modeling.

177. M. Garcia-Viloca, C. Alhambra, D. G. Truhlar, and J. Gao, *J. Comput. Chem.*, 24, 177 (2003). Hydride Transfer Catalyzed by Xylose Isomerase: Mechanism and Quantum Effects.

178. T. D. Poulsen, M. Garcia-Viloca, J. Gao, and D. G. Truhlar, *J. Phys. Chem. B*,107, 9567 (2003). Free Energy Surface, Reaction Paths, and Kinetic Isotope Effect of Short-Chain Acyl-CoA Dehydrogenase.

179. D. G. Truhlar, J. Gao, M. Garcia-Viloca, C. Alhambra, J. Corchado, M. L. Sánchez, and T. D. Poulsen, *Int. J. Quantum Chem.*, 100, 1136 (2004). Ensemble-Averaged Variational Transition State Theory with Optimized Multidimensional Tunneling for Enzyme Kinetics and Other Condensed-Phase Reactions.

180. D. G. Truhlar, in *Isotope Effects in Chemistry and Biology*, A. Kohen and H.-H. Limbach, Eds., Marcel Dekker, Inc., New York, 2006, pp. 579–620. Variational Transition State Theory and Multidimensional Tunneling for Simple and Complex Reactions in the Gas Phase, Solids, Liquids, and Enzymes.

181. M. J. Rothman, L. L. Lohr, Jr., C. S. Ewig, and J. R. Van Wazer, in *Potential Energy Surfaces and Dynamics Calculations*, D. G. Truhlar, Ed., Plenum, New York, 1981, pp. 653–660. Application of the Energy Minimization Method to a Search for the Transition State for the $H_2 + D_2$ Exchange Reaction.

182. R. Steckler and D. G. Truhlar, *J. Chem. Phys.*, 93, 6570 (1990). Reaction-Path Power Series Analysis of NH_3 Inversion.

183. D. Heidrich, in *The Reaction Path in Chemistry*, D. Heidrich, Ed., Kluwer, Dordrecht, The Netherlands, 1995, pp. 1–10. An Introduction to the Nomenclature and Usage of the Reaction Path Concept.

184. B. R. Brooks, R. E. Bruccoleri, B. D. Olafson, D. J. States, S. Swaminathan, and M. Karplus, *J. Comput. Chem.*, 4, 187 (1983). CHARMM: A Program for Macromolecular Energy, Minimisation and Dynamics Calculations.

185. G. N. Patey and J. P. Valleau, *Chem. Phys. Lett.*, 21, 297 (1973). The Free Energy of Spheres with Dipoles: Monte Carlo with Multistage Sampling.

186. G. N. Patey and J. P. Valleau, *J. Chem. Phys.*, 63, 2334 (1975). A Monte Carlo Method for Obtaining the Interionic Potential of Mean Force in Ionic Solution.

187. G. M. Torrie and J. P. Valleau, *J. Comput. Phys.*, 23, 187 (1977). Nonphysical Sampling Distributions in Monte Carlo Free Energy Estimation: Umbrella Sampling.

188. M. Garcia-Viloca, C. Alhambra, D. G. Truhlar, and J. Gao, *J. Chem. Phys.*, 114, 9953 (2001). Inclusion of Quantum Mechanical Vibrational Energy in Reactive Potentials of Mean Force.

189. D.C. Chatfield, R.S. Friedman, D.W. Schwenke, and D.G. Truhlar, J. Phys. Chem, 96, 2414 (1992). Control of Chemical Reactivity by Quantized Transition States.

190. B. J. Gertner, J.P. Bergsma, K. R. Wilson, S. Lee, and J. T. Hynes, *J. Chem. Phys.*, 86, 1377 (1987). Nonadiabatic Solvation Model for S_N2 Reactions in Polar Solvents.

191. W. P. Kierstad, K. R. Wilson, and J. T. Hynes, *J. Chem. Phys.*, 95, 5256 (1991). Molecular Dynamics of a Model S_N1 Reaction in Water.

192. J. T. Hynes, in *Solvent Effects and Chemical Reactivity*, O. Tapia and J. Bertrán, Eds., Kluwer, Dordrecht, The Netherlands, 1996, pp. 231–258. Crossing the Transition State in Solution.

193. M. J. T. Jordan and R. G. Gilbert, *J. Chem. Phys.*, 102, 5669 (1995). Classical Trajectory Studies of the Reaction $CH_4 + H \rightarrow CH_3 + H_2$.

194. J. M. Bowman, D. Wang, X. Huang, F. Huarte-Larrañaga, and U. Manthe, *J. Chem. Phys.*, 114, 9683 (1991). The Importance of an Accurate CH_4 Vibrational Partition Function in Full Dimensionality Calculations of the $CH_4 + H \rightarrow CH_3 + H_2$ Reaction.

195. F. Huarte-Larrañaga and U. Manthe, *J. Chem. Phys.*, 113, 5115 (2000). Full Dimensional Quantum Calculations of the $CH_4 + H \rightarrow CH_3 + H_2$ Reaction Rate.

196. F. Huarte-Larrañaga and U. Manthe, *J. Phys. Chem.* A, 105, 2522 (2001). Quantum Dynamics of the $CH_4 + H \rightarrow CH_3 + H_2$ Reaction. Full Dimensional and Reduced Dimensionality Rate Constants Calculations.

197. C. P. Kelly, J. D. Xidos, J. Li, J. D. Thompson, G. D. Hawkins, P. D. Winget, T. Zhu, D. Rinaldi, D. A. Liotard, C. J. Cramer, D. G. Truhlar, and M. J. Frisch, MN-GSM, version 5.2, Univeristy of Minnesota, Minneapolis, Minnesota, 55455-0431, 2005.

198. M. J. Frisch, G. W. Trucks, H. B. Schlegel, G. E. Scuseria, M. A. Robb, J. R. Cheeseman, V. G. Zakrzewski, J. A. Montgomery, R. E. Stratmann, J. C. Burant, S. Dapprich, J. M. Millam, A. D. Daniels, K. N. Kudin, M. C. Strain, O. Farkas, J. Tomasi, V. Barone, M. Cossi, R. Cammi, B. Mennucci, C. Pomelli, C. Adamo, S. Clifford, J. Ochterski, G. A. Petersson, P. Y. Ayala, Q. Cui, K. Morokuma, D. K. Malick, A. D. Rabuck, K. Raghavachari, J. B. Foresman, J. Cioslowski, J. V. Ortiz, B. B. Stefanov, G. Liu, A. Liashenko, P. Piskorz, I. Komaromi, R. Gomperts, R. L. Martin, D. J. Fox, T. Keith, M. A. Al-Laham, C. Y. Peng, A. Nanayakkara, C. Gonzalez, M. Challacombe, P. M. W. Gill, B. G. Johnson, W. Chen, M. W. Wong, J. L. Andres, M. Head-Gordon, E. S. Replogle, and J. A. Pople, *Gaussian 98, Revision A.3*, Gaussian, Inc., Pittsburgh, Pennsylvania, 1998.